REMOTE SENSING AND GIS ANALYSIS OF THE SPATIAL AND MORPHOLOGICAL CHANGES OF THERMOKARST LAKES: KOLYMA LOWLANDS, NORTHEAST SIBERIA

By

Meghan L. Tillapaugh

RECOMMENDED:

Advisory Committee Chair

Chair, Department of Geology and Geophysics

APPROVED:

Dean, College of Natural Science and Mathematics

Dean of the Graduate School

Apr 7, 2011

Date

REMOTE SENSING AND GIS ANALYSIS OF THE SPATIAL AND MORPHOLOGICAL CHANGES OF THERMOKARST LAKES: KOLYMA LOWLANDS, NORTHEAST SIBERIA

A

THESIS

Presented to the Faculty
of the University of Alaska Fairbanks

in Partial Fulfillment of the Requirements
for the Degree of

MASTER OF SCIENCE

By

Meghan L. Tillapaugh, B.S.

Fairbanks, Alaska

May 2011

Abstract

Thermokarst lakes develop when changes in the permafrost thermal regime cause degradation leading to surface subsidence and ponding. The degree of thermokarst development depends upon permafrost characteristics, topography, and geology. Changing thermokarst lake dynamics affect arctic ecosystems, hydrological patterns, albedo, and the carbon cycle through the mobilization of organic matter in the permafrost. This study used remote sensing and GIS techniques to relate lake dynamics in the Kolyma Lowlands, Siberia, to geology, elevation, geomorphological features, hydrology, and air temperature.

Highest limnicity and largest lake sizes were found in regions with low elevation, limited alluvial processes, high ground-ice content, and lithologies with small particle sizes. New lake development and erosion occurred as well.

One subregion studied showed lake area increases (Cherskii: +7.6%) while another showed a decrease (Duvanny Yar: -5.2%). Differences are attributed to variations in elevation and fluvial influences. A major cause of drainage was river tapping of lakes. Lake coalescence, flooding during river water level high stands, and lakeshore erosion were the main causes of lake expansion. The Kolyma Lowland soils have high ice and organic matter contents as well making the monitoring of thermokarst lake dynamics important as large amounts of freshwater and carbon could potentially be released.

Table of Contents

List of Figures

List of Tables

Acknowledgements

The completion of this thesis could not have been possible without the support and guidance of my advisor, Vladimir Romanovsky, as well as the members of my graduate committee, consisting of Guido Grosse, Anupma Prakash, and Jim Beget. The opportunities and knowledge they have presented to me over the past three years has been most valuable in the advancement of my education.

Chapter 1: Introduction

1.1 Permafrost and Climate Change

Permafrost is a basic component in arctic ecosystems as it supports the overlying ground surface and vegetation, and regulates surface and ground water movement (Jorgenson et al., 2010). It also acts as a foundation for human infrastructure, like buildings, roads, and pipelines. Disturbances and changing environmental conditions will often initiate permafrost degradation and thaw. Thawing permafrost will disturb the established surface conditions and when the ground ice volume exceeds the pore space of the soil, upon thaw, surface settlement will occur, a process called thermokarst (Grosse et al., 2006; Katamura et al., 2006). Thermokarst depressions allow water to accumulate and thus begin the first steps in the development of an arctic pond or lake.

Many factors influence the permafrost thermal regime and thus can cause permafrost degradation. These factors are: topography, surface and ground water movement, moisture content, soil properties, vegetation, snow cover, albedo, air temperature, and surface disturbances from human activities, including strip mining and the construction of drilling platforms and roads, as well as natural disturbances such as forest fires (Schuur et al., 2008; Jorgenson et al., 2010).

Topography affects the amount of solar radiation the ground surface receives (Jorgenson et al., 2010). North facing slopes and areas that are heavily vegetated receive less direct radiation. Less incoming radiation means less heat energy is being received by the earth's surface and is available to warm the ground. Surface water will run off the slopes and become contained within the flatter, lower-lying regions. Here, the water will be more restricted from flow and begin to pool. Surface water, once it begins to collect within thermokarst depressions, and ground water movement, within the active layer, will enhance permafrost degradation. Water has a generally low albedo and a high heat capacity and thus is able to accumulate large amounts of heat during the summer and transfer this heat to the permafrost table. Thermal conductivity, the soil property that governs the rate at which heat flows through a substance between two points at different temperatures, increases with increasing moisture content (Yoshikawa et al., 2003;

O'Donnell et al., 2009; Jorgenson et al., 2010). Soils will generally remain warmer under wet conditions than under dry conditions. Thermal conductivity also varies with other soil properties. Coarse-grained, more gravelly soils, which are normally well drained, show little difference in thermal conductivity between thawed and frozen states. Organic soils, along with silty and clayey soils, are poorly drained and have higher conductivities in the winter, when they are in a frozen state, than when they are thawed (Shur and Jorgenson, 2007; Jorgenson et al., 2010). Therefore, fine-grained and organic soils experience rapid heat loses in the winter and slow warming at depth in the summer.

Ground cover properties, like vegetation and snow, have both positive and negative feedbacks to permafrost degradation. Tall vegetation, which intercepts snow, will help keep the permafrost cold (Jorgenson et al., 2010). Less snowfall means less insulation from the colder winter air temperatures and thus colder permafrost. Increasing snowfall will insulate the permafrost from the cold winter temperatures and slow the rate of cooling (Schuur et al., 2008; Jorgenson et al., 2010). This, in return, would mean warmer permafrost temperatures going into the summer allowing for deeper thaw depths. Earlier snowmelt and later snowfall will cause solar radiation to be absorbed when it was previously reflected by the higher albedo values of the snow (Eugster et al., 2000). Moss growth and thick organic soils help insulate the permafrost from the warmer summer temperatures as well (Schuur et al., 2008). The removal of the organic layer, by fire for example, will increase ground heat fluxes and promote permafrost thaw.

With no other factors changing, warmer air temperatures will create warmer permafrost temperatures and increased permafrost degradation. Warmer temperatures will also move the forest/tundra biome border northward. Within Alaska, the treeline on the Seward Peninsula, in the Brooks Range, the Alaska Range, and the White Mountains have all moved north into the tundra throughout the 21st century (Lloyd et al., 2003; Hinzman et al., 2005).

With no vegetation present, permafrost will develop in interior Alaska at mean annual air temperatures below -6 ^{o}C (Jorgenson et al., 2010). As temperatures rise, permafrost will need negative feedbacks from outside factors to survive or to form.

Human infrastructure development will disrupt the ground surface and the established environmental conditions, favoring permafrost degradation. Permafrost acts as a substrate to build on and disturbing permafrost by building houses, pipelines, and roads can cause the permafrost to warm, reducing the load capacity of the pilings and causing slumping of the infrastructure (Hinzman et al., 2005).

Currently, 23.9% of the northern hemisphere land surface or 18,782 x 10^3 km^2 is affected by permafrost (Zhang et al., 1999; Tarnocai et al., 2009). 54% of the permafrost is within the continuous permafrost zone (Tarnocai et al., 2009) (Figure 1.1.1). However, that percentage changes with shifting environmental conditions. With such a substantial area being affected by permafrost, thermokarst development could affect a large region of the arctic. The degree to which thermokarst subsidence will occur depends on ground ice content, ground ice distribution, and thaw magnitude (Shur and Jorgenson, 2007). Beneath the active layer is often an ice-rich layer consisting of ice-wedges, segregated ice lenses and layers, along with pore-space ice (Schuur et al., 2008). The thawing of such ice-rich permafrost will cause a high degree of thermokarst terrain. The thawing of permafrost in ice-poor regions will hinder thermokarst development, as limited ground subsidence will occur. Thaw magnitude depends on the many factors listed above which influence the permafrost temperature regime.

The susceptibility of permafrost to thaw and degradation depends largely on the positive and negative feedbacks associated with changes in air temperature, ice content, and the ecological factors, which influence the permafrost temperature regime by modifying the surface energy balance. Because of the complicated interaction between all these factors, predictions based solely on future climate change are difficult. Due to these complex connections, for example, the presence of surface water is capable of thawing permafrost, to some extent, in extremely cold conditions with -20 ^{o}C mean annual air temperatures and, on the other hand, vegetation and soil properties can allow permafrost to endure at +2 ^{o}C mean annual air temperature (Jorgenson et al., 2010).

By the end of the 21st century, the global mean temperature is expected to increase between 1.8 ^{o}C and 4.0 ^{o}C (IPCC, 2007). In the arctic, north of 60^{o} latitude,

temperatures are expected to increase even more, between 2.8 ^{o}C and 4.6 ^{o}C (ACIA, 2005). With the global climate continuing to warm and human presence and activities becoming more common in the arctic, the potential for permafrost degradation, thaw, and thermokarst development is increasing and thus thermokarst research is becoming more relevant.

Figure 1.1.1. Permafrost Extent in the Northern Hemisphere (Brown et al., 1997).

1.2 Thermokarst Lakes

Thermokarst lakes occupy up to 48% of the land surface in some regions of the Arctic (Riordan et al., 2006). The size and spatial distribution of thermokarst lakes is largely a function of ground ice volume, local and regional relief, drainage patterns, age, and sediment type and texture (Sellmann et al., 1975; Smith et al., 2007). Locations with high ice content will experience a greater degree of thermokarst development when compared to regions with low ice content. The amount of ice present within the soil will determine how much settlement will occur and how much soil will be available and incorporated into the active layer. Latent heat, the amount of energy required to change a substance from a solid to a liquid, is directly proportional to ice content however. The high latent heat of ice-rich soil will impede the rate of permafrost thaw at depth (Jorgenson et al., 2010). It takes more energy to thaw ice-rich permafrost than to thaw ice-poor permafrost.

Regions with steeper relief allow better drainage. The presence of slope improves runoff, which reduces the potential for impounding water. Some sediment types, such as gravel and sand, result in better drainage because of their higher hydraulic conductivity given their high porosity and permeability. Large soil particles will also often mean less ground ice and therefore less thermokarst will develop. These characteristics hinder water accumulation and thus prevent lake development. Sediments with low hydraulic conductivities, including lacustrine and eolian silts and marine clays, impede water infiltration and enhance ponding.

Lake surface area can increase with time due to the erosion of lake banks from wave action and currents (thermal-mechanical erosion) (Frohn et al., 2005). Thawing of ice-rich permafrost beneath the lake and of the lakeshores will also cause lake expansion as will increased precipitation and surface runoff (Frohn et al., 2005; Shur and Jorgenson, 2007). Lakes may drain, fully or partially, reducing surface area due to a number of factors including underground tunnel flow through a system of ice-wedge cracks, complete thaw to the bottom of the permafrost layer under the lake, erosion by a connecting river or stream, and overflow of the lake banks in times of high water creating

a drainage outlet (Hopkins et al., 1949; Mackay, 1988; Marsh et al., 2009). A common cause of lake change occurs during times of high water when a single lake breaches its bank and drains into a lower lying lake, forming a larger, coalesced lake. This raises the water level of the second lake, initially increasing the surface area, but then it too could potentially overtop its banks and create a drainage outlet (Mackay, 1988).

Understanding and monitoring thermokarst lakes is important because of the effects lakes have on arctic environments. Formation of thermokarst lakes results in changes to permafrost stability, regional hydrological patterns, vegetation cover and ecosystem distribution, regional albedo values, and infrastructure stability (Hinzman et al., 2005; Jorgenson et al., 2010).

Thermokarst lake development can cause many changes to the hydrological network. The permafrost table, especially in regions with ice-rich permafrost, acts as an aquitard, preventing interactions between surface and sub-surface waters (Hinzman et al., 2005). Thickening of the active layer can cause ground surface subsidence, which alone can change the local hydrological patterns, and allow more surface and subsurface water to mix. Lake formation and drainage can result in rivers and streams forming or disappearing. The most obvious affect rivers have on thermokarst lakes is lake tapping by river erosion and flooding. Draining thermokarst lakes can increase freshwater runoff as well.

Thermokarst formation will increase the area of aquatic ecosystems (Jorgenson et al., 2010). Forests may be replaced by lakes, high nutrient wetlands, wet-sedge meadows, and bogs, with herbaceous plant species and forage for herbivores (Hinzman et al., 2005; Jorgenson et al., 2010). These ecosystems favor water birds and mammals, not the land based birds and mammals previously present, like caribou.

There is an inverse relationship between lake area and surface albedo values, the proportion of total incident solar radiation that is reflected from the earth's surface. Liquid water has a very low albedo (0.05), while dry, herbaceous, lichen vegetation and deciduous forests have albedo values between 0.2 and 0.3 (Jorgenson et al., 2010). Water's low albedo creates a high heat flux into the water thus allowing the transfer of

heat to the permafrost table. Thermokarst lakes act as a medium to transfer heat to the deeper layers (Yoshikawa and Hinzman, 2003). Ice has a high albedo value but with warmer temperatures, the water will be frozen for a shorter length of time, allowing solar radiation to be absorbed for a longer portion of the year. Increasing lake surface area will then decrease the regional albedo and thus the amount of heat being reflected back into the atmosphere. The amount of solar radiation being absorbed, emitted, and reflected creates changes in the radiation balance of the arctic. Currently, the Arctic's cold temperatures are sustained by a negative radiation balance in high latitudes where more radiation energy is being lost than absorbed (Hinzman et al., 2005), but with increasing lake area, the surface energy balance could change.

Lake development can occur in arctic regions where human development is ongoing. Thermokarst lakes can develop in close proximity to human infrastructure forcing the structures to be moved or rebuilt. Lake formation can also warm the surrounding permafrost causing the ground to settle and structures to become unstable.

Besides shifting ecosystem structure and distribution, thermokarst lake formation affects the global carbon cycle. The northern hemisphere permafrost region contains approximately 1,672 Pg (1 Pg = 1 billion metric tons) of organic carbon in its soils; approximately 50% of the global belowground organic carbon reservoir (Tarnocai et al., 2009). This measurement includes soil carbon in permafrost soils from 0-300 cm, Yedoma deposits for an average depth of 25 m, and seven major arctic river deltas, with an average depth of 50 m (Yedoma is described in greater detail on the following page). Carbon is incorporated into the permafrost in two ways. The first is by syngenetic permafrost growth. Due to sedimentation and peat formation, the ground surface and the permafrost table rises and the organic matter at the bottom of the former active layer is incorporated into the permafrost (Schuur et al., 2008). The second method is by cryoturbation (Ping et al., 2008; Walker et al., 2008). Plant root growth, organisms, and freeze-thaw cycles mix the soils, forcing organic matter to deeper and deeper depths.

As permafrost thaws, organic matter contained within the soil will thaw and become available for microbial decomposition. In uplands, active layer thickening and

talik formation will make carbon available for aerobic decomposition, releasing carbon dioxide. Thermokarst lake formation is less common in uplands allowing decomposition to occur in an oxygen-rich environment. In the lowlands, where thermokarst lake formation is more common, thawed soil from permafrost degradation often accumulates at the bottom of lakes, promoting decomposition in anaerobic conditions (Schuur et al., 2008). When decomposition occurs in oxygen-deprived environments, methane is released. The amount of carbon within northern hemisphere permafrost is roughly twice the current atmosphere carbon pool (Schuur et al., 2008). With increasing air temperatures and continual soil warming, the rate of microbial decomposition of the carbon will increase.

Yedoma, organic-rich and ice-rich Pleistocene sediment, underlies an estimated 10^6 km^2 of northern Siberia; this amounts to 7.6% of the total permafrost area north of 45^o latitude (Walter et al., 2007b) (Figure 1.2.1). About 475 Pg of organic carbon is contained within the Yedoma deposits (Zimov et al., 1997; Walter et al., 2006, 2007b). Yedoma soils are densely populated with thermokarst lakes giving these soils the potential to release a large amount of methane upon thaw. Lakes act as a channel to: 1) transfer heat deeper into the soil; and 2) bring deep and old permafrost carbon to the surface in the form of microbially produced greenhouse gas methane. A positive feedback system therefore exists between thawing permafrost and thermokarst lake formation and the arctic atmospheric methane concentrations. Methane has 25 times the global warming potential that carbon dioxide does over a 100-year period (ACIA, 2005; IPCC, 2007). This allows Yedoma lakes to be a larger factor in climate warming than previously thought.

The above-mentioned effects of degrading permafrost and thermokarst lake formation provide evidence that the underlying permafrost is either: 1) in an unstable state, such as the case in southern, discontinuous permafrost zones; or 2) responding to disturbances, such as climate warming, fires, or hydrological changes, causing the near-surface permafrost to thaw/degrade. The latter occurs in continuous permafrost regions where the permafrost is cold and climatically stable so far. With thermokarst lake

formation, permafrost will be thawing, while in locations where thermokarst lakes are draining, the ground refreezes. It is important to understand the factors that are affecting permafrost degradation, thermokarst development, thermokarst lake formation and drainage because of their effects on the arctic environment, which include effects on atmospheric carbon concentrations.

Figure 1.2.1. Yedoma Distribution in Siberia (G. Grosse, unpublished map, based on Romanovskii, 1993).

1.3 Changes during the Pleistocene-Holocene Transition

A large proportion of the arctic surface permafrost sediments formed during the multiple Pleistocene cooling periods, which occurred between 1.8 million and 12 k years BP (Smith et al., 1995; Walter et al., 2006; Veremeeva and Gubin, 2009). However, arctic environments changed during the Pleistocene-Holocene warming period when an approximate 20 ^{o}C rise in temperature occurred (Shur and Jorgenson, 2007). Between 20 and 10 k years BP, following the Last Glacial Maximum (24-21 k years BP), there was an increase in air temperature of approximately 2 ^{o}C/millennium (ACIA, 2005). This temperature information has been recorded within the Greenland ice sheets (Severinghaus et al., 1998). A large percentage of permafrost disappeared and much of the terrain, up to 50%, experienced thermokarst development during this time (Veremeeva and Gubin, 2009). The relationship between warming climate and thermokarst development during the Pleistocene-Holocene transition shows that warming temperature trends can cause permafrost degradation.

1.4 Pervious Siberian Lake Change Studies

Described here are the three most recent thermokarst lake change studies available, which have been completed in Siberia. The first one, Smith et al. (2005), was done across 515,000 km^2 of west Siberia. Landsat Multispectral Scanner satellite images from the early 1970's and multispectral optical-mechanical radiometer images from the Russian RESURS-1 satellite from the late 1990s to early 2000s were used. Minimum lake size in this analysis was 40 ha. The study showed that the number of lakes during this time decreased by 11%. That means that from the studied 1,170 lakes, 125 lakes drained to below the 40 ha cutoff. Lake area lost was 93,000 ha or six percent.

A regional pattern was revealed in this study. In the continuous permafrost regions, lake area increased by 13,300 ha (12%), while in discontinuous, sporadic, and isolated permafrost regions, lake area decreased by 13%, 12%, and 11% respectively. Lake drainage; however, far outpaced the rate of lake expansion.

The second study was completed by Walter et al. (2006), along the Kolyma River near Cherskii, Russia. The study region was 12,000 km^2 and located in continuous

permafrost. 1974 Landsat Multispectral Scanner images and 2000 Landsat Enhanced Thematic Mapper Plus images were analyzed and showed a 14.7% increase in lake area.

The most recent study by Veremeeva and Gubin (2009), was completed within the Kolyma Lowlands on the northern Yakutia coastal lowlands using Landsat Multispectral Scanner images from 1973 and Landsat Enhanced Thematic Mapper images from 2001. The study region was 6,500 km^2, within the continuous permafrost zone, and lakes larger than 0.1 ha were mapped. The results showed that the area occupied by lakes had decreased during this period. Percent change values range from 0.9% to 10.7% for different landscape settings, the highest occurring within river valleys. Drainage appeared to occur due to thermo-erosion processes associated with warming ground and air temperatures.

1.5 Goal of This Research

Climate warming will likely have considerable impact on the stability of permafrost and the near-future development or drainage of thermokarst lakes. Understanding thermokarst lake dynamics is a crucial component to better understand changes in arctic environments and the carbon contribution the arctic lakes will make to the global carbon budget.

In order to better understand how thermokarst lakes are changing over time, this research project characterized thermokarst lakes in the Kolyma Lowlands based on lakes' spatial distribution and morphological changes from 1965 to 2007. This was accomplished using multi-sensor satellite imagery along with geographic information system (GIS) methods. Relationships between lake drainage and topography and geology were also identified. Other data sources used included a geological map (Russian Geological Research Institute VSEGEI, 2000), a digital elevation map (DEM) (Ferranti, 2009), and the International Permafrost Association (IPA) Circum-Arctic Permafrost Map (Brown et al., 1997). ArcGIS was used to complete the analysis. Specific goals included: 1) calculation of changes in lake surface area over time; 2) calculation of thermokarst lake drainage rates; and 3) calculation of high-resolution lake erosion rates for Yedoma deposits within the study area.

Chapter 2: Study Region

The study region for this research is located in the Kolyma Lowlands of Northeast Siberia. This is an unglaciated region located north of the Arctic Circle. The closest large settlement in the region is Cherskii. To the north, the study region is bound by the East Siberian Sea, and the Kolyma River runs through the region. To the east are the Rodinka Mountains (max. elev. roughly 1000 m) (Smith et al., 1995) and to the south is the Kolymskiy Range (Smith et al., 1995). To the west are the Kolyma Lowlands (elev. less than 20 m) (Smith et al., 1995) and the Yedoma uplands (elev. less than 60 m). The study region is located between 156°E and 163°E and 68°N and 70°N (Figure 2.1.1; Figure 2.1.2; Figure 2.1.3).

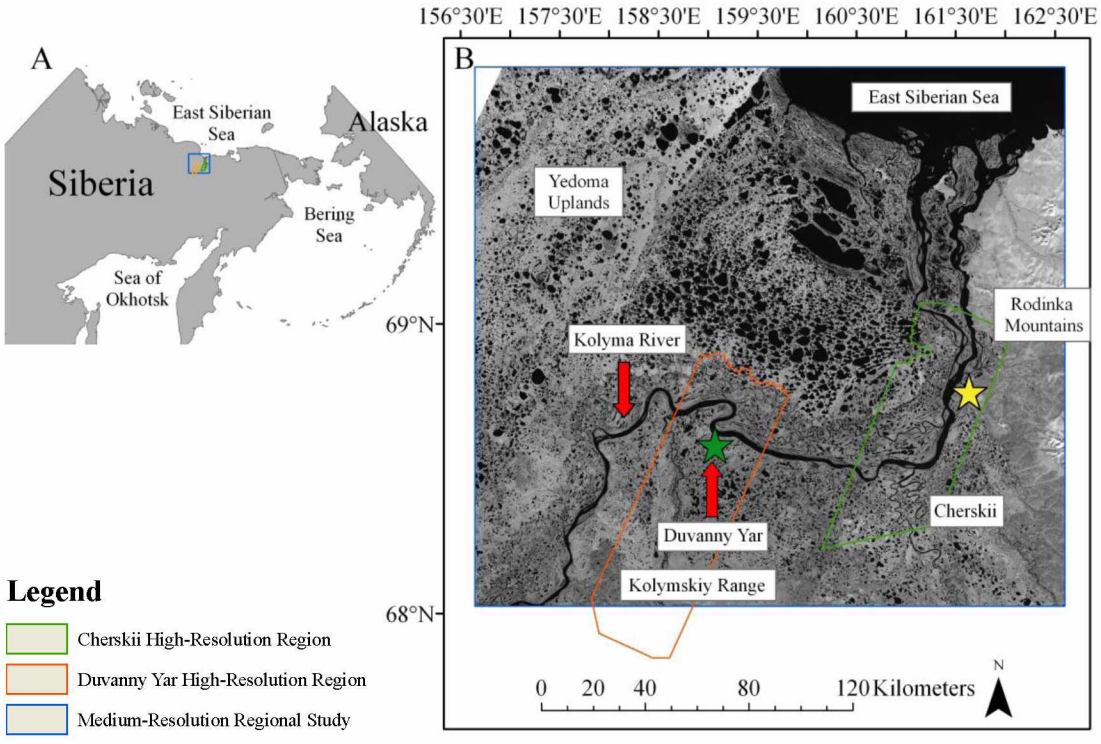

Figure 2.1.1. Study Region. A. Location of the Kolyma Lowlands in Northeast Siberia. B. Detailed map of the study region.

Figure 2.1.2. Kolyma Riverbank Erosion. Photo courtesy of A.L. Kholodov, University of Alaska, Fairbanks.

Figure 2.1.3. Kolyma Riverbank Degradation. Photo courtesy of A.L. Kholodov, University of Alaska, Fairbanks.

The majority of the study region, 3.9 million hectares (90%), are lowlands consisting of continuous permafrost (permafrost underlies > 90% of the terrain) that is predominately ice-rich (> 20% of excess ice in the upper 20 m of permafrost) (Brown et al., 1997). The elevation of this region is between zero and 60 meters above sea level. The eastern boundary of the study region along with a portion of the southern region is continuous permafrost with a slightly lower excess-ice content (between zero and 10%). These regions consist of mountains and highland ridges and plateaus (Smith et al., 1995; Brown et al., 1997). The elevations of the highlands range from 60 meters to just under 1,000 meters above sea level.

Permafrost depth in the Kolyma Lowlands ranges from 400 meters near Cherskii to over 800 meters (Bakermans et al., 2006; Grosse et al., 2008; Kosterin and Sivtseva, 2009). The majority of the surface permafrost deposits are of late Pleistocene origin, 100 k to 12 k years old (Smith et al., 1995; Gradstein et al., 2004; Walter et al., 2006; Veremeeva and Gubin, 2009). Some deposits developed during the Holocene, with the coldest period being between 1650 and 1859, the Little Ice Age (Schuur et al., 2008). The current topography, consisting of thermokarst lakes, drained thermokarst lake basins, and Yedoma uplands, started to develop during the Pleistocene/Holocene transition. The most active period of thermokarst development occurred between 9-8 k years BP, during the Holocene Climatic Optimum (Lozhkin et al., 1975; Kaplina and Lozhkin, 1982, cited within Veremeeva and Gubin, 2009). A second, less active period of thermokarst development occurred in the Middle to Late Holocene, 5-4 k years BP (Veremeeva and Gubin, 2009). Many thermokarst basins formed within previously developed basins during this time.

The permafrost in the Kolyma Lowland (Figure 2.1.1) region is ice-rich, as mentioned above, and also high in organic carbon. Several 100 Pg of organic carbon accumulated in soils and sediments in the northern Siberian plains during the late Pleistocene (Zimov et al., 1997). Parts of the study region belong to the Yedoma Suite (Late Pleistocene in age; 100-12 k years BP). Yedoma deposits are polygenetic and included nival sediments, wind-blown loess, alluvial silts, and re-transported silt-sized

sediment with high organic matter content, very high segregated ground ice content, (60% to 120% by weight), and very large ice wedges (up to 50% of total soil volume) (Schirrmeister et al., 2008). Yedoma contains between two and five percent organic matter and averages around 25 meters thick (Zimov et al. 2006). Grass roots, stems and leaves along with organic detritus are common (Schirrmeister et al., 2008) giving Yedoma the potential to release large amounts of fresh water and carbon should it thaw. Therefore, thermokarst lakes forming in Yedoma regions are capable to release large amounts of methane produced during microbial decomposition of this previously permafrost-stored organic carbon.

Land cover and soils for the region vary by location. The higher elevations (> 400 m) around Cherskii consist of alpine tundra vegetation covering frost-shattered bedrock. The lower-lying areas and hill slopes consist mainly of loess and colluvium deposits (Smith et al., 1995). Massive ground ice is common in the lower elevation loess deposits. *Pinus pumila* (Siberian dwarf pine) and *Larix dahurica* (larch) are common along with a shrub layer consisting of *Betula* (birch), *Salix* (willow), *Alnus* (alder) and *Ledum palustre* (marsh Labrador tea) (Smith et al., 1995). This region is well to slightly moderately drained. The active layer in this region ranges from > 1 m on the hilltops to < 40 cm at lower elevations (Smith et al., 1995; Nakano et al., 2000). Landform topography consists of mountain slopes, pediments (flat rock surfaces of low relief that are often covered with rock debris), and thermokarst depressions (Smith et al., 1995).

The Duvanny Yar region of the Kolyma Lowlands (elevation < 60 m) consists of lacustrine, colluvium, alluvium, and loess deposits with massive ground ice (Smith et al., 1995; Brown et al., 1997; Russian Geological Research Institute VSEGEI, 2000). Drainage varies from very poor to moderate. Vegetation consists of an open taiga (Subarctic coniferous) forest composed of *Larix dahurica*. An understory consisting of *Betula*, *Salix*, and *Ledum* (Labrador tea) exists along with a lichen covered forest floor. Upland Yedoma surfaces are covered with *Larix dahurica*. Grass species, *Ledum palustre*, and *Vaccinium vitis-idaea* (lingonberry, mountain cranberry, lowbush cranberry) dominate the understory (Smith et al., 1995). The active layer is generally <

40 cm, however, it is slightly deeper (80 cm) on the active Kolyma River floodplain. The landscape consists mostly of thermokarst lakes and basins (Smith et al., 1995; Veremeeva and Gubin, 2009).

The northern region of the Kolyma Lowlands bordering the East Siberian Sea is mostly composed of sediments containing large amounts of ground ice, and is highly affected by stream erosion and thermokarst action. Moderately to well drained alluvium and loess deposits make up the soils. The elevation is < 40 m. Vegetation consists of *Arctagrostis latifolia* (broadleaf polargrass), *Carex* (sedges), *Festuca* (perennial fescue grasses), *Alopecuris* (foxtail grass), and *Salix*. The active layer ranges from 60 cm to 40 cm (Smith et al., 1995).

The climate of the Kolyma Lowlands is extremely continental, receiving between 220 and 240 mm precipitation a year inland and under 200 mm along the East Siberian Sea Coast (Smith et al., 1995). Average annual air temperature is between -10 and -15 degrees Celsius; averaging around -33 ^{o}C in January and 11 ^{o}C in July (Kolyma Lowland National Weather Data, Smith et al., 1995; Nakano et al., 2000). The permafrost is also relatively cold. Most of the region has permafrost temperatures around -8 ^{o}C with the exception of the region around Cherskii, which is warmer, and at some locations may be as warm as -3 ^{o}C (Romanovsky, V., personal communication) (Figure 2.1.4; Figure 2.1.5; Figure 2.1.6).

The maps in Figure 2.1.4, Figure 2.1.5, and Figure 2.1.6 are from Kotlyakov and Koronkevitch (2002). The data from these maps was obtained between 1961 and 1990. The temperature and precipitation data used to create the maps is from Climate Research Unit's global dataset of mean monthly surface climate, and the permafrost temperature and extent data is from The World Atlas of Snow and Ice Resources, Institute of Geography at the Russian Academy of Sciences, Moscow, Russia. The data is from paper maps with scales ranging from 1:20 million to 1:40 million.

Another reason to study lakes in this region is because of the limited number of thermokarst lake studies completed in the Kolyma Lowlands. This region is densely

populated with arctic lakes and lake changes could significantly alter the current conditions of the Lowlands.

The Kolyma Lowlands are at low elevations, consist of lacustrine and marine clays, silts, and soils rich in organic matter within the continuous permafrost zone. These characteristics made the Kolyma Lowlands heavily influenced by thermokarst formation in the past and thus they are prone to high levels of thermokarst lake formation in the future.

Average Temperature for July

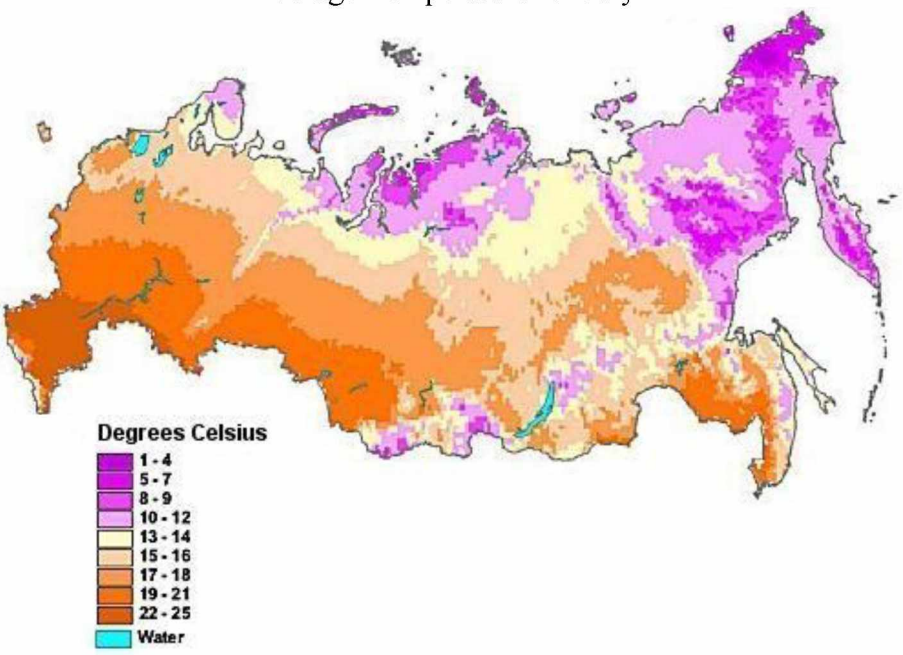

Average Temperature for January

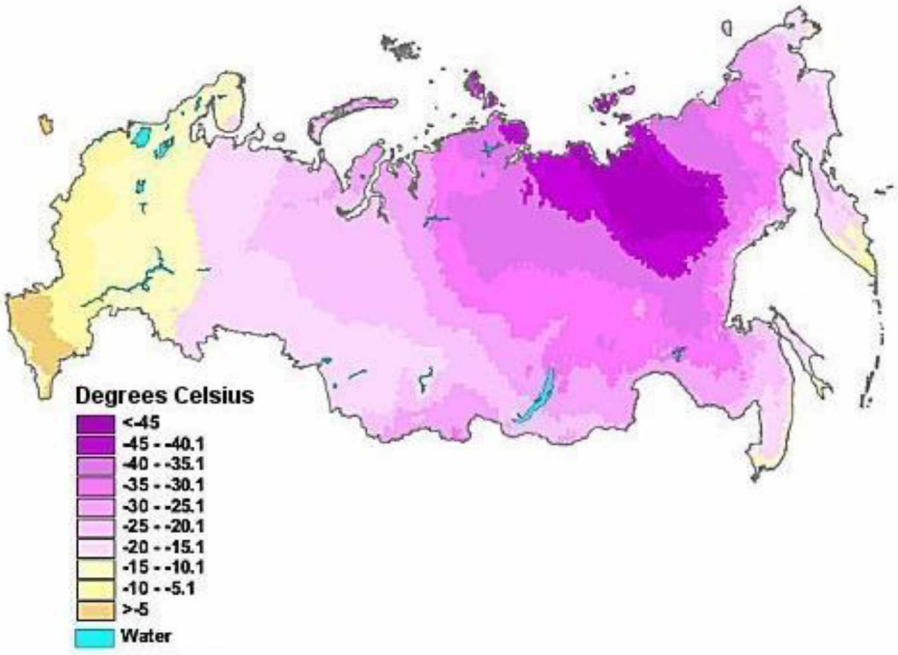

Figure 2.1.4. January and July Temperature Maps for Siberia. Data and maps are from Kotlyakov and Koronkevitch, 2002. Data was acquired between 1961 and 1990.

Average Annual Temperature

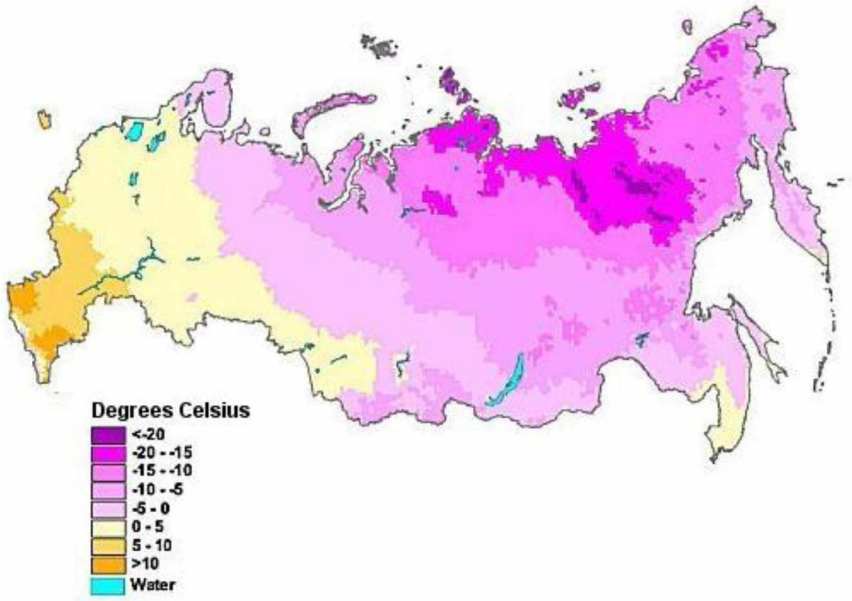

Average Annual Precipitation

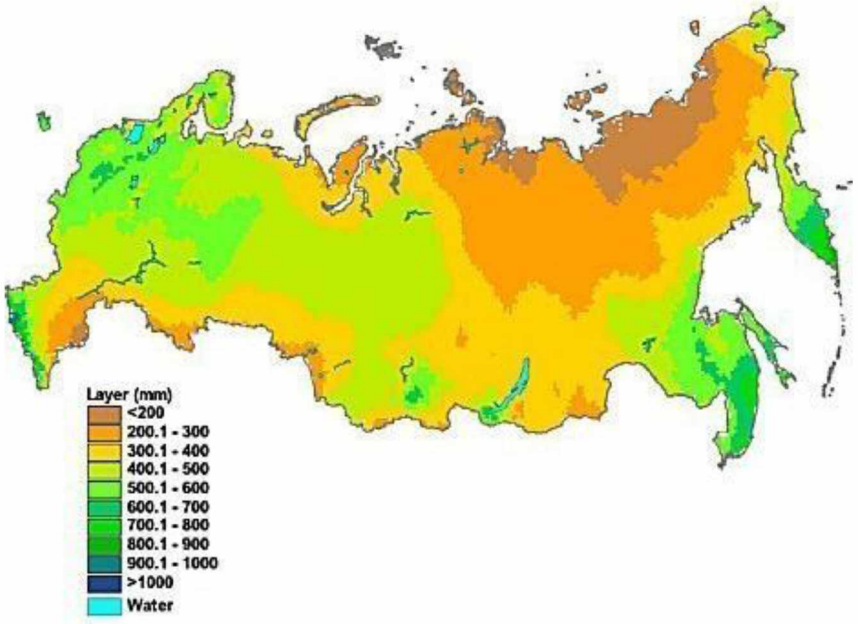

Figure 2.1.5. Mean Annual Temperature and Precipitation Maps for Siberia. Data and maps are from Kotlyakov and Koronkevitch, 2002. Data was acquired between 1961 and 1990.

Temperature of Permafrost

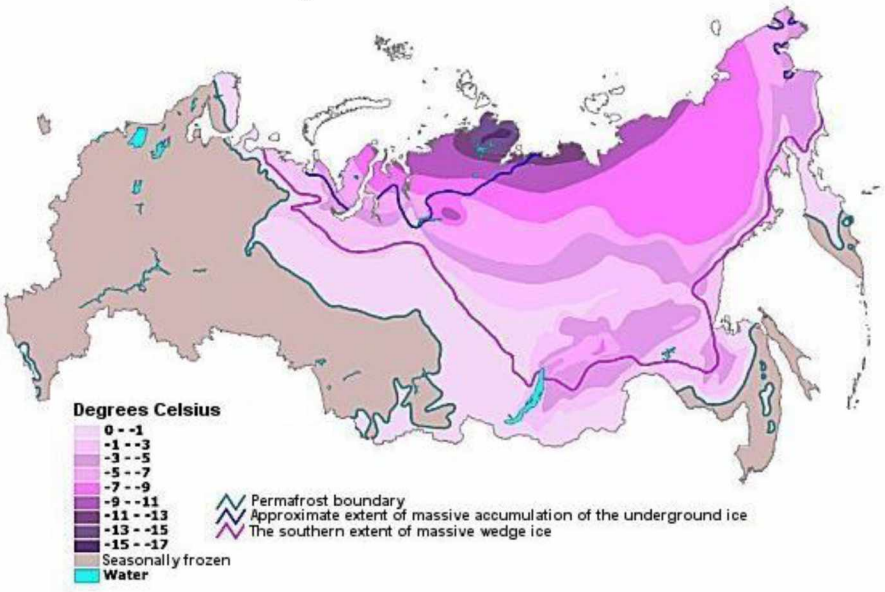

Extent of Permafrost

Figure 2.1.6. Permafrost Temperature and Extent Maps for Siberia. Data and maps are from Kotlyakov and Koronkevitch, 2002. Data was acquired between 1961 and 1990.

Chapter 3: Methods

In order to characterize spatial, temporal, and morphometric changes occurring to thermokarst lakes in the Kolyma Lowlands, I employed satellite remote sensing and GIS analysis. The image types used were medium-resolution Landsat Multispectral Scanner (MSS; 79 m resolution), Thematic Mapper (TM; 30 m resolution), and Enhanced Thematic Mapper Plus (ETM+; 30 m resolution) along with high-resolution Advanced Land Observing Satellite (ALOS) PRISM (2.5 m resolution), Hexagon (6-9 m resolution), and Corona (2.5 m resolution) images (Figure 3.1.1).

3.1 Medium-Resolution Landsat Images

The Landsat program started in 1967 and was a combined effort between NASA and the United States Department of Interior to develop a series of earth observing satellites. The satellites were called Earth Resource Technology Satellites (ERTSs) until 1975 when NASA officially renamed the ERTSs program the Landsat program and they became known as Landsat satellites (Lillesand et al., 2004). Today, the Landsat program is a joint program between NASA and the United States Geological Survey (USGS) with the primary receiving station for the data being located in Sioux Falls, South Dakota at the Earth Resource Observation System (EROS) Data Center. To date, there have been seven Landsat satellites, launched between 1972 and 1999, and five types of sensors have been used, Return Beam Vidicon (RBV), Multispectral Scanner (MSS), Thematic Mapper (TM), Enhanced Thematic Mapper (ETM; Launched on Landsat 6 and failed) and Enhanced Thematic Mapper Plus (ETM+) (Lillesand et al., 2004). Global coverage of Landsat data is available with the exception of the polar latitudes greater than 82^{o} (Avery and Berlin, 1992).

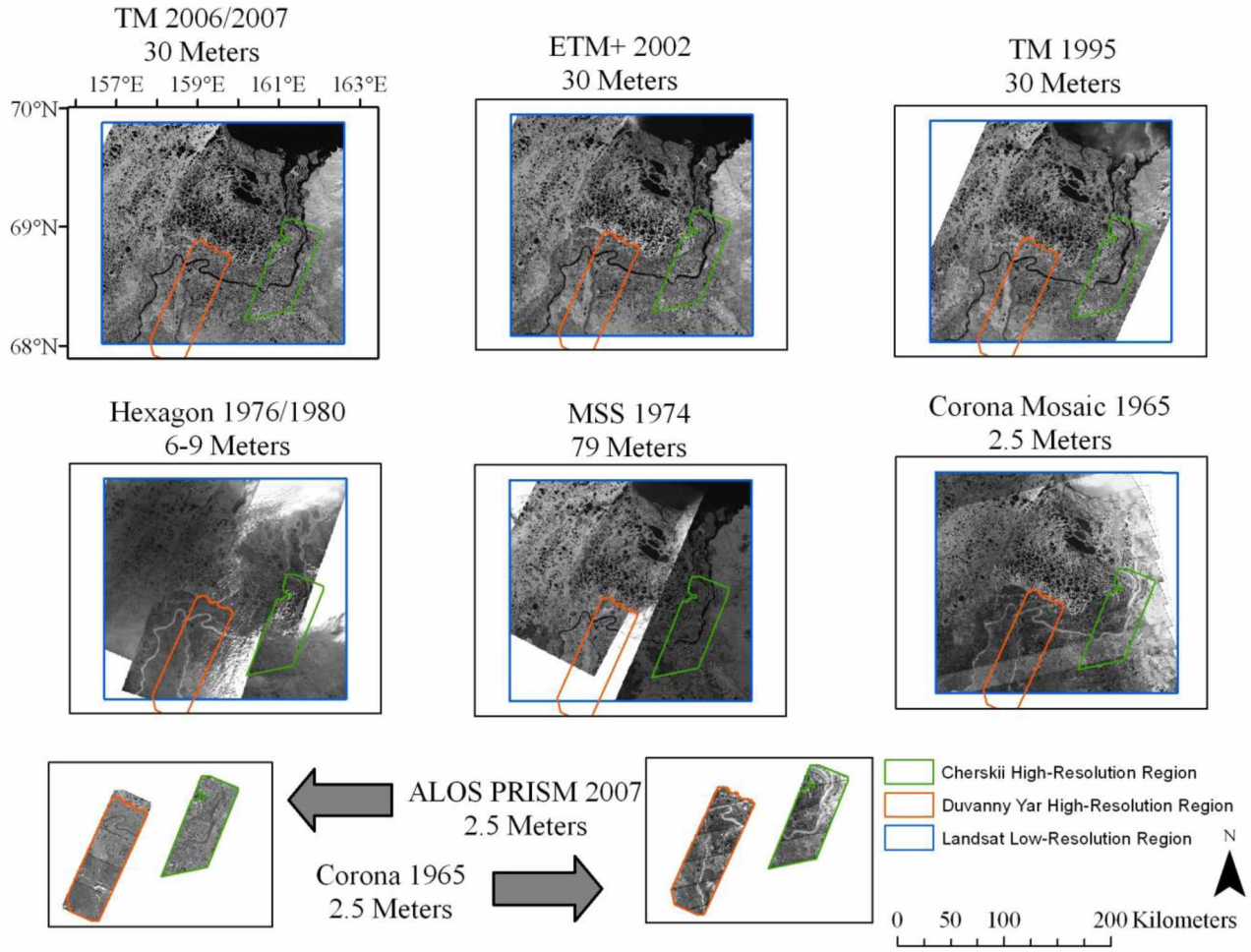

Figure 3.1.1. Subsets of all Image Mosaics Used. Image type, date, and ground resolution are listed for each image.

Some limitations of the Landsat data include cloud cover and noise from sensor variations during recording or transmission. The USGS established the Global Orthorectified Landsat Dataset containing high quality, relatively cloud-free images, which is available to the public (Tucker et al., 2004). This data set contains MSS images from the 1970's, TM images from the 1990's, and ETM+ images from the 2000's. The images are from Landsat's 1-5 and 7 (Tucker et al., 2004).

Landsat images used in this study included terrain-corrected (L1T) (Williams, 2009) MSS, TM, and ETM+ (Table 3.1.1) from Landsat's 1, 5, and 7 respectively (Table 3.1.2).

Table 3.1.1. List of the Landsat Images Used in This Study.

Image Type	Date	Path/Row
Landsat TM	7/10/2007	104/011
Landsat TM	7/10/2007	104-012
Landsat TM	7/12/2006	107/011
Landsat TM	7/12/2006	107/012
Landsat TM	9/9/1995	106/011
Landsat TM	9/9/1995	106/012
Landsat ETM+	8/5/2002	104/011
Landsat ETM+	8/5/2002	104/012
Landsat ETM+	8/10/2002	107/011
Landsat ETM+	8/10/2002	107/012
Landsat MSS	7/11/1974	113/011
Landsat MSS	7/11/1974	113/012
Landsat MSS	8/1/1974	116/010
Landsat MSS	8/1/1974	116/011
Landsat MSS	8/2/1974	117/011

Table 3.1.2. Orbital Characteristics for Landsat Satellites (Avery and Berlin, 1992; Lillesand et al., 2004).

Satellite/ Sensor	Launch Date	Decommissioned Date	Ground Resolution (m)	Orbit Altitude (km)	Repeat Coverage Interval (days)
Landsat 1/MSS	July 23, 1972	January 6, 1978	79	900	18
Landsat 5/TM	March 1, 1984	Still Operational	30*	705	16
Landsat 7/ETM+	April 15, 1999	Still Operational	30**	705	16

* Band six, the thermal band, has a ground resolution of 120 m
** Band six, the thermal band, has a ground resolution of 60 m and band eight, the panchromatic band, has a ground resolution of 15 m (Lillesand et al., 2004)

The Landsat 1 MSS images selected for this study were acquired in July and August 1974. The orbit was sun-synchronous, meaning it kept pace with the sun's westward progression as the earth rotated. A sun-synchronous orbit insures repeated illumination conditions for every orbit, however, it does not account for changes in solar angle azimuth, or intensity as they change with location and season.

The MSS system onboard Landsat 1 was a four-band system, designated as bands one through four (Table 3.1.3). It is an across-track (whiskbroom) sensor that scans from west to east with the southward progression of the satellite. Each image takes 25 seconds to complete (Avery and Berlin, 1992), resulting in an image that is a parallelogram, not a square, because of the earth's rotation. An onboard AC to DC converter converts the analog signal recorded by each detector into a six-bit

Table 3.1.3. List of MSS Bands Onboard Landsat 1 (Avery and Berlin, 1992; Lillesand et al., 2004).

Band Number	Wavelength (μm)	Region
1	0.5-0.6	Green
2	0.6-0.7	Red
3	0.7-0.8	Near IR
4	0.8-1.1	Near IR

digital signal (Avery and Berlin, 1992; Lillesand et al., 2004).

The four bands of the MSS sensor are targeted for different land-use applications. Bands allow different wavelength regions to be recorded separately. Because different surface features react differently at different wavelengths, certain bands are better suited for different studies. Band 1 is most useful for studying water features; it is able to penetrate water and is responsive to sediment and pollution patterns. It is very sensitive to haze though. Band 2 consists of wavelengths best absorbed by chlorophyll and therefore exhibits good contrast between vegetated and non-vegetated surfaces. Bands 3 and 4 are responsive to the amount and type of vegetation present. They are useful for differentiating different crop types and timber types, along with separating bare soil from vegetated soil, planted and natural vegetation. Both bands are in the near infrared (IR) range. Water is a good absorber of IR radiation, hence water appears nearly black in this band and is easily distinguished. This also helps distinguish moist land from dry land (Avery and Berlin, 1992; Lillesand et al., 2004). Band 4 was chosen in this study as the tonal contrast between water and land is slightly greater than in band 3 (Avery and Berlin, 1992).

The Landsat TM images used were from September 1995 and from July 2006 and 2007. These were from Landsat 5, which was also sent into a circular, near-polar, sun-synchronous orbit. Landsat 5 carried both MSS and TM sensors. The TM sensor is an across-track scanner with a seven-channel system, designated as bands one through seven (Table 3.1.4). The TM employs an oscillating scan mirror, which scans in both the west-to-east and east-to-west directions. This allows for a slower rate of oscillation and thus increased time for the sensors to record spectral

Table 3.1.4. List of TM Bands Onboard Landsat 5 (Avery and Berlin, 1992; Lillesand et al., 2004).

Band Number	Wavelength (μm)	Regions
1	0.45-0.52	Blue
2	0.52-0.60	Green
3	0.63-0.69	Red
4	0.76-0.90	Near IR
5	1.55-1.75	Mid IR
6	10.4-12.5	Thermal IR
7	2.08-2.35	Mid IR

signatures from the earth. Longer recording times make for less noise to be recorded in the images. The onboard AC to DC converter uses an 8-bit system (Avery and Berlin, 1992; Lillesand et al., 2004).

The August 2002 ETM+ images used in this research came from Landsat 7. The ETM+ was the only sensor onboard (Lillesand et al., 2004). A major improvement of the ETM+ sensor over the TM sensor was the addition of a panchromatic band (0.50-0.90 um) with a spatial resolution of 15 m (Lillesand et al., 2004). The first seven bands are identical to Landsat 5's TM sensor with the exception being that the thermal band (band 6) now has a spatial resolution of 60 m and not 120 m.

The TM and ETM+ bands are also responsive to certain surface features depending upon their characteristics. Band 1 is a water penetration band best used for water bathymetric and coastal studies. It is also good at differentiating soil, vegetation, and rock. It is extremely sensitive to atmospheric haze however and thus may lack tonal contrast. Band 2 is similar to MSS band 1. It is good for monitoring water turbidity and because it contains the reflectance peak for leaf surfaces (0.6 um), it can be used to distinguish broad classes of vegetation (Lillesand et al., 2004). Band 3 is similar to MSS band 2. Again, it is a strong absorption band for chlorophyll and a strong reflectance band for bare soils. It is good for plant species studies. Band 4 is similar to MSS band 3. This band is best for distinguishing vegetation health based on moisture content, and water bodies from dry and moist soils. Band 4 is the best spectral region to distinguish vegetation varieties and conditions. It is useful for studies of coastal wetlands, swamps, and flooded regions. Band 5 is most responsive to changes in leaf-tissue water content (Avery and Berlin, 1992). Lower reflectance means lower moisture content. This band can also delineate moisture content of soils. Snow verses clouds can be distinguished using this band and thus it is good for use in studies determining snow pack. Band 6 is a thermal IR band and is useful for surface temperature monitoring studies for temperatures between -100 ^{o}C and +150 ^{o}C; differences area discernable up to 0.6 ^{o}C (Avery and Berlin, 1992). Examples of studies include those looking at different rock types and thermal water pollution. Band 7 is a good absorption band for hydrous minerals like

clays and micas, and different mineral and rock types. This makes it useful for lithological mapping and detecting clay alteration zones associated with mineral deposits such as copper (Avery and Berlin, 1992). Band 8, located on the ETM+ sensor, is a panchromatic band allowing for a higher resolution.

The differentiation between land and water surfaces in our study region was best in band 5 and thus band 5 was used in this study. Band 5 also exhibits the least variation in the spectral signatures of the water pixels (Frazier and Page, 2000). The band 4 infrared range is more designed to monitor changes in vegetation moisture, vigor, and biomass content (Lillesand et al., 2004). Band 5 also has more depth penetration than band 4. Band 5 therefore allows more absorption of infrared radiation making water pixels appear slightly darker in color than they would in band 4. The spectral signature recorded in band 4, for water pixels, would reflect more of the surface properties. This would create a lighter, more land-like spectral signature for water bodies with a vegetated surface or ones that are sediment-laden.

3.2 High-Resolution Images

Higher resolution image types used in this study included Corona, Hexagon, and ALOS PRISM images (Table 3.2.1). Corona images (also know as Key Hole (KH) -1 through KH-4B) are declassified images from United States intelligence missions, which operated between August 1960 and May 1972 (Grosse et al., 2005; Dashora et al., 2006). The images were taken by a rotating panoramic camera system that used photographic panchromatic film. The earliest missions had a single camera while the later had two, a forward and rear looking camera, allowing acquisition of stereo images. The images used in this study were from the KH-4A mission, which operated from August 1963 to October 1969 (Bayram et al., 2004). The flight altitude was between 150 and 203 km (McDonald, 1995), and the resolution of these images is roughly two meters (Bayram et al., 2004). The exposed film was released and captured mid-air by an aircraft. Corona images became declassified in 1995 by an executive order signed by United States President William Clinton (Dashora et al.,

Table 3.2.1. High-Resolution Images Selected for This Study.

Image Type	Date	Image File
Hexagon	8/19/1976	DZB1212 500213L003001
Hexagon	7/31/1980	DZB1216 500227L002001
Hexagon	9/4/1980	DZB1216 500316L001001
ALOS Prism	7/29/2007	12836 2195-01B2G
ALOS Prism	7/29/2007	12836 2200-01B2G
ALOS Prism	7/29/2007	12836 2205-01B2G
ALOS Prism	7/29/2007	12836 2210-01B2G
ALOS Prism	7/29/2007	DO 662195 01B2
ALOS Prism	7/29/2007	DO 662200 01B2
ALOS Prism	7/29/2007	DO 662205 01B2
ALOS Prism	7/29/2007	DO 662210 01B2
Corona	7/21/1965	DS1022-1019 DF 009
Corona	7/21/1965	DS1022-1019 DF 010
Corona	7/21/1965	DS1022-1019 DF 011
Corona	7/21/1965	DS1022-1019 DF 012
Corona	7/21/1965	DS1022-1019 DF 013
Corona	7/21/1965	DS1022-1019 DF 014
Corona	7/21/1965	DS1022-1019 DF 015
Corona	7/21/1965	DS1022-1019 DF 016
Corona	7/21/1965	DS1022-1019 DF 017
Corona	7/21/1965	DS1022-1019 DF 018
Corona	7/21/1965	DS1022-1019 DF 019
Corona	7/21/1965	DS1022-1019 DF 020
Corona	7/21/1965	DS1022-1019 DF 021

2006). Corona image are available for the Soviet Union, China, the Middle East, and Southeast Asia (Bayram et al., 2004).

Aerial images for much of Russia remain classified and are unavailable to foreign researchers for remote sensing-based research. Therefore, Corona images are the best available option for historic high-resolution remote sensing data. In addition, they cover a very large footprint of approximately 20 x 266 km per image (Tappan et al., 2000). Corona images are readily available for much of Russia and are useful for many different applications, including studies in periglacial geomorphology and archaeology (Grosse et al., 2005; Casana and Cothren, 2008). Corona images have also been used for detailed mapping and the generation of DEMs from stereo pairs (Casana and Cothren, 2008; Galiatsatos et al., 2008).

The Hexagon images (also known as KH-9A and KH-9B images) used in this study were from August 1976 and July and September of 1980. Hexagon images were taken during United States military space reconnaissance missions. The first Hexagon satellites were launched in the 1970's and the last in the early 1980's (Surazakov et al., 2008). Hexagon images are panchromatic; taken by photographic mapping cameras (Hese et al., 2010). The United States government declassified Hexagon images in September 2002. The spatial resolution ranges between six and nine meters (Surazakov et al., 2008; Schneider et al., 2009).

Like the Corona images for the 1960's, Hexagon images are the best available image data for Siberia in the 1970's and early 1980's. Hexagon images have been used for studies in Central Asia studying glacier inventory in the Tien Shan Mountains (Surazakov et al., 2008). Surazakov et al. (2008) created DEMs from Hexagon images with horizontal accuracies of under six meters for flat terrain and ten meters for mountainous terrain. Glacier studies in the Russian Arctic were also completed using Hexagon images by Grant et al. (2009).

The third type of high-resolution imagery used in this study was ALOS PRISM images. The platform for the Panchromatic Remote-Sensing Instrument for Stereo Mapping (PRISM) sensor was the Japanese Advanced Land Observing Satellite (ALOS).

It was launched on January 24, 2006 from the Tanegashima Space Center in Japan. The satellite is in a sun-synchronous orbit with an altitude of 691.65 km. The repeat coverage time is 46 days (ALOS Data User Handbook, 2007). The ALOS satellite has two additional sensors onboard that were not used in this study, the Advanced Visible and Near Infrared Radiometer type-2 (AVNIR-2) and the Phased Array type L-band Synthetic Aperture Radar (PALSAR) (ALOS Data User Handbook, 2007).

The PRISM sensor is an along track (push broom) scanner and has a single panchromatic band (0.52-0.77um) (ALOS Data User Handbook, 2007). It has forward, nadir, and rear looking sensors with swath widths of 70 km individually or 35 km when all three are imaging together. The digital images are 8 bit and have a spatial resolution of 2.5 m (ALOS Data User Handbook, 2007). The PRISM images used in this study are from July 2007. Other examples of PRISM imagery usage include monitoring widespread snow cover, extraction of roads within Brazil, and creating a wetland and aquatic surface inventory in Sologne, north-central France and the Al'Tamin province in northern Iraq (ALOS Data User Handbook, 2007; Gonga-Saholiariliva et al., 2008; Castro and Centeno, 2010).

3.3 Non-Image Data Sources

Other data sources used to characterize the Kolyma Lowland landscape included: 1) a geological map with a 1: 1,000,000 scale (Russian Geological Research Institute VSEGEI, 2000); 2) a 90 m digital elevation model (DEM) derived from 1: 200,000 topographic maps (Ferranti, 2009) (Figure 3.3.1.); and 3) the 1:10,000,000 scale International Permafrost Association (IPA) Circum-Arctic Permafrost Map (Brown et al., 1997) (Figure 3.3.2.). All three datasets are the best available data covering the entire region. The DEM is an important component as elevation plays an important role in the hydrological network and thus the development of thermokarst lakes.

Air temperature data was available from three Russian national weather stations around the Kolyma Lowlands: Cherskii, Kolymskaya, and Buhta Ambarcik (Figure 3.3.3). This data were used to see if any trends in air temperature could be related to the changes occurring to thermokarst lakes.

Evaporation data for the Kolyma Lowland region is unavailable and the precipitation data recorded at the weather stations was incomplete and patchy covering the period from 1965 to 2007. Therefore, calculations relating trends in evaporation and precipitation to changes that are occurring to thermokarst lakes were not made.

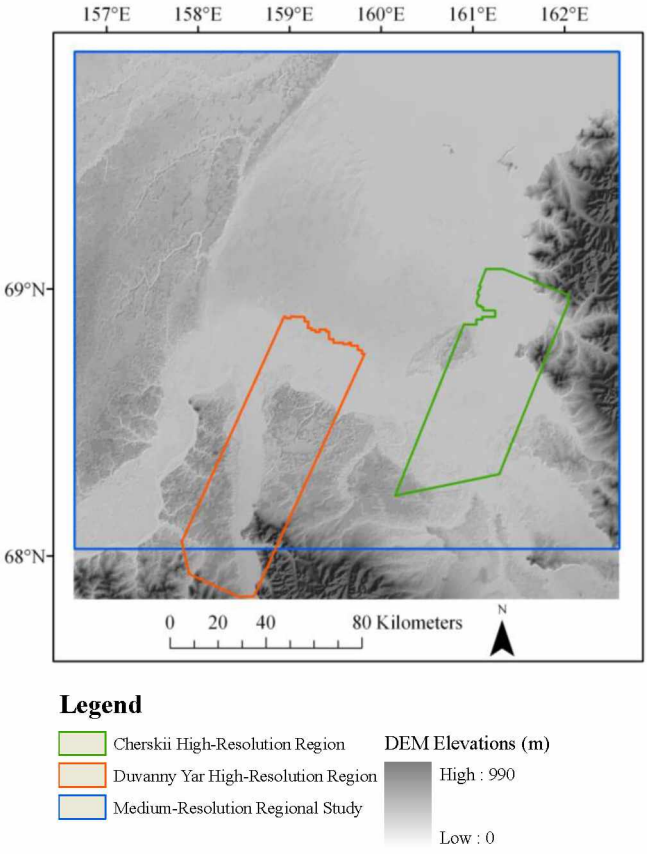

Figure 3.3.1. Hillshade overlaid by a DEM of Study Region. DEM based on 1:200,000 topographic maps (Ferranti, 2009).

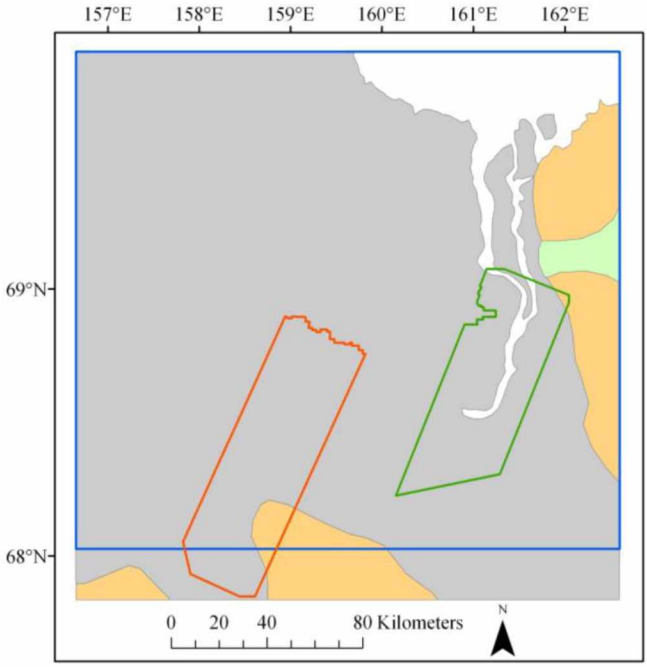

Legend

- Cherskii High-Resolution Region
- Duvanny Yar High-Resolution Region
- Medium-Resolution Regional Study
- Continuous, Ice-rich permafrost (>20%), lowlands
- Continuous, Ice-rich permafrost (>10%), Mountains, highland ridges and plateaus with exposed bedrock
- Continuous, Ice-poor permafrost (0-10%), Mountains, highlands ridges and plateaus with exposed bedrock

Figure 3.3.2. IPA Permafrost Map of the Study Region. Derived from Brown et al., 1997.

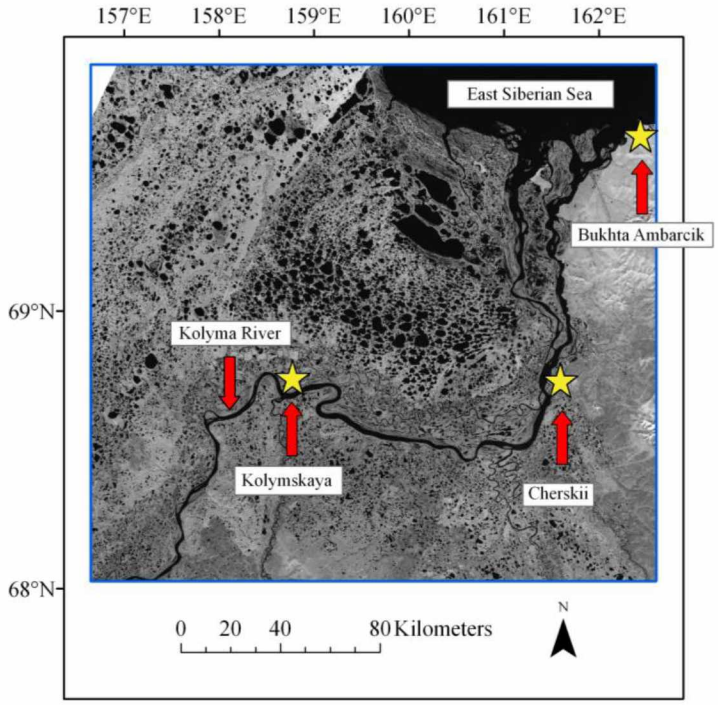

Figure 3.3.3. National Weather Stations within the Kolyma Lowlands. Locations of National Weather Stations in the Kolyma Lowlands.

3.4 GIS Analysis

Image processing, including geo-referencing and creating image mosaics, was completed in ESRI ArcGIS 9.3. Polygonal shapefiles of thermokarst lakes and the different geological units present in the region were also created in ArcGIS. The identification of relationships between thermokarst lakes and the underlying geology, elevation, geomorphology, and permafrost conditions was done using ArcGIS.

3.4.1 Geo-Referencing and Image Mosaics

All Landsat images used in this study were processed with the Standard Terrain Correction (Level 1T). This level of correction provides radiometric and geometric accuracy by using ground control points.

The geographic coordinate system assigned to the Landsat TM and ETM+ data sets accurately projected the images upon receiving them from the USGS EROS Data Center in Sioux Falls. However, the Landsat MSS images were poorly geo-referenced possibly due to erroneous ground control points (GCP) in the processing chain. To correct this displacement, the MSS images were co-registered to the terrain-corrected TM images from 2006/2007 (Table 3.4.1.1). For each MSS scene, 18 to 23 GCPs were identified in both the base TM image and the MSS image. For GCPs, mostly small lakes and ponds that appeared to be stable in both images were used. Image transformation was done using a third order polynomial warping method and a bilinear pixel resampling (weighted average of the four nearest pixels on the original image). With the resolution of the MSS images of 79 m being the limiting resolution, the average root mean square (RMS) error was 18.4 m with the highest being 19.6 m.

The Hexagon images were geo-referenced to the Landsat TM images from 2006/2007 as well. A third order polynomial warping method and a bilinear resampling interpolation was again employed. The number of ground control points ranged between 20 and 46. The limiting spatial resolution came from the TM images at 30 m, giving an average RMS value of 11.1 m, the highest being 12.9 m.

After complete geo-referencing, image mosaics were created for several time slices represented by all the Landsat images (MSS, TM, ETM+) along with the Hexagon

images (Figure 3.1.1). These were completed using the mosaic-to-new-raster application in ArcGIS.

The third image type that needed geo-referencing was the Corona images. These were geo-referenced to the ALOS PRISM images, which had a predefined geographic coordinate system. A third order polynomial warping method and a bilinear resampling interpolation was applied. The number of ground control points ranged from 22 to 48, with the average being 29 (Table 3.4.1.1). As both image types have a spatial resolution of roughly 2.5 m, the average RMS error was 4.0 m, the highest being 4.5 m.

Table 3.4.1.1. Image Geo-Referencing Specifications.

Georeferenced Image Identification	Image Type	Image Ground Resolution (m)	Number of GCP	Base Image Used for Georeferencing	Target Projection	Target Datum	RMS Error (m)	Output Pixel Size
MSS_07-11-1974_Subset_LM1113011007419210_B7.tif	Landsat MSS	79	23	TM_07-10-2007_Subset_L5104011_01120070710_B50.TIF and TM_07-10-2007_Subset_L5104012_01220070710_B50.TIF and TM_07-12-2006_Subset_L5107011_01120060712_B50.TIF and TM_07-12-2006_Subset_L5107012_01220060712_B50.TIF	UTM 58N	WGS-1984	18	60 meters
MSS_07-11-1974_Subset_LM1113012007419210_B7.tif	Landsat MSS	79	20	TM_07-10-2007_Subset_L5104011_01120070710_B50.TIF and TM_07-10-2007_Subset_L5104012_01220070710_B50.TIF and TM_07-12-2006_Subset_L5107011_01120060712_B50.TIF and TM_07-12-2006_Subset_L5107012_01220060712_B50.TIF	UTM 57N	WGS-1984	17.7	60 meters
MSS_08-01-1974_Subset_LM1116010007421310_B7.tif	Landsat MSS	79	18	TM_07-10-2007_Subset_L5104011_01120070710_B50.TIF and TM_07-10-2007_Subset_L5104012_01220070710_B50.TIF and TM_07-12-2006_Subset_L5107011_01120060712_B50.TIF and TM_07-12-2006_Subset_L5107012_01220060712_B50.TIF	UTM 57N	WGS-1984	18.6	60 meters
MSS_08-01-1974_Subset_LM1116011007421310_B7.tif	Landsat MSS	79	20	TM_07-10-2007_Subset_L5104011_01120070710_B50.TIF and TM_07-10-2007_Subset_L5104012_01220070710_B50.TIF and TM_07-12-2006_Subset_L5107011_01120060712_B50.TIF and TM_07-12-2006_Subset_L5107012_01220060712_B50.TIF	UTM 57N	WGS-1984	18.1	60 meters
MSS_08-02-1974_Subset_LM1117011007421410_B7.tif	Landsat MSS	79	22	TM_07-10-2007_Subset_L5104011_01120070710_B50.TIF and TM_07-10-2007_Subset_L5104012_01220070710_B50.TIF and TM_07-12-2006_Subset_L5107011_01120060712_B50.TIF and TM_07-12-2006_Subset_L5107012_01220060712_B50.TIF	UTM 57N	WGS-1984	19.6	60 meters
DZB1216-500316L001001_1_a.tif	Hexagon	2.5	28	TM_07-10-2007_Subset_L5104011_01120070710_B50.TIF and TM_07-10-2007_Subset_L5104012_01220070710_B50.TIF and TM_07-12-2006_Subset_L5107011_01120060712_B50.TIF and TM_07-12-2006_Subset_L5107012_01220060712_B50.TIF	UTM 57N	WGS-1984	9.3	5 meters
DZB1216-500316L001001_1_b.tif	Hexagon	2.5	20	TM_07-10-2007_Subset_L5104011_01120070710_B50.TIF and TM_07-10-2007_Subset_L5104012_01220070710_B50.TIF and TM_07-12-2006_Subset_L5107011_01120060712_B50.TIF and TM_07-12-2006_Subset_L5107012_01220060712_B50.TIF	UTM 57N	WGS-1984	6.9	5 meters
DZB1216-500227L002001_2_a.tif	Hexagon	2.5	22	TM_07-10-2007_Subset_L5104011_01120070710_B50.TIF and TM_07-10-2007_Subset_L5104012_01220070710_B50.TIF and TM_07-12-2006_Subset_L5107011_01120060712_B50.TIF and TM_07-12-2006_Subset_L5107012_01220060712_B50.TIF	UTM 57N	WGS-1984	12.3	5 meters
DZB1216-500227L002001_2_b.tif	Hexagon	2.5	46	TM_07-10-2007_Subset_L5104011_01120070710_B50.TIF and TM_07-10-2007_Subset_L5104012_01220070710_B50.TIF and TM_07-12-2006_Subset_L5107011_01120060712_B50.TIF and TM_07-12-2006_Subset_L5107012_01220060712_B50.TIF	UTM 57N	WGS-1984	15	5 meters
DZB1212-500213L003001_3_a.tif	Hexagon	2.5	25	TM_07-10-2007_Subset_L5104011_01120070710_B50.TIF and TM_07-10-2007_Subset_L5104012_01220070710_B50.TIF and TM_07-12-2006_Subset_L5107011_01120060712_B50.TIF and TM_07-12-2006_Subset_L5107012_01220060712_B50.TIF	UTM 57N	WGS-1984	12.9	5 meters
DZB1212-500213L003001_3_b.tif	Hexagon	2.5	30	TM_07-10-2007_Subset_L5104011_01120070710_B50.TIF and TM_07-10-2007_Subset_L5104012_01220070710_B50.TIF and TM_07-12-2006_Subset_L5107011_01120060712_B50.TIF and TM_07-12-2006_Subset_L5107012_01220060712_B50.TIF	UTM 57N	WGS-1984	9.9	5 meters
DS1022-1019DF015_15_b.tif	Corona	2.5	25	ALOS_PSM_N_D0662190_0_1B2 29Jul07.tif and ALOS_PSM_N_D0662195_0_1B2_29Jul07.tif	UTM 57N	WGS-84	3.38	2.5 m
DS1022-1019DF016_16_b.tif	Corona	2.5	23	ALOS_PSM_N_D0662195_0_1B2 29Jul07.tif and ALOS_PSM_N_D0662200_0_1B2_29Jul07.tif	UTM 57N	WGS-84	4.37	2.5 m
DS1022-1019DF017_17_b.tif	Corona	2.5	35	ALOS_PSM_N_D0662200_0_1B2 29Jul07.tif and ALOS_PSM_N_D0662205_0_1B2_29Jul07.tif	UTM 57N	WGS-84	4.19	2.5 m
DS1022-1019DF018_18_b.tif	Corona	2.5	30	ALOS_PSM_N_D0662205_0_1B2 29Jul07.tif and ALOS_PSM_N_D0662210_0_1B2_29Jul07.tif	UTM 57N	WGS-84	4.51	2.5 m
DS1022-1019DF019_19_b.tif	Corona	2.5	22	ALOS_PSM_N_D0662210_0_1B2 29Jul07.tif	UTM 57N	WGS-84	4.41	2.5 m
DS1022-1019DF020_20_b.tif	Corona	2.5	25	ALOS_PSM_N_D0662210_0_1B2 29Jul07.tif	UTM 57N	WGS-84	4.09	2.5 m

3.4.2 Digitizing of the Lakes

Thermokarst lake boundaries were digitized both manually and by automated methods creating polygonal shapefiles. Automated mapping was done using Feature Analyst 4.2 for ArcGIS. Feature Analyst is an automated feature extraction program, which uses a manually created, well-balanced, representative training set. A training set was created using a range of spectral signatures coming from the thermokarst lakes, as well as other attributes including size, shape, and spatial association. Feature Analyst uses all these elements when conducting feature extraction. Extraction settings used were as follows: learning was set up as a water-mass feature, the Manhattan input representation was used, and the learning algorithm was set to approach 1. Water-mass feature was chosen because lakes have very distinctive morphometric shapes and spatial characteristics when compared to trees, rivers, and man-made features like buildings. Lakes are often rounded or elliptical, vary in size from very small to hundreds of hectares, and are scattered throughout the landscape. The Manhattan input representation was the best pattern to use, as lakes are relatively symmetrical in a circular or elliptical shape and are a relatively large land cover feature. Approach 1 was used because it was a basic feature extraction that was being performed. Approach 2 is best for removing clutter and extracting small objects. Feature Analyst did not include high amounts of clutter in the extraction of thermokarst lakes. Approach 3 is less accurate and is designed for simple extractions. The resulting shapefile produced by Feature Analyst was corrected manually.

Manual digitizing of lake boundaries, whether it was to create training sets, to correct lake boundaries produced by Feature Analysts, or to create new shapefiles, was completed at a scale of 1:5,000 for the Corona and ALOS PRISM images and for the Landsat and Hexagon images, digitizing was done at a scale of 1:20,000.

3.4.3 Remaining Data Processing

The geological map for the study region (Russian Geological Research Institute VSEGEI, 2000) was manually digitized at a scale of 1:50,000 (Figure 3.4.3.1). Seven geological units containing a different set or combination of litho-genetic sediment types were present in the study region (Table 3.4.3.1). Separate shapefiles were created for each geological unit. The DEM (Ferranti, 2009) and the Circum-Arctic Permafrost Map (Brown et al., 1997) were uploaded into ArcGIS already in digital format. Contour lines were created from the DEM using the raster-to-surface-contour feature in Arc Toolbox. The contour interval was set to 20 m.

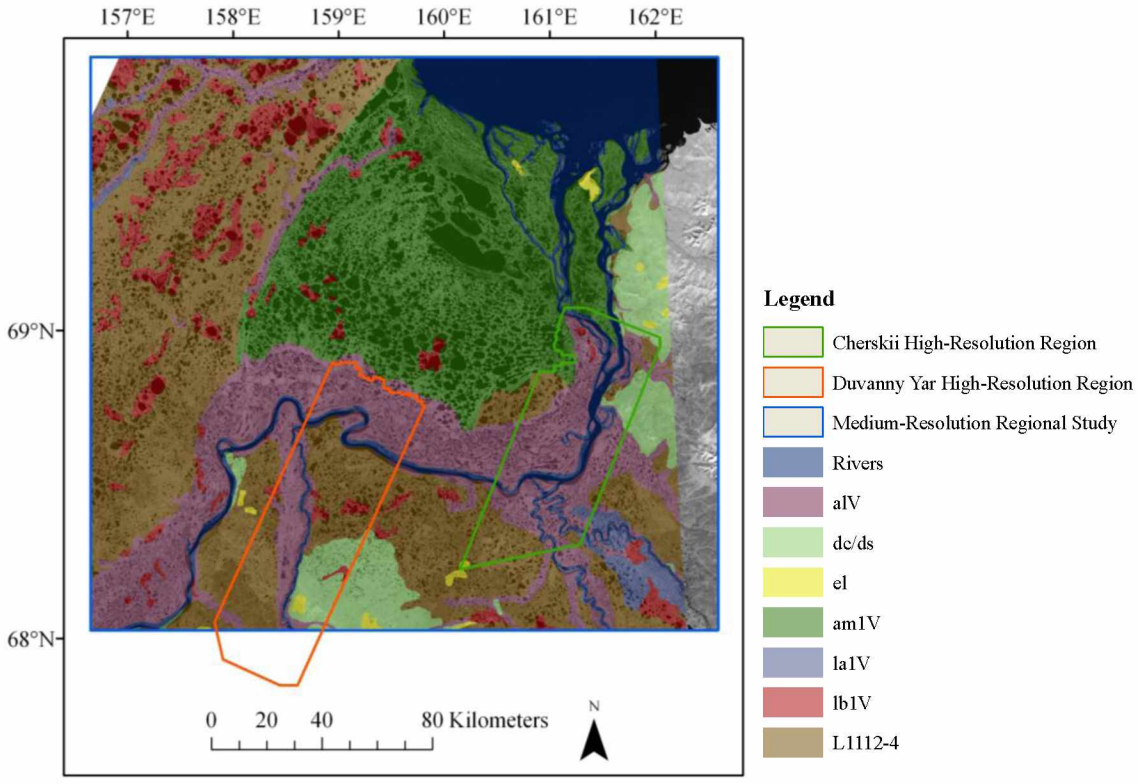

Figure 3.4.3.1. Digitized Geological Map. Geological map digitized at a scale of 1:50,000 and based on a 1:1,000,000 scale geological map (Russian Geological Research Institute VSEGEI, 2000).

Table 3.4.3.1. Litho-Genetic Sediment Types Found within the Study Region.

Geological Unit	Deposit Types	Approximate Time Period
alv	Alluvial	Middle Pleistocene though the Holocene
am1V	Alluvial Marine	Upper Pleistocene through the Holocene
dc/ds	Deluvial-Solifluction Deluvial-Colluvial	Pleistocene/Holocene
el	Eluvial	Holocene
la1V	Alluvial Lacustrine	Middle Pleistocene though the Lower Holocene
lb1V	Bog Lacustrine	Lower and Upper Holocene
$L111_{2-4}$	Alluvial Lacustrine Loess-Like (Yedoma)	Upper Pleistocene

3.5 Regions of Lake Analysis

3.5.1 High-Resolution Study Regions

The Corona (1965) and ALOS PRISM (2007) images were used to create two separate high-resolution study regions: region 1, designated as Duvanny Yar and region 2, designated as Cherskii (Figure 3.5.1.1).

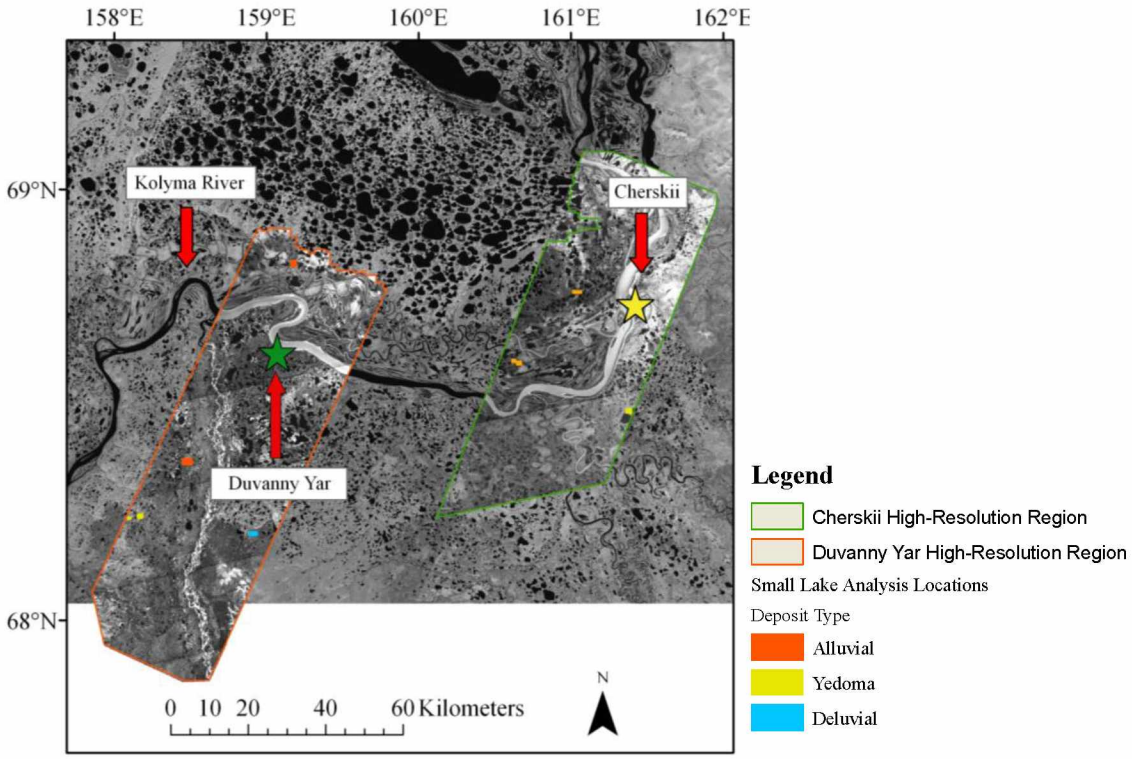

Figure 3.5.1.1. High-Resolution and Small-Lake Study Locations. High-resolution Duvanny Yar and Cherskii regions with the small-lake study locations shown. The small-lake analysis locations, indicated by the small rectangles within the larger Cherskii and Duvanny Yar study regions, are color-coded by the deposit type they are located in.

The Cherskii and Duvanny Yar regions were selected based on available cloud-free, high-resolution satellite imagery covering a large, multi-decadal time period. The Duvanny Yar region is approximately 4,192 km^2 with a center coordinate of roughly $68^{o}24'N/158^{o}5'E$. The geological projection and datum for this region was UTM 57N and WGS-84 respectively. The Cherskii region is slightly smaller, approximately 3,362 km^2, and has a center coordinate of about $68^{o}4'N/161^{o}1'E$. The geological projection for this region was also UTM 57N and the datum was WGS-84. Lake polygon shapefiles for both locations and image types were created using Feature Analyst and then manually corrected. Lake shapefiles were clipped to each geological unit. All lake files were imported into a geodatabase, where surface area for each lake was calculated. Net change in lake number, percent area change, and relationships between thermokarst lakes and the underlying geology were identified using Microsoft (MS) Excel. Generalized conclusions relating thermokarst lakes to the elevation and permafrost conditions were done in ArcGIS.

The Corona and ALOS PRISM lake files were then visually scanned for lakes that showed lake area loss; these lakes were placed into a separate shapefile. These lakes showing lake area loss in 2007 were spatially joined to the 1965 lakes and the two files were imported into a geodatabase and MS Excel. Percent lake area loss was calculated for each lake and those showing lake area loss greater than 20% (from here on referred to as L_{20}) were analyzed with respect to geological unit, elevation, and permafrost conditions.

Results from the Duvanny Yar and the Cherskii regions were then compared to each other in an attempt to understand if thermokarst lake behavior was the same under similar conditions: permafrost, elevation, and underlying geology.

Minimum size of an individual lake mapped for these high-resolution studies was 0.5 ha, approximately 800 pixels. The threshold was a result of the panchromatic imagery. Panchromatic images produce a varied spectral signature for water bodies, especially smaller, vegetated, and shallower, sediment heavy lakes. As automated

systems could not accurately extract these features and manual digitizing would have been to time consuming, the smallest lakes were not included and analyzed.

Within the Cherskii and Duvanny Yar study regions, select areas were chosen to determine if new thermokarst lakes were forming (Figure 3.5.1.1). These locations were chosen in alluvial, deluvial, and Yedoma sediments. For these smaller locations, there was no minimum lake size; every visible water body was manually digitized. There were five locations in the Duvanny Yar region and three in the Cherskii region; study sites ranged between 40 and 375 ha. As before, these lake files were loaded into a geodatabase to calculate area and then into MS Excel to complete lake area analysis.

3.5.2 Medium-Resolution Regional Study

The Corona, Hexagon, and Landsat image mosaics were used to create a series of time steps from 1965 to 2007. The entire area covered by the oldest images (Corona) and the most recent images (TM 2006/2007) is 43,543 km^2 (Figure 3.5.2.1). The center coordinate is around 60°1'N/159°29'E. To start, all the lakes on the TM 2006/2007 images were mapped using Feature Analyst and then manually corrected. This lake file was then overlaid on the Corona mosaic. The image was visually scanned for lakes that showed substantial area loss. Those lakes were manually mapped on the Corona image and placed into a new shapefile. The TM and Corona lake files were then imported into a geodatabase and MS Excel; percent lake area loss was calculated. Those lakes showing $L_{20,}$ or large lakes showing substantial lake area loss less than 20%, were manually mapped on all the six different image sets in the series. Lake files were clipped to the individual geological units and to the region that was cloud-free on all the images (Figure 3.5.2.1). The region has an irregular shape as areas with cloud cover in any one of the time slices of the image series were masked out. The cloud-free area of the multi-temporal image set is 26,179 km^2. Lakes showing substantial lake area loss were then manually assigned an elevation range based on the contour map: 0-20 m, 20-40 m, 40-60 m, 60-80 m, 80-100 m.

The geological projection and datum for the medium-resolution study region was UTM 57/58N and WGS 1984 respectively. The minimum lake size mapped was five ha

(50,000 m^2 or 0.05 km^2). The limiting factor was the MSS images, where five ha equals eight pixels.

All the lake files created in the above steps were imported into a geodatabase and MS Excel. Surface area change for the lakes that experienced substantial lake area loss was calculated over the entire 42-year period as well as between the individual time steps for the lakes within the cloud-free zone: 1965-1975; 1975-1980; 1980-1995; 1995-2002; 2002-2007. Comparisons were made between the drained lakes and the underlying geology, elevation, permafrost conditions, and temperature trends. Relationships between the thermokarst lakes and the permafrost conditions were identified visually.

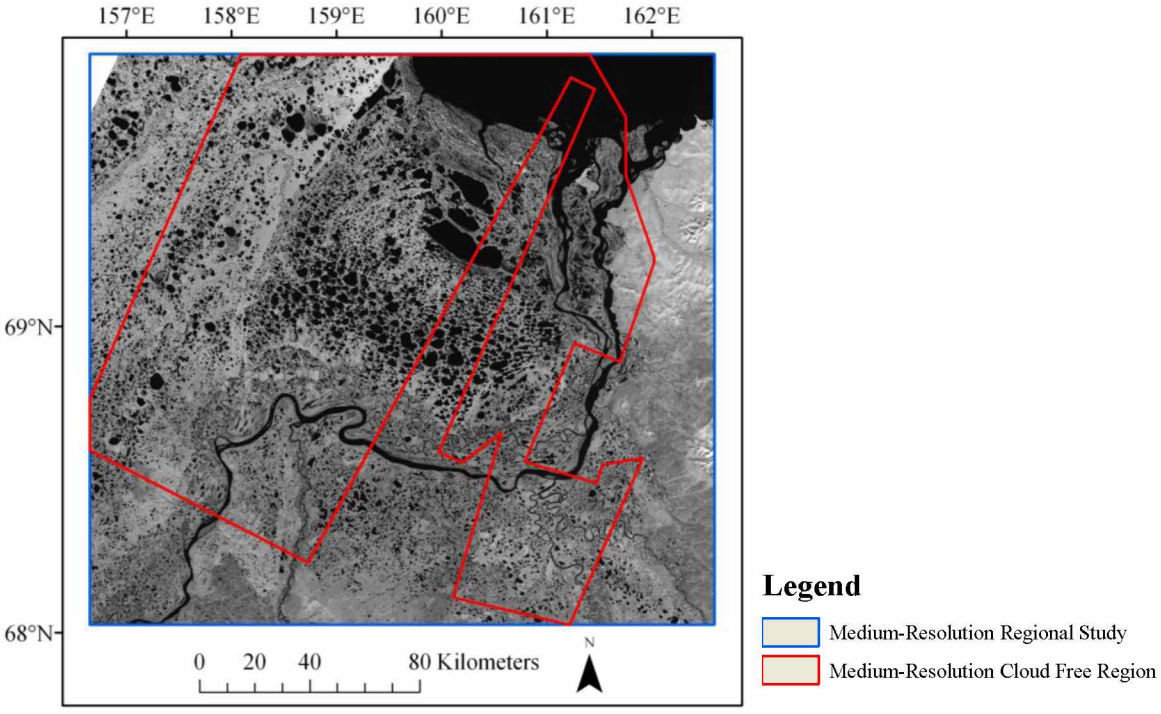

Figure 3.5.2.1. Medium-Resolution Regional Study Area. The cloud-free area in six time slices of the image datasets is shown as well.

3.5.3 Lake Erosion Rates within Yedoma Deposits

The final part of this study looked at lake erosion rates in the loess-like, silty deposits (Yedoma) in the high-resolution Duvanny Yar and Cherskii study regions (Figure 3.5.3.1). This was done using the Digital Shoreline Analysis System (DSAS) extension for ArcGIS. A baseline was created by buffering the 1965 shoreline by two meters to the offshore side. Baseline smoothing distance was set to 20 meters and transects were cast 100 meters apart. Shoreline transects were casts for all lakes within the Yedoma. Those values showing no change, a negative value, or only intersecting a single shoreline, implying that lake surface area did not change or the lake shoreline retreated, were removed from the results. The DSAS results were imported into a geodatabase and MS Excel where erosions rates were calculated for the 42-year period, 1965-2007.

3.5.4 Calculating Albedo Changes

Changes in albedo were calculated for the high-resolution Cherskii and Duvanny Yar study region. This was done by multiplying the land area, in ha, for the 1965 image by 0.2 (the designated albedo for tundra) and then multiplying the water area for 1965 by 0.05 (the designated albedo for the arctic lakes). These resulting values were then added together and divided by the total area of the study region. This was then done for the 2007 image as well. The difference between the two albedo values was then calculated providing the change in albedo that occurred due to changes in lake surface area.

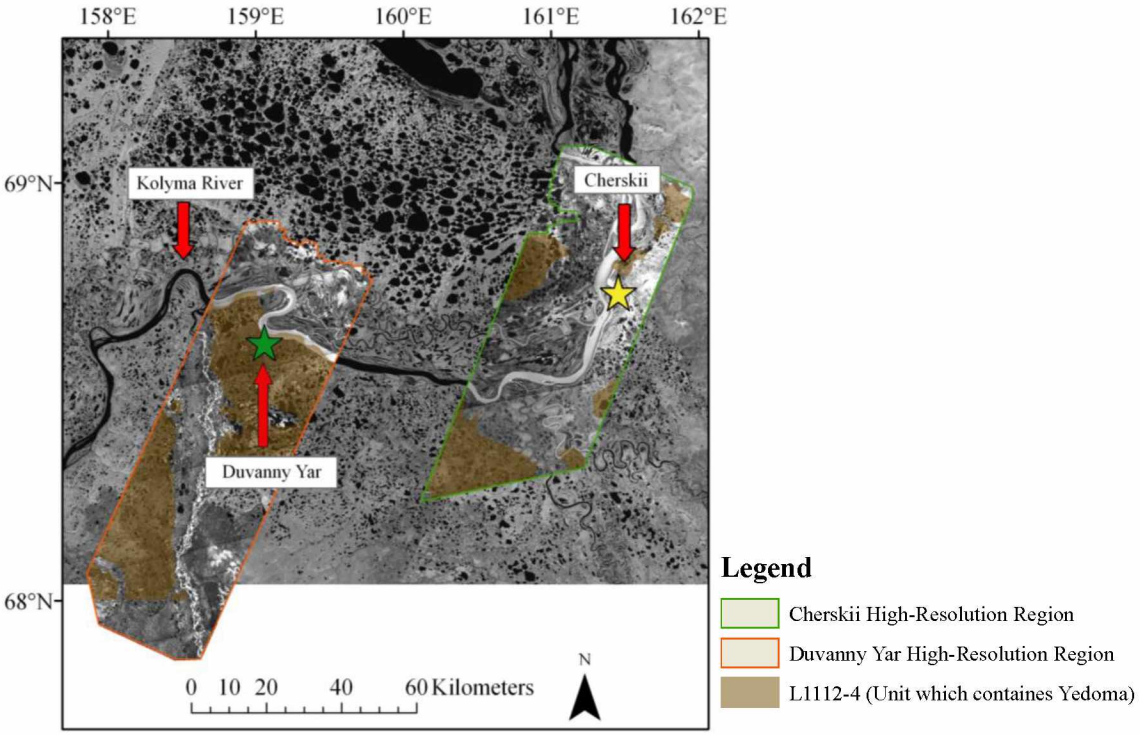

Figure 3.5.3.1. Location of Yedoma Deposits. Yedoma deposits located within the Duvanny Yar and Cherskii Regions.

Chapter 4: Results

4.1 High-Resolution Local Studies

4.1.1 Lake Area in the Duvanny Yar Region: Lakes > 0.5 ha

The Duvanny Yar region (Figure 3.5.1.1) experienced an overall decrease in lake surface area of 2,185.3 ha or 5.2% between 1965 and 2007. Over the 42-year period, this would account for a linear rate of decrease of 53.2 ha per year. Lake area in 1965 and 2007 was 42,730.0 ha and 40,495.9 ha respectively. Limnicity (lake area per total area) for the study region decreased from 10.2% in 1965 to 9.6% in 2007. This is a decrease of 0.5 ha per 100 ha of land. There was however, an overall increase in the total number of lakes by 69. In 1965, there were 2,264 lakes larger than 0.5 ha and in 2007, there were 2,333 lakes larger than 0.5 ha (Figure 4.1.1.1). A decrease was largely observed for large lakes > 50 ha, while lake numbers increased in most size categories of lakes < 50 ha.

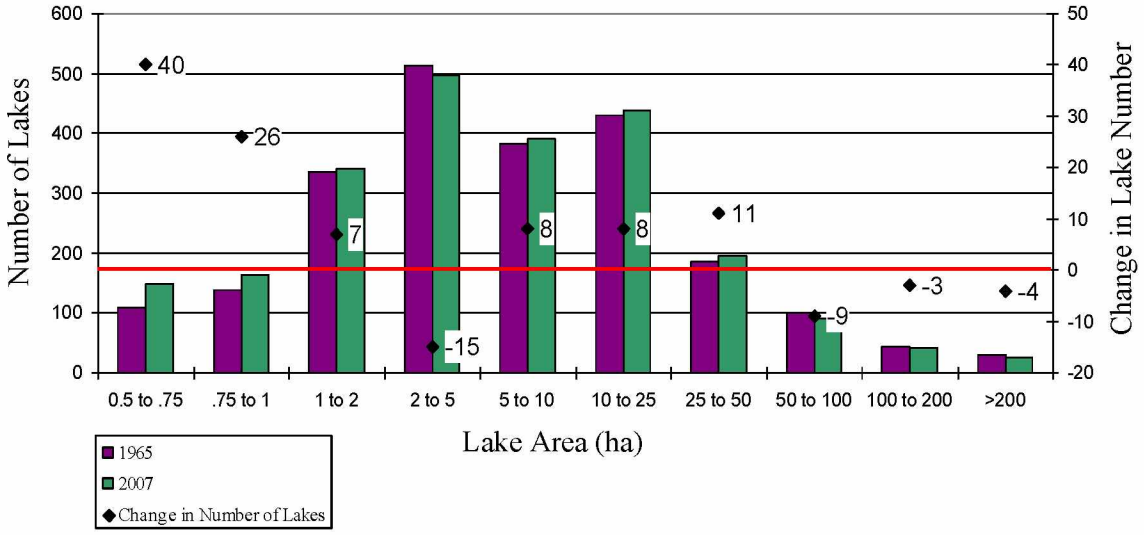

Figure 4.1.1.1. Duvanny Yar Lake Size Distribution. Lake size distribution (left axis; colored bars) and change in lake numbers per size category (right axis; black diamonds) for all lakes larger than 0.5 ha in the Duvanny Yar region from 1965 to 2007. The red line indicates zero change in lake number per size category.

Based on the 1:1.000,000 scale surface geological map (Russian Geological Research Institute VSEGEI, 2000), seven different geological units were present within the Duvanny Yar region (Figure 4.1.1.2). The $L111_{2\text{-}4}$ unit (containing Yedoma), the *alV* unit, and the *dc/ds* unit make up the majority of the study region. When lake area is analyzed by geological unit, all those units containing thermokarst lakes experienced a net decrease in lake area (Table 4.1.1.1). The highest normalized lake area (% of lake area) was found in the *lb1V* deposits followed by the $L111_{2\text{-}4}$ deposits. Normalized lake area was calculated by dividing the total lake area, in ha, for a single geological unit, by the total area of that geological unit, in ha; this value was then multiplied by 100. The resulting value represents the lake area present in 100 ha of a geological unit if the lake area was evenly distributed throughout. This allowed lake areas to be compared for the different geological units regardless of how much area the geological unit occupied within the study region.

The $L111_{2\text{-}4}$ deposits experienced the highest normalized lake area loss (-0.7%), followed by *alV* deposits (-0.6%) (Figure 4.1.1.3).

The *la1V* deposits makes up an extremely small part of the study region, < 1,000 ha. No lakes were located in these deposits. In the *am1V* deposits, there are only portions of two lakes. Both deposits combined account for 0.25% of the study region. Neither deposit is visible at the scale of Figure 4.1.1.2.

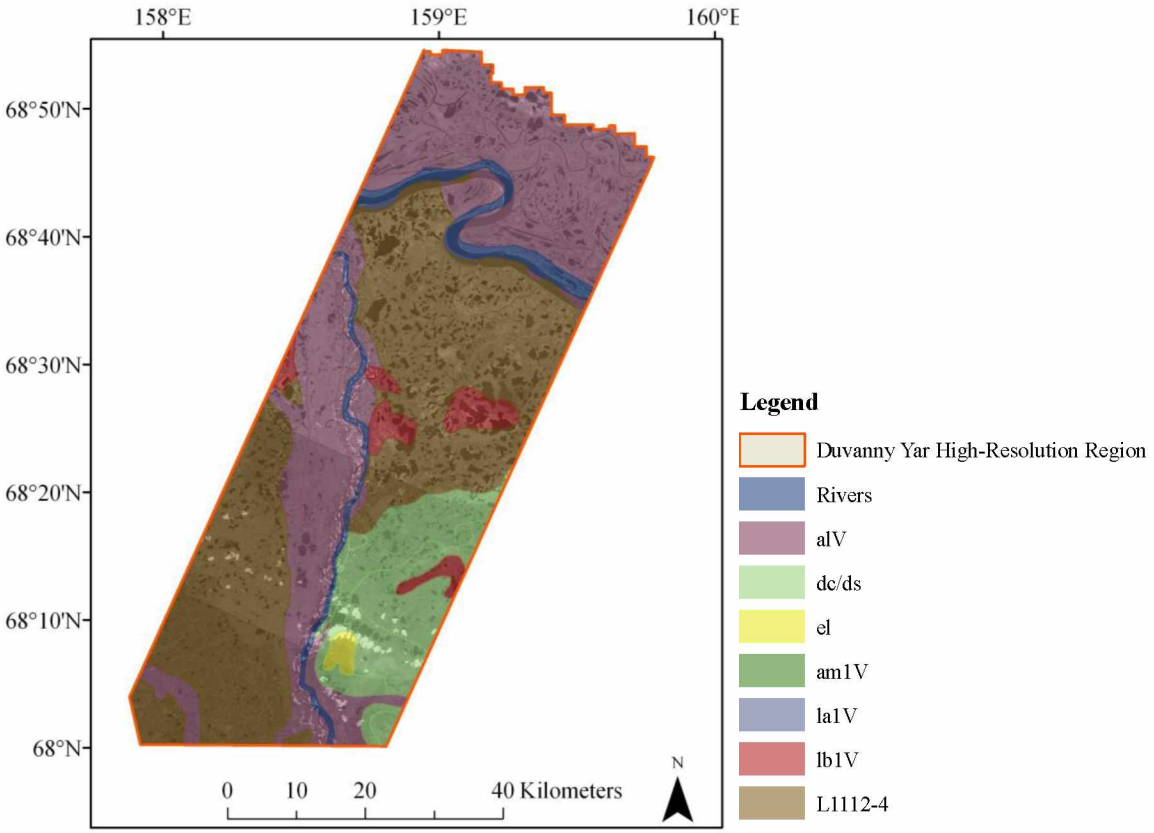

Figure 4.1.1.2. Duvanny Yar Geological Map. Map showing the different types of underlying geology present within the Duvanny Yar study region. Lake area calculations based on geology may vary slightly from the lake analysis values for the entire region as the geological map did not cover the entire Duvanny Yar high-resolution study region. Geological data from Russian Geological Research Institute VSEGEI, 2000.

Table 4.1.1.1. Analysis of Lakes Greater Than 0.5 ha by Geological Unit in the Duvanny Yar Region.

Geological Unit	Area (ha)	1965 Lake Area (ha)	2007 Lake Area (ha)	1965 Lake Area per Unit (%)	2007 Lake Area per Unit (%)	Difference in Lake Area (ha)	Difference in Lake Area per Unit (%)	Lake Area Drained per Unit (%)	Pecent of Total Lake Area Loss Accounted for per Unit (%)	Normalized Percent of Total Lake Area Loss Accounted for per Unit (%)
alV	156,226.6	12,445.9	11,582.1	8.0	7.4	-863.8	-0.6	-6.9	39.5	21.9
am1V	35.7	1.2	1.0	3.4	2.9	-0.2	-0.5	-15.5	0.0	20.9
dc/ds	47,317.8	3,128.2	2,969.4	6.6	6.3	-158.9	-0.3	-5.1	7.3	13.3
el	2,128.2	2.8	0.6	0.1	0.0	-2.2	-0.1	-79.7	0.1	4.1
la1V	933.0	0.0	0.0	0.0	0.0	0.0	0.0	-----	0.0	0.0
lb1V	13,275.8	3,486.6	3,445.5	26.3	26.0	-41.1	-0.3	-1.2	1.9	12.3
$L111_{2-4}$	162,176.8	22,757.9	21,638.7	14.0	13.3	-1,119.1	-0.7	-4.9	51.2	27.4
Totals		41,822.6	39,637.3	-----	-----	-2,185.3	-2.5	-----	100.0	100.0

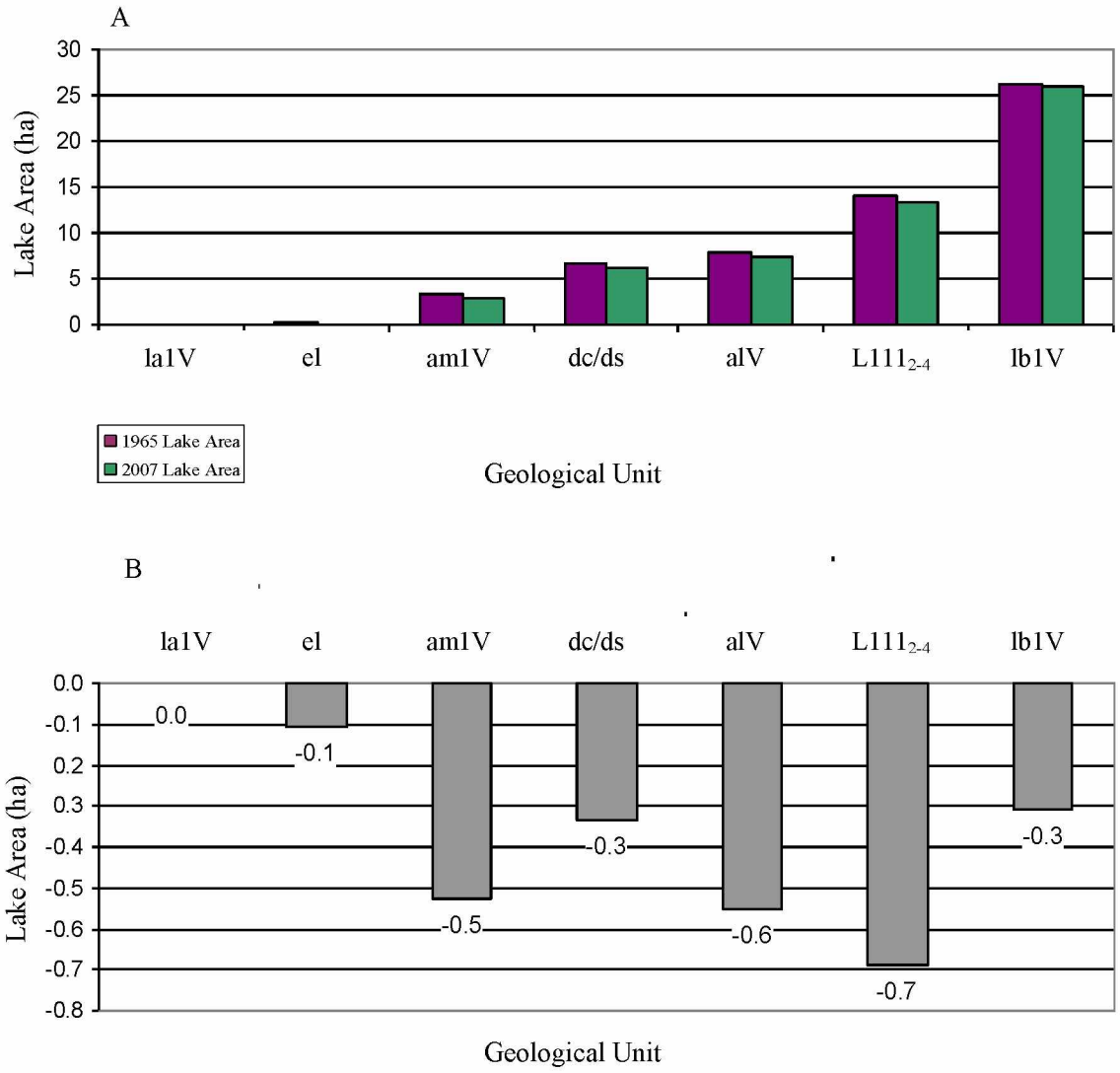

Figure 4.1.1.3. Duvanny Yar Normalized Lake Area by Geological Unit. A. Normalized lake area for each geological unit. B. Decrease in normalized lake area over the 42-year period.

4.1.1.1 Lakes Showing Area Loss Greater Than 20%

Within the Duvanny Yar region, 133 lakes > 0.5 ha decreased more than 20% from their size in 1965 and 13 lakes disappeared completely (Table 4.1.1.1.1; Figure 4.1.1.1.1). In further discussions, this subset of lakes is referred to as L_{20}. These 133 lakes in L_{20} accounted for a loss in lake area of 2,281 ha (Figure 4.1.1.1.2). Some of the larger lakes separated into multiple smaller lakes during shrinkage. This resulted in an overall increase in L_{20} lake numbers by 112 between 1965 and 2007. No definitive relationship exists between percent drainage and the size of individual lakes (Figure 4.1.1.1.3). Large lakes (larger than 50 ha) appear to be equally affected by shrinkage processes as the smaller lakes. The highest percent lake area loss occurred to lakes between one and 10 ha.

Table 4.1.1.1.1. Duvanny Yar Summary of Lakes Showing L_{20}.

	Lake Area (ha)	Number of Lakes	Mean Lake Size (ha)	Median Lake Size (ha)
1965	4,093.7	133	30.8	6.6
2007	1,812.5	245	7.4	1.3
Difference	2,281.2	112	23.4	5.3

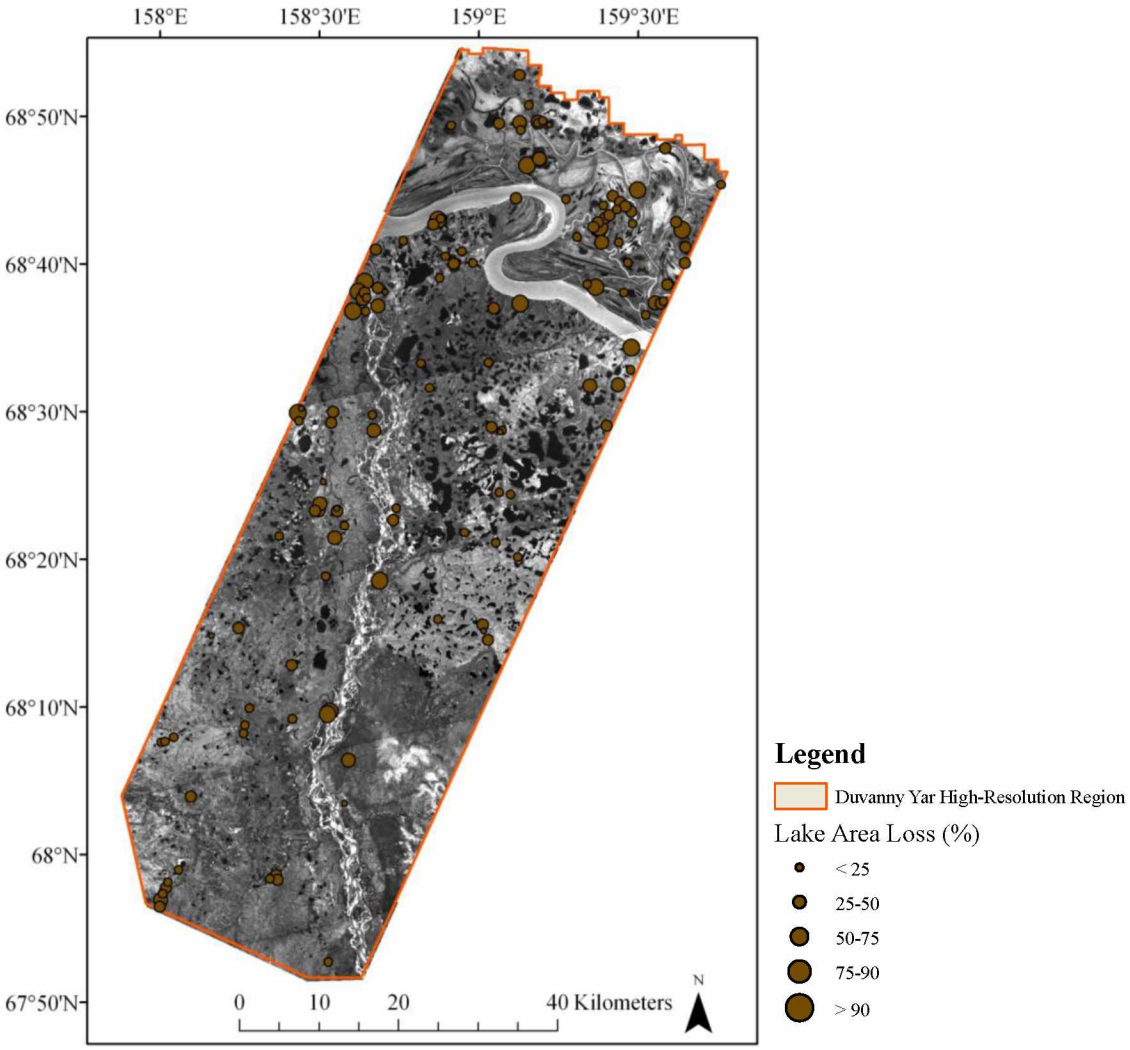

Figure 4.1.1.1.1. Location of L_{20} Lakes Shown by Percent Lake Area Loss.

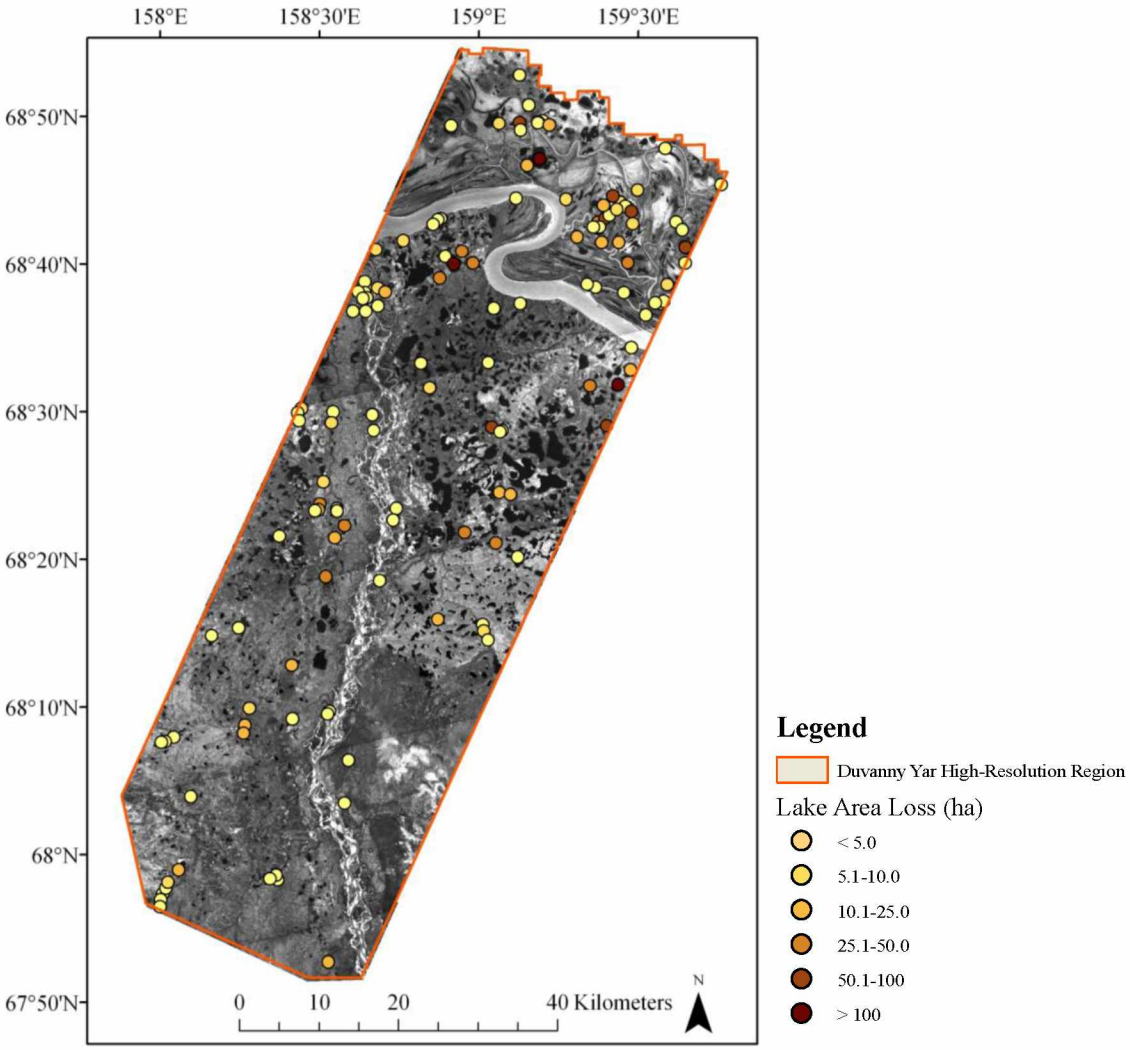

Figure 4.1.1.1.2. Location of L_{20} Lakes Shown by the Size of Lake Area Loss.

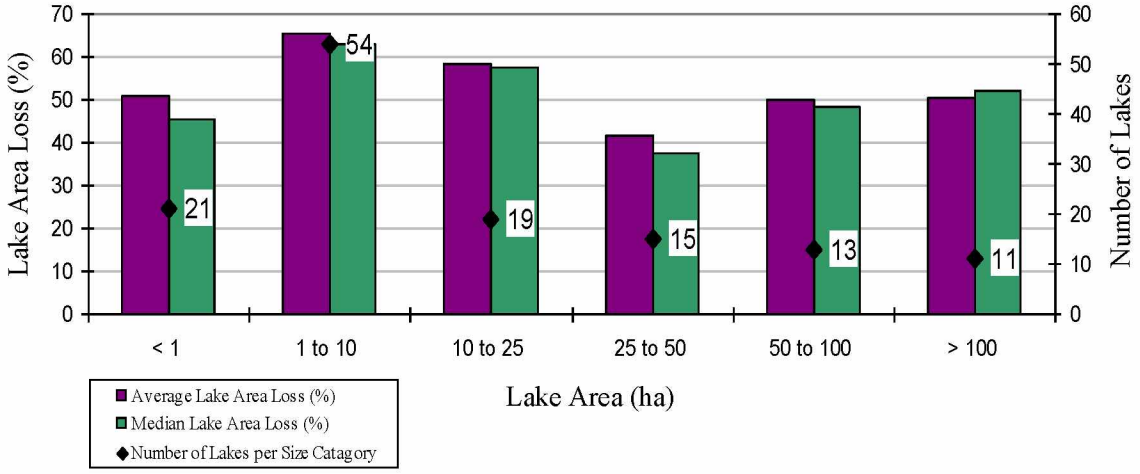

Figure 4.1.1.1.3. Duvanny Yar Mean and Median Lake Area Loss. Mean and median lake area loss related to lake area size (colored bars correspond to left axis). Lake size distribution is also shown (black diamonds correspond to right axis). No distinctive trend is seen.

When the lakes from the L_{20} subset were analyzed by geological unit (Table 4.1.1.1.2), the *alV* unit accounted for the greatest lake area loss (0.8 ha per 100 ha of geological unit) (Figure 4.1.1.1.4). This amount is close to 50% of the total lake area loss within the Duvanny Yar region. Lakes in $L111_{2\text{-}4}$ deposits accounted for the second highest rate of lake area loss, 0.6 ha per 100 ha of geological unit or over 33% of the total lake area loss within the Duvanny Yar region. The *la1V* deposits and the *am1V* deposits did not contain any L_{20} lakes. The remaining geological units had much lower drainage values, typically 0.1 ha per 100 ha of geological unit or four to seven percent of the total lake area loss.

Even though in the Duvanny Yar region lake area loss is the dominant process, lake expansion is occurring as well. In the *alV* deposits for example, overall lake area decreased by 863.8 ha. Lake area loss from L_{20} lakes in the *alV* deposits was 1,285.1 ha. The difference of 421.3 ha is accounted for by lake expansion within the *alV* deposits.

Table 4.1.1.1.2. Geological Analysis of L_{20} Lakes within Duvanny Yar. Geological analysis of lakes greater than 0.5 ha from the L_{20} subset within the Duvanny Yar study region.

Geological Unit	Area (ha)	1965 Lake Area (ha)	2007 Lake Area (ha)	1965 Lake Area per Unit (%)	2007 Lake Area per Unit (%)	Lake Area Loss (ha)	Percent of Total Lake Area Loss per Unit (%)	Difference in Lake Area Loss per Unit (%)	Normalized Percent of Total Lake Area Loss Accounted for per Unit (%)
alV	156,226.6	2,210.4	925.3	1.4	0.6	-1,285.1	-57.5	-0.8	49.6
am1V	35.7	0.0	0.0	0.0	0.0	0.0	0.0	0.0	0.0
dc/ds	47,317.8	81.1	48.9	0.2	0.1	-32.2	-1.4	-0.1	4.1
el	2,128.2	2.8	0.6	0.1	0.0	-2.2	-0.1	-0.1	6.3
la1V	933.0	0.0	0.0	0.0	0.0	0.0	0.0	0.0	0.0
lb1V	13,275.8	49.8	35.5	0.4	0.3	-14.3	-0.6	-0.1	6.5
$L111_{2-4}$	162,176.8	1,635.1	734.2	1.0	0.5	-901.0	-40.3	-0.6	33.5
Totals		3,979.2	1,744.4	-------	-------	-2,234.8	-100.0	-1.7	100.0

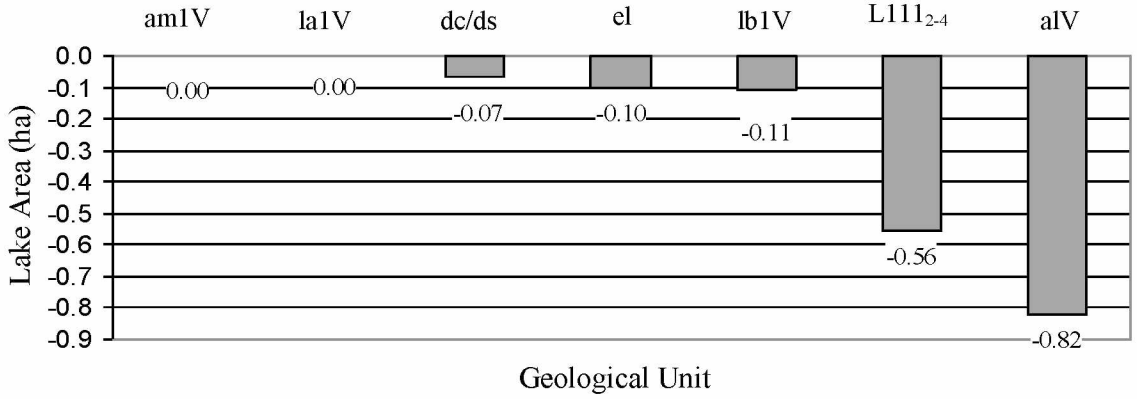

Figure 4.1.1.1.4. Decrease in Normalized Lake Area per 100 ha of Geological Unit for the L_{20} Lakes Subset in the Duvanny Yar Region.

4.1.1.2 DEM and Permafrost Analysis

Based on the 1:200,000 DEM (Ferranti, 2009), half of the Duvanny Yar region has elevations of more than 20 m above sea level. However, over $^2/_3$ of the thermokarst lake area is located below 20 meters. Because the study region is relatively small and the lakes are generally located at lower elevations, precise elevation/lake change calculations were not done. General relationships between the region's elevation and its overall effect on lake area loss and expansion will be addressed in the discussion section. The same is true for relationships between lake area change and permafrost data. Based on the 1:10,000,000 Circum-Arctic Permafrost Map (Brown et al., 1997), the permafrost in the Kolyma Lowland region is continuous and mostly ice rich (> 20%). The data available is broad and generalized over all of Siberia. A detailed assessment of the relationships between thermokarst lakes and permafrost character is therefore not possible with the presently available data. Any influence permafrost characteristics may have on the changes occurring to thermokarst lakes is described in the discussion.

4.1.1.3 Small-Lake Dynamics

Five small areas, that upon visually scanning the satellite images showed lake development, were selected to demonstrate that new lakes were forming between 1965 and 2007 (Figure 4.1.1.3.1; Figure 4.1.1.3.2). All lakes, the smallest being 0.003 ha (29.8 m^2), were analyzed. Two regions were located in alluvial deposits, two in Yedoma, and one in deluvial deposits (Table 4.1.1.3.1). These rates of lake development are not representative of the entire geological unit as they were chosen because lake development was occurring there; they were not randomly selected. Increase in lake area within these five regions is shown in Table 4.1.1.3.2.

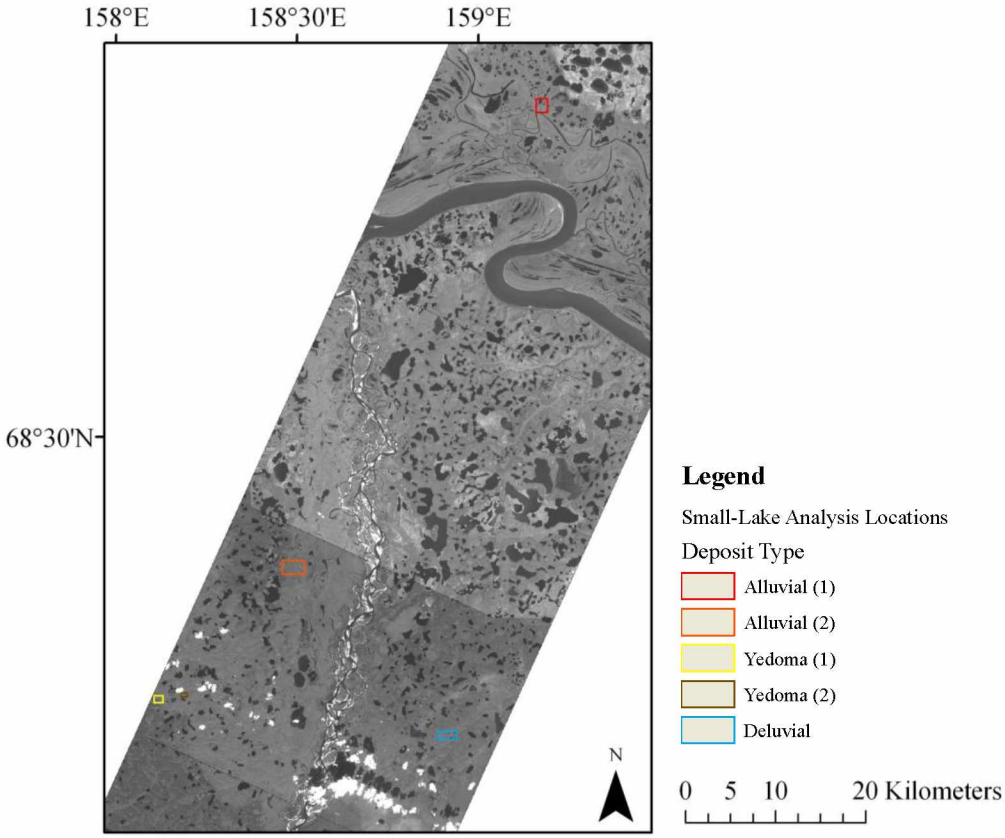

Figure 4.1.1.3.1. Location of Duvanny Yar Small-Lake Analysis Sites.

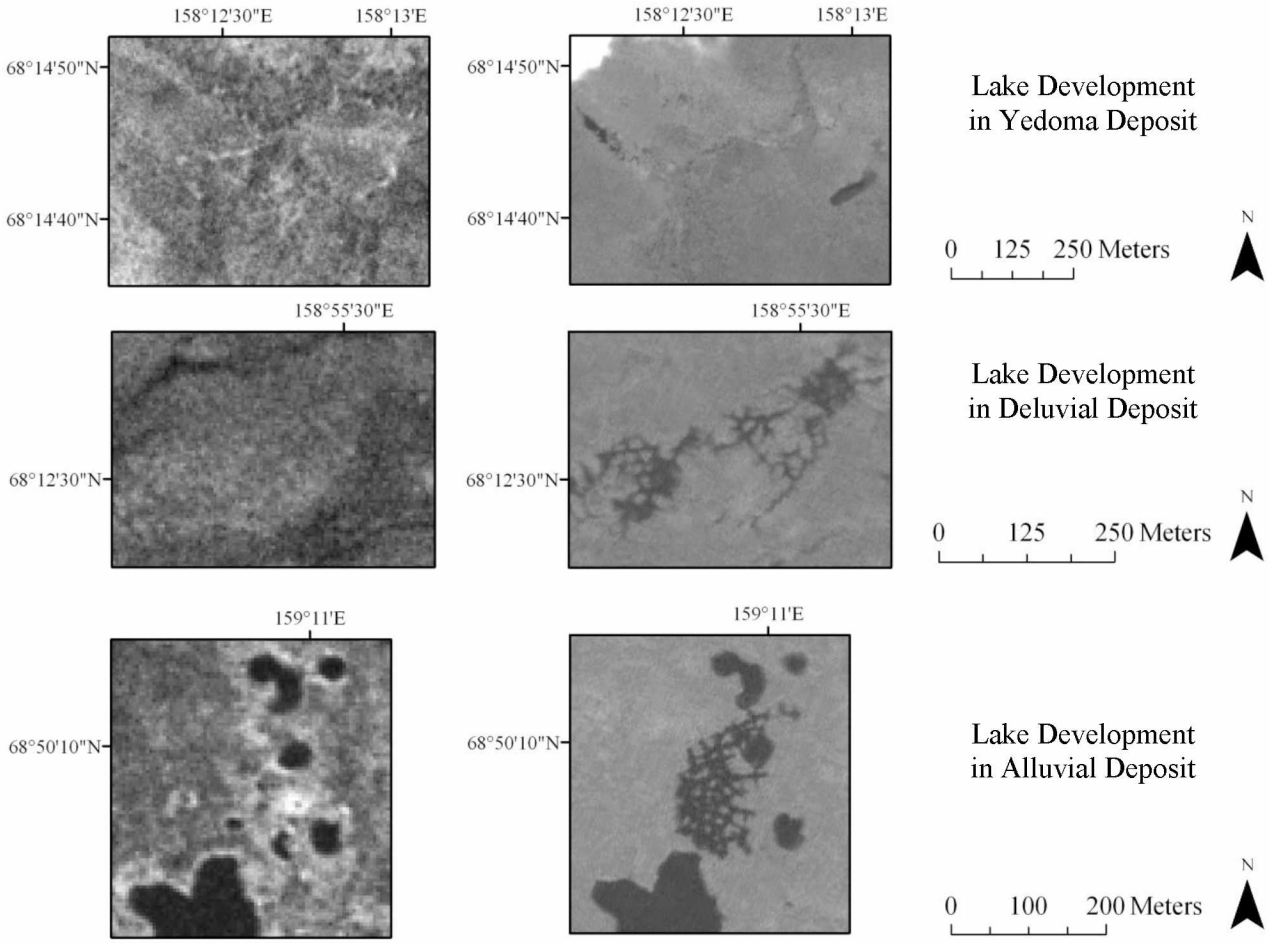

Figure 4.1.1.3.2. Examples of Lake Development in the Duvanny Yar Region Between 1965 (Left) and 2007 (Right).

Table 4.1.1.3.1. Development of New Lakes within the Duvanny Yar Region. Lake distribution by size (ha) is shown along with the total change in lake number.

Sediment Type	Lake Size (ha)	Number of Lakes 1965	Number of Lakes 2007	Change in Number of Lakes
Alluvial (1)	< 0.01 ha	0	10	10
	0.01 ha -0.05 ha	7	8	1
	0.05 ha- 0.1 ha	5	7	2
	0.1 ha - 0.5 ha	11	10	-1
	0.5 ha -1 ha	1	0	-1
	< 1 ha	4	4	0
	Total	28	39	11
Alluvial (2)	< 0.01 ha	0	22	22
	0.01 ha -0.05 ha	3	18	15
	0.05 ha- 0.1 ha	1	6	5
	0.1 ha - 0.5 ha	0	1	1
	0.5 ha -1 ha	0	1	1
	< 1 ha	0	0	0
	Total	4	48	44
Yedoma (1)	< 0.01 ha	0	6	6
	0.01 ha -0.05 ha	0	1	1
	0.05 ha- 0.1 ha	0	0	0
	0.1 ha - 0.5 ha	0	2	2
	0.5 ha -1 ha	0	0	0
	< 1 ha	0	0	0
	Total	0	9	9
Yedoma (2)	< 0.01 ha	0	4	4
	0.01 ha -0.05 ha	1	3	2
	0.05 ha- 0.1 ha	1	2	1
	0.1 ha - 0.5 ha	1	0	-1
	0.5 ha -1 ha	0	0	0
	< 1 ha	0	0	0
	Total	3	9	6
Deluvial	< 0.01 ha	0	3	3
	0.01 ha -0.05 ha	3	7	4
	0.05 ha- 0.1 ha	1	3	2
	0.1 ha - 0.5 ha	0	6	6
	0.5 ha -1 ha	2	2	0
	< 1 ha	2	2	0
	Total	8	23	15

Table 4.1.1.3.2. Change in Lake Area for the Small-Lake Analysis Locations. Lake area statistics for the Duvanny Yar small-lake analysis locations.

Sediment Type	Study Area (ha)	Total Lake Area 1965 (ha)	Total Lake Area 2007 (ha)	Difference (ha)	Linear Rate of Increase per Year (ha)	Linear Rate of Increase per Year (m^2)
Alluvial (1)	191.16	25.98	27.80	1.82	0.04	432.49
Alluvial (2)	374.72	0.12	1.79	1.67	0.04	396.52
Yedoma (1)	33.21	0.00	0.48	0.48	0.01	114.97
Yedoma (2)	76.03	0.22	0.24	0.02	0.00	5.38
Deluvial	185.45	5.17	9.19	4.03	0.10	958.66

The following statistics do not account for lakes which were present in 1965 but had completely dried up by 2007, nor does it account for an increase in lake number that may have occurred because a larger lake dried into multiple smaller ones. These results reflect only new lakes that formed between 1965 and 2007. Alluvial (1) region had 15 new lakes develop, accounting for 1.5 ha of lake area. Alluvial (2) had 48 new lakes develop with 1.8 ha of lake area. The majority of these lakes, 40 out of the 48, were smaller than 0.05 ha. Yedoma (1) had 9 new lakes in 2007 (0.5 ha) and Yedoma (2) had 7 new lakes (0.2 ha). These lakes were also very small, all under 0.1 ha in size. The deluvial region developed the most new lake area (2.4 ha) with 14 new lakes in this region.

4.1.2 Lake Area in the Cherskii Region: Lakes > 0.5 ha

The Cherskii region (Figure 3.5.1.1) experienced an overall increase in thermokarst lake surface area of 3,622.3 ha (+7.7%), between 1965 and 2007. Over the 42-year period, this accounts for a linear rate of increase of 87.9 ha per year. Lake area in 1965 and 2007 was 47,114.9 ha and 50,807.3 ha respectively. Limnicity for the study region increased from 14.0% in 1965 to 15.1% in 2007. This is an increase of 1.10 ha of lake area per 100 ha of land area. There was an increase in the overall number of lakes by 72. In 1965, there were 3,246 lakes larger than 0.5 ha in size and in 2007, there were 3,318 lakes of this size (Figure 4.1.2.1).

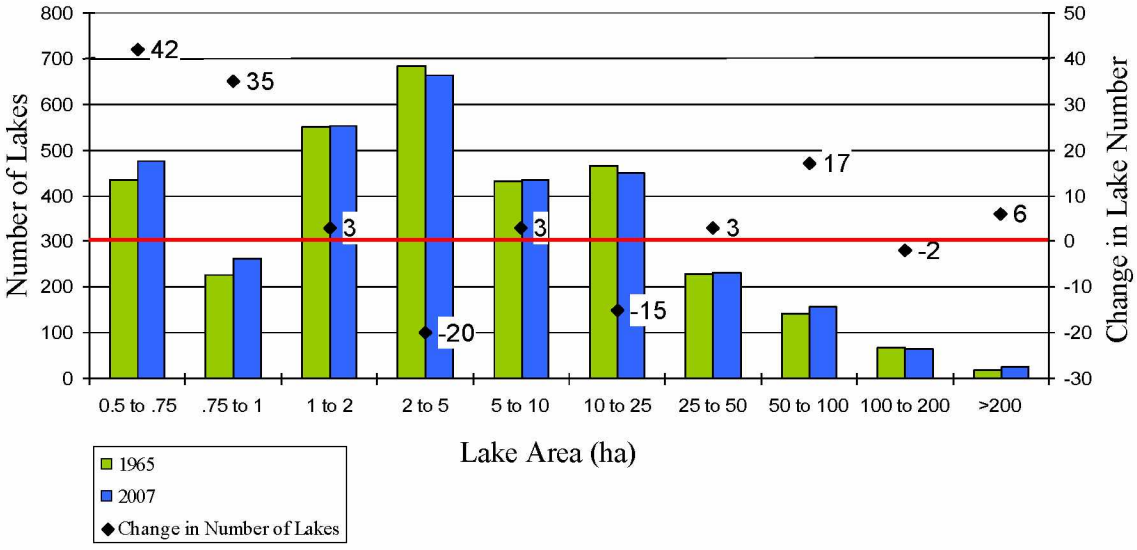

Figure 4.1.2.1. Cherskii Region Lake Size Distribution. Lake size distribution (left axis; colored bars) and change in lake number per size category (right axis; black diamonds) for all lakes larger than 0.5 ha in the Cherskii region from 1965 to 2007. The red line indicates zero change in lake number per size category.

Both the Duvanny Yar and Cherskii regions had an increase in lake number with the greatest increase coming from small lakes; both regions had an increase of over 70 lakes whose areas were less than 2.0 ha. However, the source of this increase is different. In the Duvanny Yar region, the increase in number of small lakes mostly came from larger lakes transforming into multiple smaller lakes (Mackay, 1988) (Figure 4.1.2.2). In the Cherskii region, while some larger lakes did drain into multiple smaller ones, many lakes that were outside of the studies size range (< 0.5 ha) in 1965, increased in size to an area larger than 0.5 ha by 2007.

Between 1965 and 2007, the size distribution of larger lakes changed as well. In the Duvanny Yar region, the number of lakes larger than 50 ha decreased from 173 to 157, a reduction of 16 lakes. However, within the Cherskii region, there was an increase of 21 lakes with areas larger than 50 ha. This increase is mainly caused by several larger lakes, sometimes up to five, adjoining through an outlet too wide and too short to be considered a river. This resulted in no definitive lake boundary. Most of the regions where lake areas are substantially increasing in size were heavily influenced by rivers and streams (Figure 4.1.2.3). Upon examining the imagery, the expanded lake areas were often lighter in color, possibly indicating that the expansion was due to seasonal flooding and not necessarily lake growth by thermokarst processes.

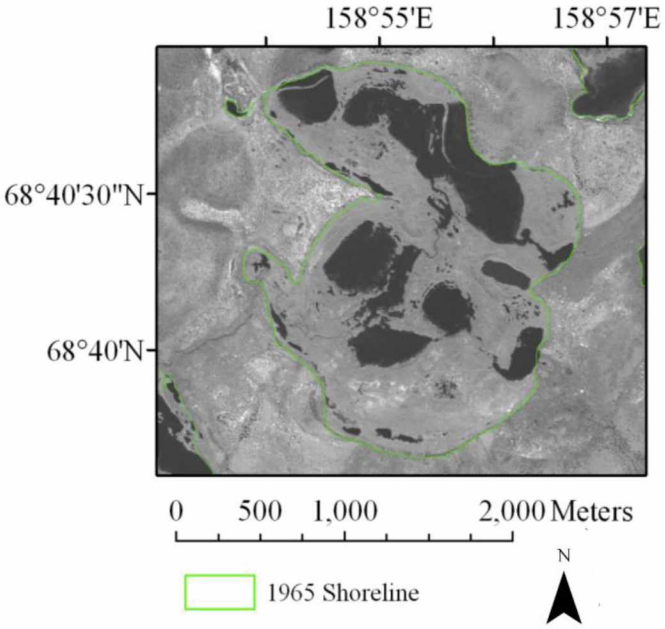

Figure 4.1.2.2. Larger Lake Transforming into Multiple Smaller Lakes. Base image is from 2007; 1965 lake area was 298.1 ha. Lake is located within Yedoma sediment.

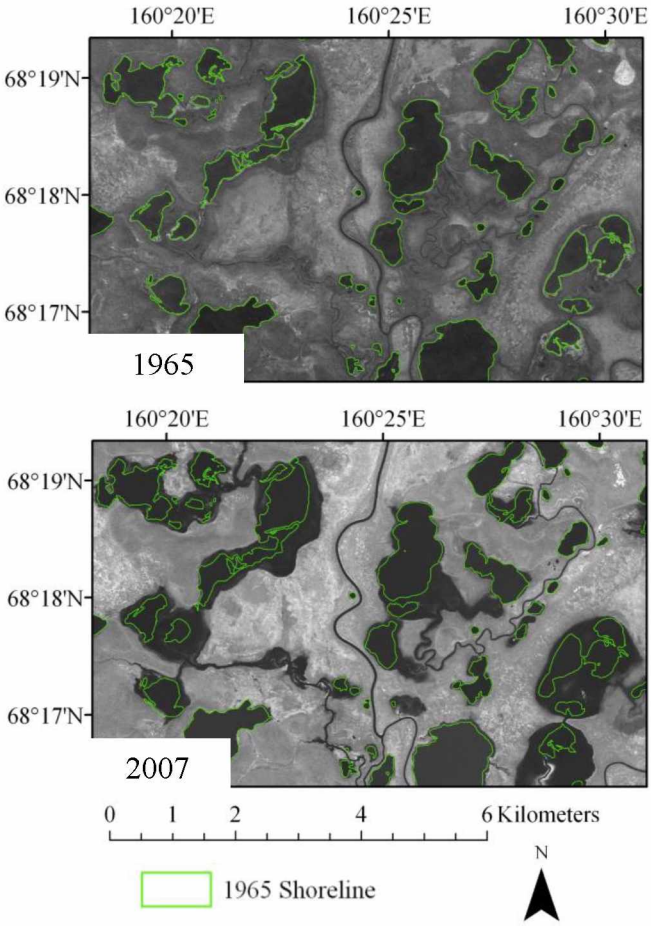

Figure 4.1.2.3. Large Lake Growth in the Cherskii Study Region. This region is heavily affected by a network of rivers and streams and therefore by possible flooding episodes.

Variations in river water level and volume can affect lake levels if the two are connected by a water channel. Often, river waters rise due to seasonal change, which include snowmelt in the spring and rain-induced episodes throughout the summer (Marsh and Hey, 1989). Marsh and Hey (1989) studied river influenced flooding in the Mackenzie Delta lakes near Inuvik, Canada. They discovered the degree of flooding is controlled by four factors: 1) water level regime of the major distributary channel, 2) whether there is a single channel connecting the lake to the distributary channel or multiple channels, 3) the distance the lake is from the distributary channel, and 4) the lakes elevation in relation to the distributary channel. Lakes at lower elevations and with a single connecting channel experienced the greatest level of flooding. The lakes experiencing flooding in the Cherskii region of the Kolyma Lowlands are at elevations less than 20 m average sea level and are relatively close to the distributary channels. However, a second channel often connects multiple lakes together. This allows the flooding caused by the increase in river volume to affect multiple lakes in the region.

Much of the study region is composed of *alV* deposits and $L111_{2\text{-}4}$ deposits (Figure 4.1.2.4). When analyzed by geological unit, all those that contained lakes showed an increase in lake surface area (Table 4.1.2.1). The *am1V* deposits and the $L111_{2\text{-}4}$ deposits had the first and second highest limnicity respectively. Between 1965 and 2007, increase in normalized lake area was roughly the same for the *am1V*, $L111_{2\text{-}4}$, *lb1V*, and *la1V* units. This increase ranges between 2.3 ha and 2.0 ha per 100 ha of a geological unit. *alV*, *dc/ds*, and *el* deposits showed an increase in lake area as well but values were much smaller, less than 0.8 ha per 100 ha of geological unit.

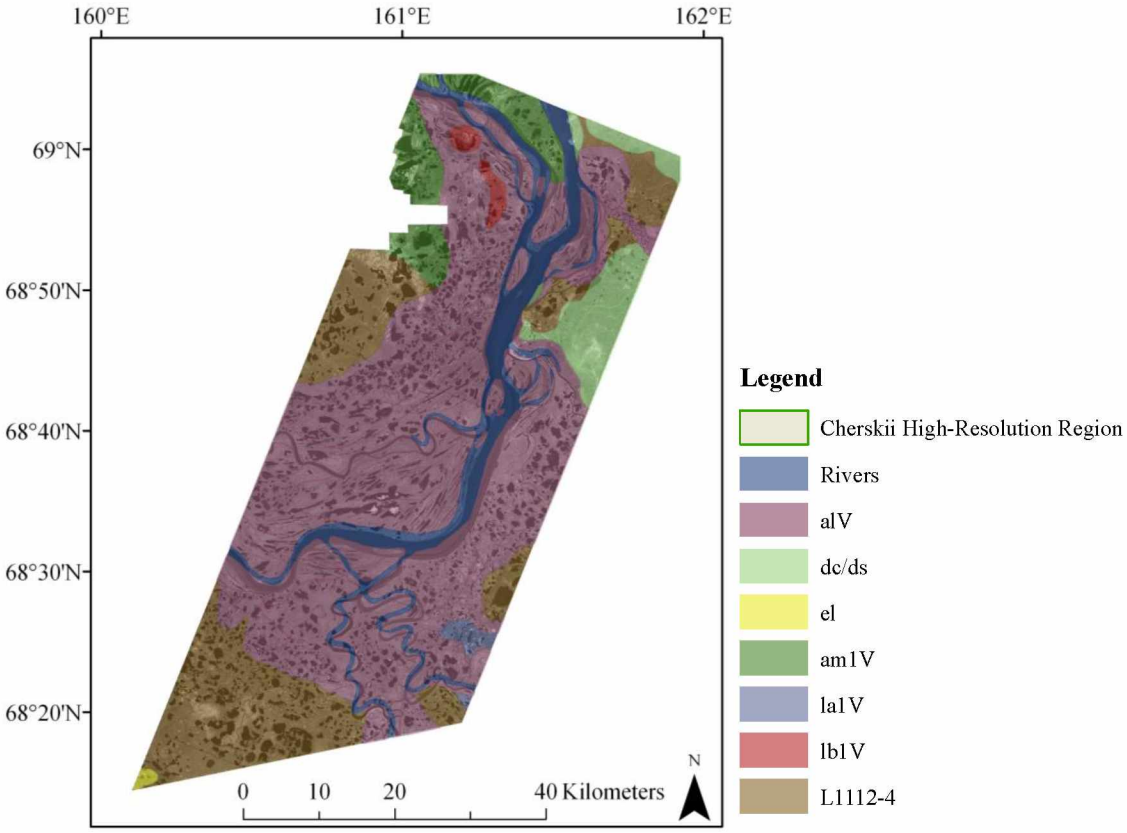

Figure 4.1.2.4. Cherskii Region Geological Map. Map showing the different types of underlying geology present within the Cherskii study region. Geological data from Russian Geological Research Institute VSEGEI, 2000.

Table 4.1.2.1. Analysis of Lakes Greater Than 0.5 ha by Geological Unit in the Cherskii Region.

Geological Unit	Area (ha)	1965 Lake Area (ha)	2007 Lake Area (ha)	1965 Lake Area per Unit (%)	2007 Lake Area per Unit (%)	Difference in Lake Area (ha)	Difference in Lake Area per Unit (%)	Increase in Lake Area per Unit (%)	Percent of Total Lake Area Increase Accounted for per Unit (%)	Normalized Percent of Total Lake Area Increase Accounted for per Unit (%)
alV	227,548.9	30,587.3	32,216.3	13.4	14.2	1,629.1	0.7	5.3	45.0	7.5
am1V	18,162.7	3,626.2	4,004.5	20.0	22.0	378.3	2.1	10.4	10.4	21.9
dc/ds	16,114.9	406.6	443.3	2.5	2.8	36.7	0.2	9.0	1.0	2.4
el	578.9	64.0	64.1	11.1	11.1	0.1	0.0	0.1	0.0	0.2
la1V	2,387.8	257.1	304.9	10.8	12.8	47.8	2.0	18.6	1.3	21.0
lb1V	2,967.1	421.1	490.6	14.2	16.5	69.6	2.3	16.5	1.9	24.6
$L111_{2-4}$	68,393.9	11,824.1	13,284.8	17.3	19.4	1,460.7	2.1	12.4	40.3	22.4
Totals		47,186.3	50,808.6	-------	-------	3,622.3	9.5	-------	100.0	100.0

Normalized lake area distribution by geological unit for the Cherskii region was slightly different than for the Duvanny Yar region. With the exception of the *dc/ds* deposits, lake area is more evenly distributed (Figure 4.1.2.5). The deluvial deposits are located at higher elevations where there is exposed bedrock and less soil for lakes to develop in. There are fewer lakes here and those that exist are small. Average size of these lakes is around eight ha with a median around four ha. The eluvial deposits make up a small percentage of the study region and also have very small lake areas. The five remaining geological units have normalized lake area values within 11 ha of each other, namely between 12 and 22 ha. The more even distribution of lake area may be caused by the higher alluvial influence that the Cherskii region has over the Duvanny Yar region.

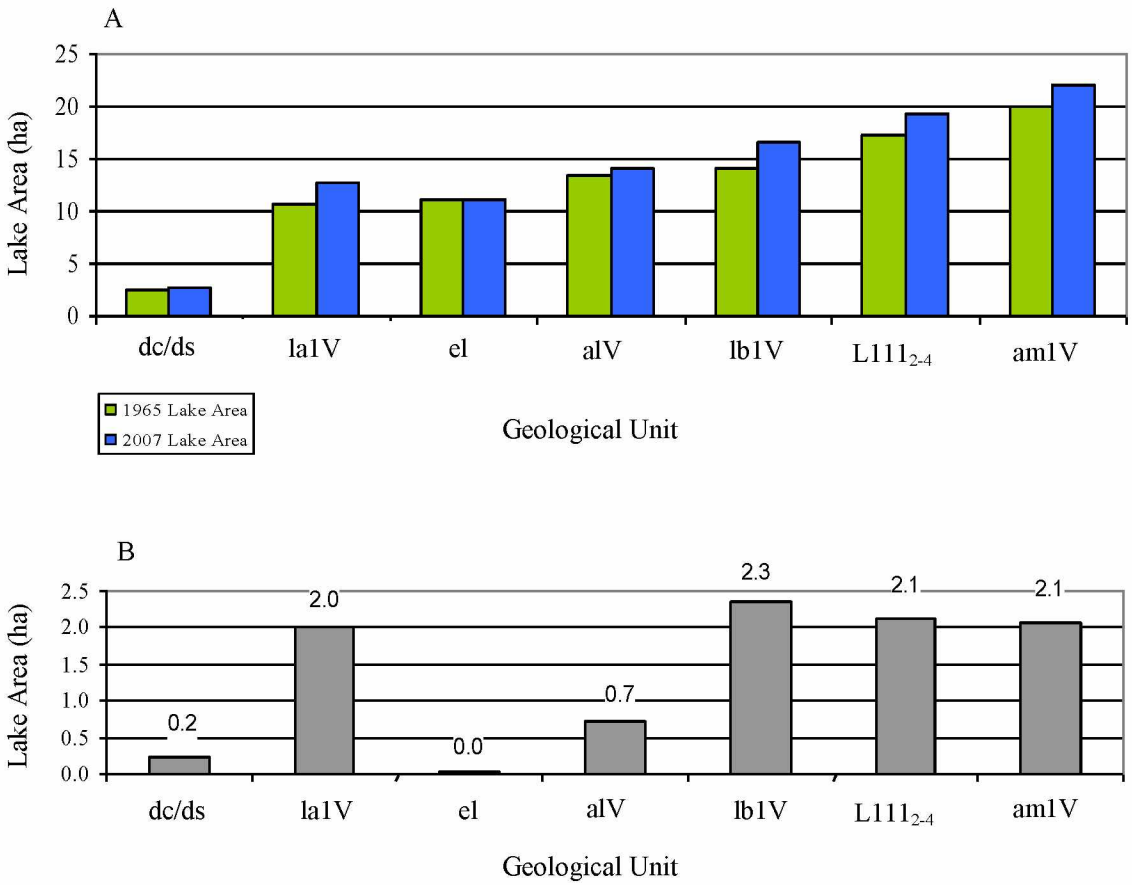

Figure 4.1.2.5. Cherskii Normalized Lake Area by Geological Unit. A. Normalized lake area for each geological unit. B. Increase in normalized lake area over the 42-year period.

4.1.2.1 Lakes Showing Area Loss Greater Than 20%

Within the Cherskii region, 166 lakes decreased more than 20% in size between 1965 and 2007 and 1,761.6 ha of lake area was lost (Table 4.1.2.1.1; Figure 4.1.2.1.1; Figure 4.1.2.1.2). Of these, 14 lakes drained completely. The total number of lakes increased as the larger lakes often separated into multiple smaller lakes during shrinkage. There was an increase of 74 lakes between 1965 and 2007. However, the average lake size dropped by over 15 ha. When comparing lake size to percent lake area loss, lakes < 10 ha experienced a higher percent of lake area loss than lakes > 10 ha (Figure 4.1.2.1.3). Average percent lake area loss for lakes < 10 ha was around 50% while larger lakes, on average, experienced lake area loss of between 10 and 15 percent less.

As with the Duvanny Yar region, both lake area loss and lake growth is occurring. Overall, the Cherskii region experienced an increase in lake area of 3,622.3 ha. Lakes that belong to the L_{20} subset accounted for a loss of 1,761.6 ha, therefore, an increase in lake area of at least 5,383.9 ha occurred in other lakes.

Table 4.1.2.1.1. Summary of Lakes from the L_{20} Subset in the Cherskii Region.

	Lake Area (ha)	Number of Lakes	Mean Lake Size (ha)	Median Lake Size (ha)
1965	4,565.0	166	27.5	7.3
2007	2,803.4	240	11.7	2.6
Difference	1,761.6	74	15.8	4.7

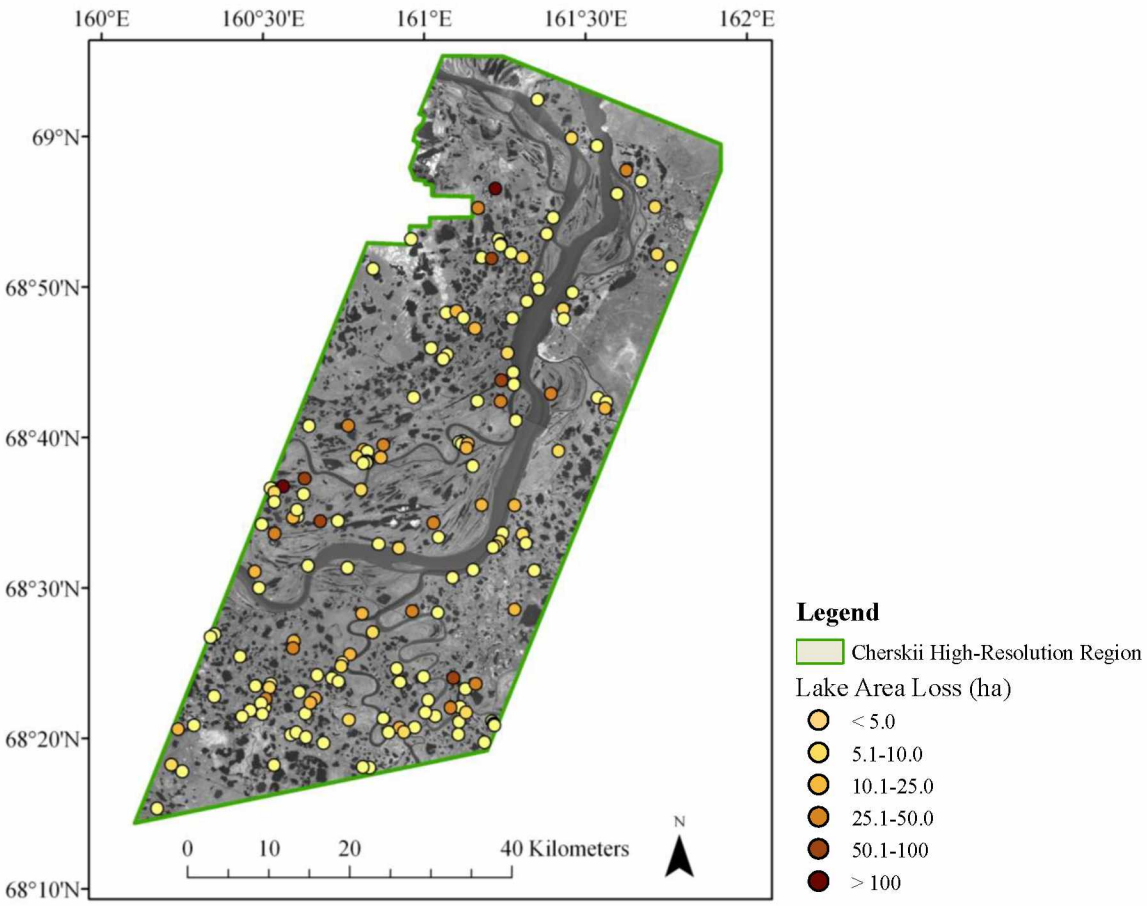

Figure 4.1.2.1.1. Location of L_{20} Lakes Shown by the Size of Lake Area Loss.

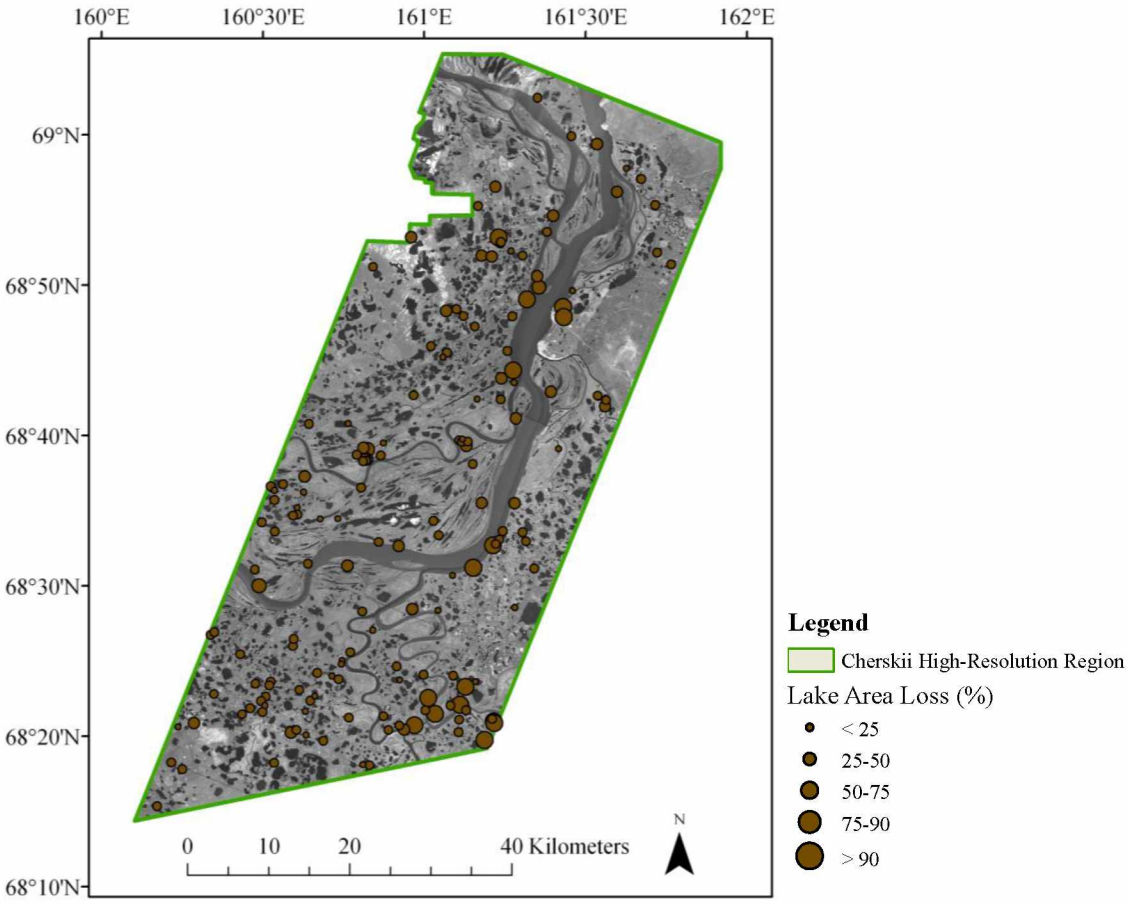

Figure 4.1.2.1.2. Location of L_{20} Lakes Shown by Percentage of Lake Area Loss.

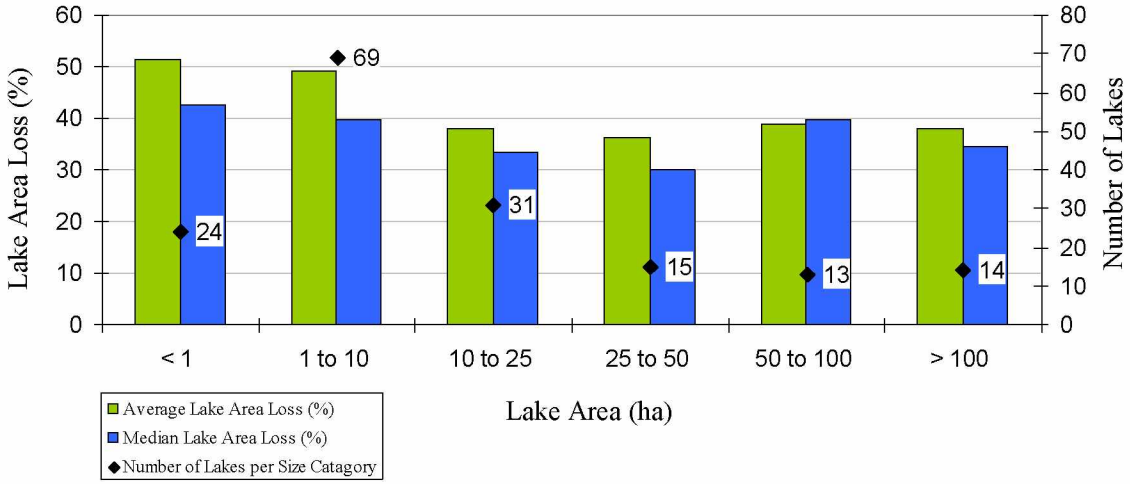

Figure 4.1.2.1.3. Mean and Median Lake Area Loss Related to Lake Area in the Cherskii Region. Lake size distribution is also shown. Smaller lakes show greater lake area loss then larger lakes.

When the lakes from the L_{20} subset were analyzed by geological unit (Table 4.1.2.1.2), *alV* sediments accounted for the largest amount of lake area loss, namely 0.70 ha per 100 ha of geological unit, which comprises 55.2% of the total lake area loss within the Cherskii region (Figure 4.1.2.1.4). This closely resembles the area loss accounted for by *alV* deposits in the Duvanny Yar region (49.9%). Alluvial sediments in the regions largely consist of sand-sized particles, which have higher hydraulic conductivity values and thus provide better drainage. Alluvial processes (i.e. flooding, erosion) also influence lake drainage. Alluvial deposits will have generally lower ice content as well due to the larger sediment size. Ice content is one factor that influences permafrost degradation and lake drainage. Less thermokarst processes will occur upon the thawing of ice-poor permafrost when compared to ice-rich permafrost.

The remaining geological units individually accounted for less than 16% of the total lake area loss in the Cherskii region; under 0.20 ha for 100 ha of geological unit. There were no L_{20} lakes in the *lb1V* deposits.

Table 4.1.2.1.2. Geological Analysis of L_{20} Lakes within the Cherskii Region. Geological analysis of L_{20} lakes greater than 0.5 ha within the Cherskii study region.

Geological Unit	Area (ha)	1965 Lake Area (ha)	2007 Lake Area (ha)	1965 Lake Area (%)	2007 Lake Area (%)	Lake Area Loss (ha)	Percent of Total Lake Area Loss per Unit (%)	Difference in Lake Area Loss per Unit (%)	Normalized Percent of Total Lake Area Loss Accounted for per Unit (%)
alV	227,548.9	4,054.6	2,451.7	1.8	1.1	-1,602.9	-91.0	-0.7	55.2
am1V	18,162.7	27.5	13.5	0.2	0.1	-14.0	-0.8	-0.1	6.0
dc/ds	578.9	18.8	12.4	0.1	0.1	-6.4	-0.4	0.0	3.1
el	2,967.1	2.9	2.0	0.5	0.4	-0.8	0.0	-0.1	11.2
la1V	2,387.8	3.2	0.5	0.1	0.0	-2.8	-0.2	-0.1	9.1
lb1V	16,114.9	0.0	0.0	0.0	0.0	0.0	0.0	0.0	0.0
$L111_{2-4}$	68,393.9	458.0	323.2	0.7	0.5	-134.8	-7.7	-0.2	15.4
Totals		4,565.0	2,803.4	-----	-----	-1,761.6	-100.0	-1.3	100.0

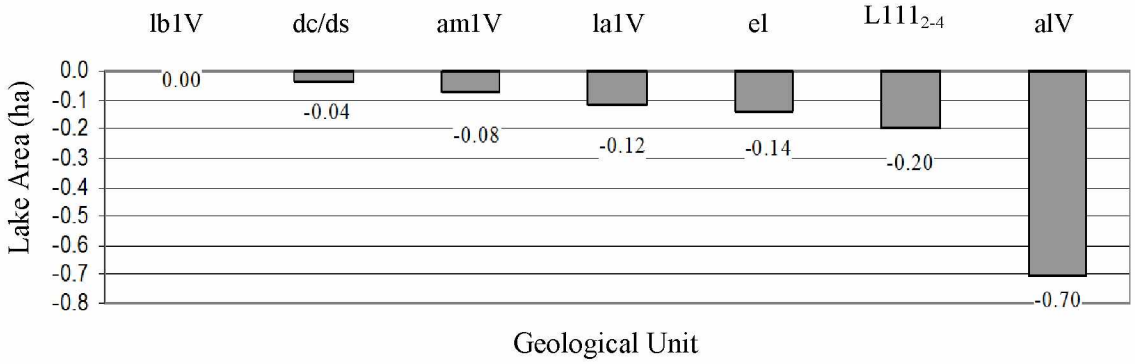

Figure 4.1.2.1.4. Decreased in Normalized Lake Area in the Cherskii Region. Decrease in L_{20} lakes area for 100 ha of geological unit.

4.1.2.2 DEM and Permafrost Analysis

According to the 1:200,000 DEM (Ferranti, 2009), the Cherskii region has an elevation generally less than 20 meters above sea level and therefore the majority of the lakes are located at lower elevations. Only five lakes were located at more than 20 meters above sea level. The data from the Circum-Arctic Permafrost Map (Brown et al., 1997), labels the permafrost in this region as continuous with mostly high ice content (> 20%). The coarse scale map places all the thermokarst lakes in the Cherskii region in the continuous, ice-rich permafrost zone. As with the Duvanny Yar region, relationships and affects of elevation and permafrost conditions on thermokarst lake behavior will be presented in the discussion.

4.1.2.3 Small-Lake Dynamics

Within the Cherskii region, three small regions that showed thermokarst lake development were chosen to verify that new lake formation was occurring. Two of the regions were in alluvial sediments and one in Yedoma (Figure 4.1.2.3.1). Between 1965 and 2007, new lakes formed in all three regions (Table 4.1.2.3.1). Changes in lake area within these regions are shown in Table 4.1.2.3.2.

Like for the Duvanny Yar region, these calculated rates of lake growth are not representative for the entire study region as these areas were specifically selected because they were experiencing new lake development, demonstrating that new lakes are forming in this area of the Kolyma Lowlands. As only lakes greater than 0.5 ha were mapped in the previous results, the majority of these new lakes would not be accounted for, as most are less than 0.5 ha in area.

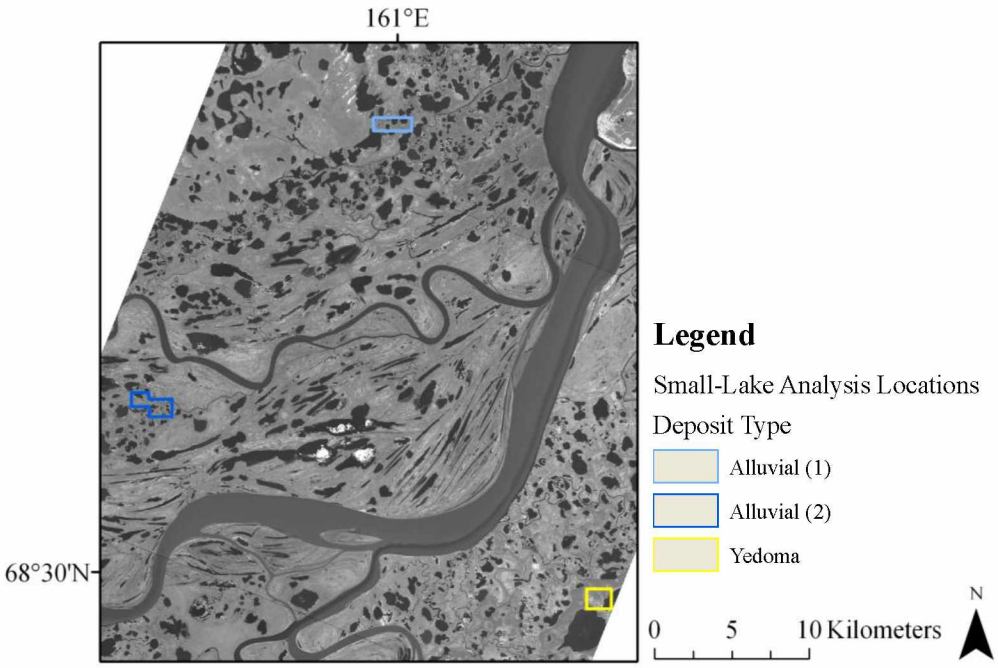

Figure 4.1.2.3.1. Location of Small-Lake Analysis Sites within the Cherskii Region.

Table 4.1.2.3.1. Development of New Lakes within the Cherskii Region. Lake distribution by size (ha) is shown along with the total increase in lake number.

Sediment Type	Lake Size (ha)	Number of Lakes 1965	Number of Lakes 2007	Change in Number of Lakes
Alluvial (1)	< 0.01 ha	0	8	8
	0.01 ha -0.05 ha	0	37	37
	0.05 ha- 0.1 ha	1	7	6
	0.1 ha - 0.5 ha	2	8	6
	0.5 ha -1 ha	0	3	3
	> 1 ha	6	6	0
	Total	9	69	60
Alluvial (2)	< 0.01 ha	0	12	12
	0.01 ha -0.05 ha	2	33	31
	0.05 ha- 0.1 ha	0	7	7
	0.1 ha - 0.5 ha	3	10	7
	0.5 ha -1 ha	2	9	7
	> 1 ha	6	6	0
	Total	13	77	64
Yedoma	< 0.01 ha	0	15	15
	0.01 ha -0.05 ha	5	18	13
	0.05 ha- 0.1 ha	2	5	3
	0.1 ha - 0.5 ha	4	2	-2
	0.5 ha -1 ha	0	1	1
	> 1 ha	1	1	0
	Total	12	42	30

Table 4.1.2.3.2. Change in Lake Area for the Small-Lake Analysis Locations in the Cherskii Region.

Sediment Type	Location Area (ha)	Total Lake Area 1965 (ha)	Total Lake Area 2007 (ha)	Difference (ha)	Linear Rate of Increase per Year (ha)	Linear Rate of Increase per Year (m^2)	Normalized Rate of Increase per Year (m^2 per 100 ha of geology)
Alluvial (1)	208.93	44.47	46.73	2.26	0.05	537.12	257.08
Alluvial (2)	273.65	43.28	49.22	5.94	0.14	1,413.24	516.44
Yedoma	203.67	37.07	37.15	0.08	0.00	18.77	9.21

Again, the following analysis does not account for lakes present in 1965 but had completely dried up by 2007 or for an increase in lake number that may have occurred because a larger lake dried into multiple smaller ones. These results reflect only the new lake formation that took place between 1965 and 2007. Alluvial (1) had 59 new lakes with a total area of 4.2 ha and Alluvial (2) had 67 new lakes accounting for 7.8 ha in total area. In Alluvial (2), 14 of the lakes were larger than 0.1 ha. In the Yedoma location, 41 lakes developed accounting for a total area of 1.7 ha. As with the Duvanny Yar region, the majority of these new lakes in the Yedoma are less than 0.05 ha.

New lakes within alluvial sediments were often larger and rounder than those which occurred within Yedoma deposits (Figure 4.1.2.3.2). Lakes developing in Yedoma deposits and thermokarst basins were often initiated within ice wedge polygon formations (Figure 4.1.2.3.3).

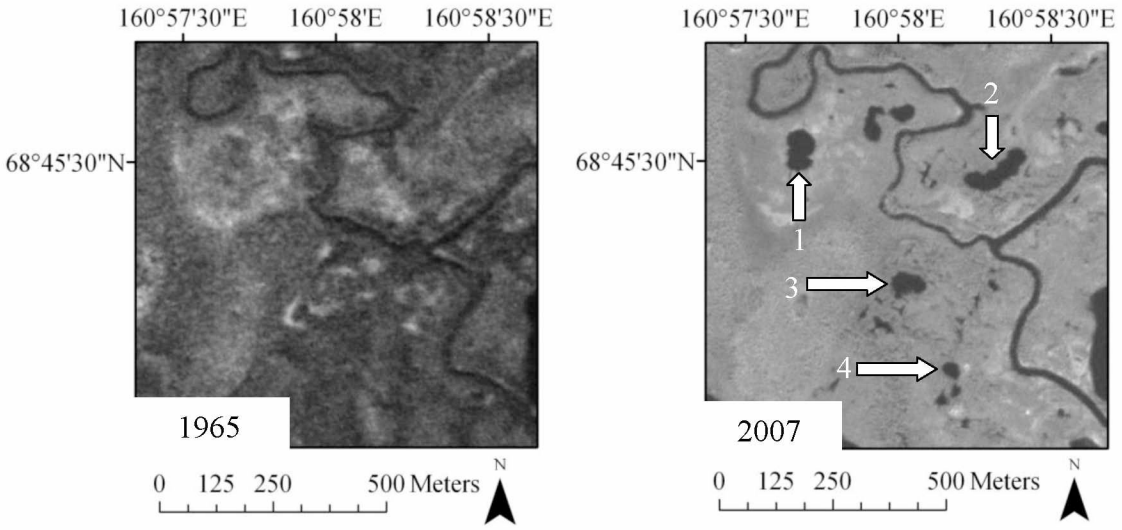

Figure 4.1.2.3.2. Lake Formation within Alluvial Sediments. Lake areas for the selected lakes are as follows: lake 1: 0.46 ha lake 3: 0.32 ha lake 2: 0.60 ha lake 4: 0.11 ha

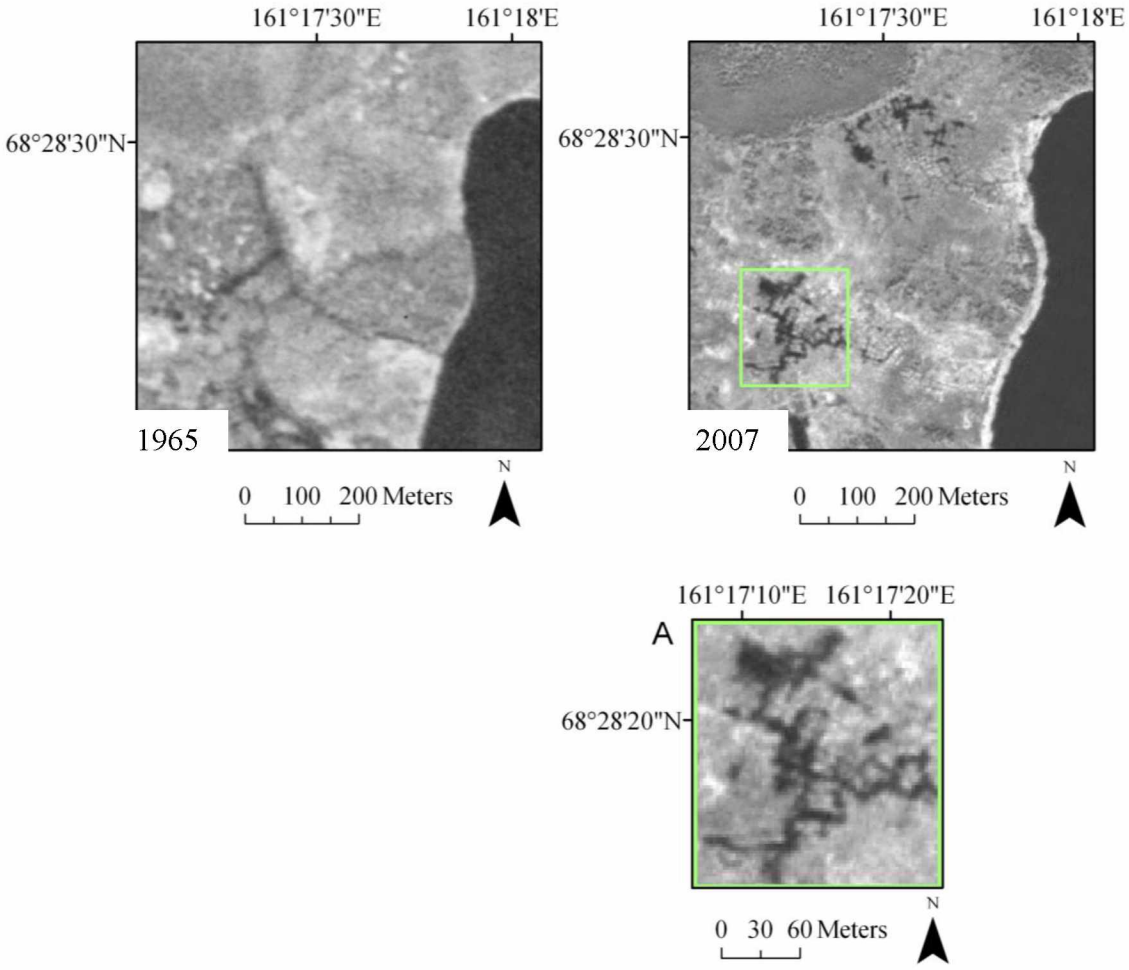

Figure 4.1.2.3.3. Permafrost Degradation within a Thermokarst Basin. This basin was located within the Yedoma geological unit. A. Subset from 2007 image showing lake development initiating within ice wedge polygons. With continual permafrost degradation and thaw, a thermokarst lake could develop. Water surface area within A is roughly 3.81 ha.

4.2 Lakeshore Erosion Rates in Yedoma Deposits

Erosion rates for lakes within the $L111_{2\text{-}4}$ deposits were calculated for both the Cherskii and Duvanny Yar regions (Figure 3.5.3.1). In the Duvanny Yar region, at least one transect on 858 lakes experienced erosion and in the Cherskii region, 647 lakes experienced erosion. Both regions showed similar rates of erosion occurring (Table 4.2.1). Processes that cause lake expansion include thawing of ground-ice around the lake perimeter and lakeshore erosion by wind-generated water currents crashing against the lake banks (Walter et al., 2006; Martin et al., 2009). In the Cherskii region, the southern most $L111_{2\text{-}4}$ deposit (designated as region A; Figure 4.2.1) is heavily affected by a network of small streams and rivers. Lake expansion rates in this region are strongly impacted by water level fluctuations related to river and stream annual cycles, suggesting that observed strong lake expansion is not erosion but largely flooding. The stream network and the many inlets and outlets greatly affect the water level of the lakes. Most thermokarst lake basins are closed systems and thus lake expansion is likely to be caused by permafrost thaw and bank erosion. That is not the case in region A. The lakes are not closed systems and lake levels rise and fall with river and stream volume. To avoid erosion rates being reported higher than what is actually occurring, region A was analyzed separately and was not included in the overall Cherskii Yedoma lakes erosion calculations.

Table 4.2.1. Average, Median, and Maximum Erosion Rates in the Duvanny Yar and Cherskii Region.

	Average Erosion Rate (m/yr)	Median Erosion Rate (m/yr)	Maximum Erosion Rate (m/yr)
Cherskii $L111_{2\text{-}4}$ Lakes	0.28	0.21	1.80
Duvanny Yar $L111_{2\text{-}4}$ Lakes	0.21	0.17	1.89

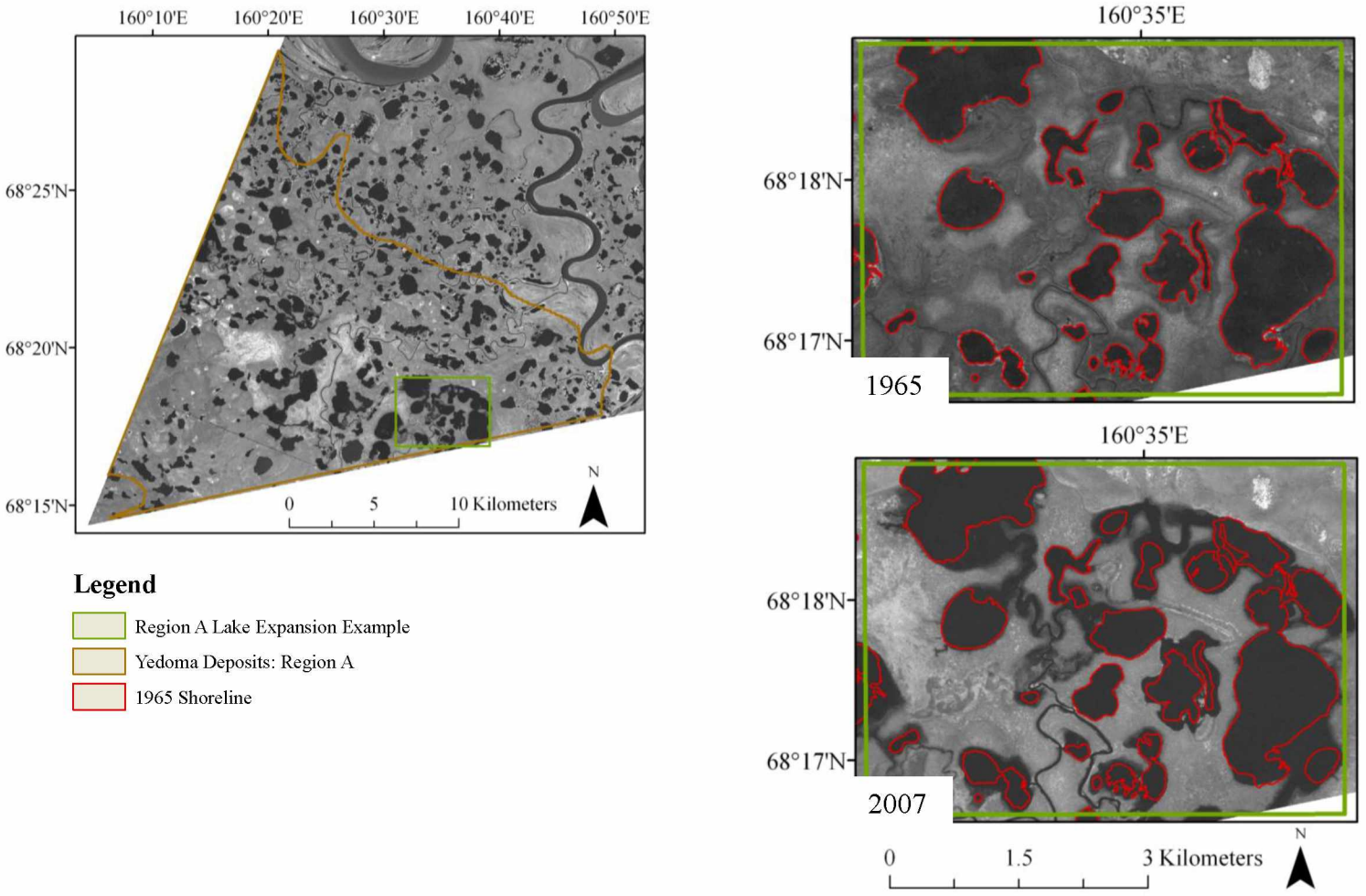

Figure 4.2.1. Lake Expansion Occurring in Cherskii *L111*$_{2\text{-}4}$ Region A. Lake expansion is caused by alluvial flooding.

On the satellite images, ALOS PRISM and Corona, the lake expansion regions occurring in region A are often lighter in color. This is caused by more radiation being reflected back to the sensor and less being absorbed by the water. The darker the spectral signature, the more pure the water is. The lighter spectral signature possibly indicates that the water is shallower and sediment loaded and probably indicates a flooding event, but not true erosion of the permafrost. The water has simply overflowed the lake banks and is covering the ground surface. It is not expansion due to erosion along the lake perimeter.

The average expansion rate for the Cherskii and Duvanny Yar study regions was 0.28 m/yr and 0.21 m/yr, respectively (Table 4.2.1). The maximum erosion rate for the Cherskii and Duvanny Yar regions is 1.80 m/yr and 1.89 m/yr, respectively.

Examples of the erosion occurring within Duvanny Yar and Cherskii Yedoma (excluding region A) are given in Figure 4.2.2 and Figure 4.2.3.

The scale of the geological map, 1:1,000,000 (Russian Geological Research Institute VSEGEI, 2000) is much smaller than the scale of the lake dataset (ground resolution of 2.5 m). Therefore, the $L111_{2\text{-}4}$ unit on the geological map contains Yedoma uplands, along with other geomorphological surfaces. These include thermokarst lake basins, small fluvial valleys, streams, and floodplains. Erosion rates for all the surface types located within the Yedoma unit on the geological map are included in the erosion rate calculations.

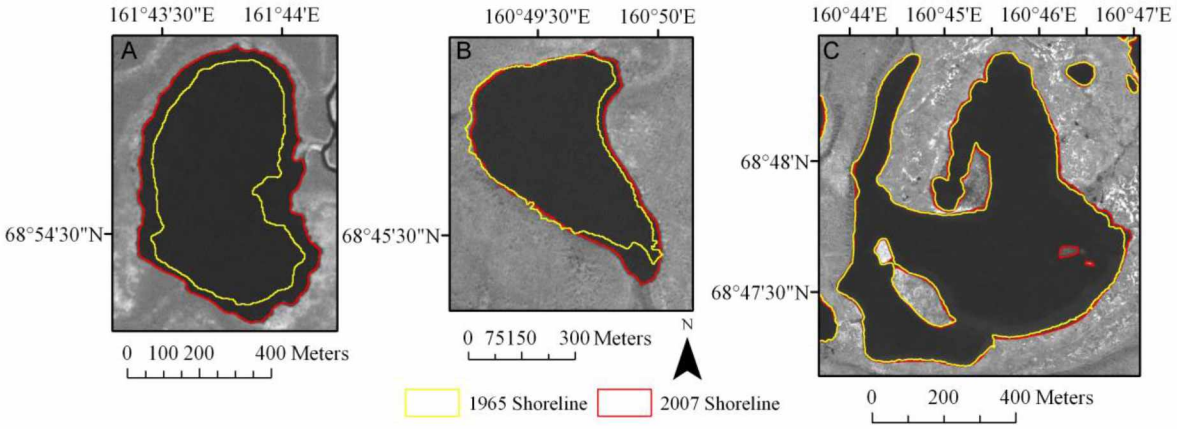

A. Erosion rates vary from 1.09 to 0.37 m/yr. Increase in area of 7.94 ha.

--- 1965: 20.72 ha
--- 2007: 28.66 ha

B. Erosion rates vary from 1.74 m/yr at the south tip to 0.53 and 0.23 m/yr on the east side. Minimal erosion was experienced on the west side. Increase in area of 1.48 ha.

--- 1965: 17.20 ha
--- 2007: 18.68 ha

C. Erosion rates vary between 0.03 and 0.71 m/yr. Area increased by 6.26 ha.

--- 1965: 247.96 ha
--- 2007: 254.22 ha

Figure 4.2.2. Cherskii Shoreline Erosion Examples. Image A, B, and C correspond to captions A, B, and C respectively

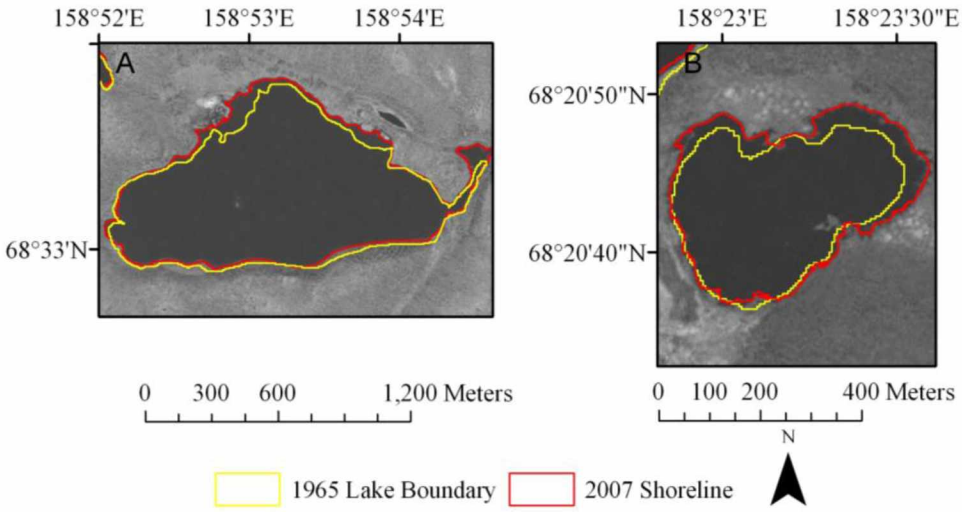

A. Erosion rates vary from 1.89 to 0.36 m/yr. South shoreline showed retreat. Increase in area of 3.90 ha.

--- 1965: 80.05 ha
--- 2007: 83.95 ha

B. Erosion rates were negligible on the west side while they vary from 0;47 m/yr to the north and 1.11 m/yr to the east. Increase in area of 2.17 ha.

--- 1965: 10.77 ha
--- 2007: 12.94 ha

Figure 4.2.3. Duvanny Yar Shoreline Erosion Examples. Figure A and B correspond to caption A and B respectively.

Section 4.3 Albedo

With changes in the ratio of land to water, changes in albedo can be expected. As surface vegetation changes from tundra to shrub to a forest of black spruce, and with increasing water area, albedo values will decrease (Harris, 2002; Hinzman et al., 2005; Jorgenson et al., 2010). Albedo values for dry, tundra vegetation average around 0.17 to 0.20 (Chapin et al., 2005; Jorgenson et al., 2010), while albedo values for shrub vegetation range around 0.15 and are close to 0.11 for a sub-Arctic forest (Chapin et al., 2005). The albedo for standing water is extremely low, around 0.05 (Jorgenson et al., 2010).

Using an average albedo value for tundra of 0.2 and an albedo of 0.05 for water, changes in albedo were calculated for both the Duvanny Yar and Cherskii high-resolution study regions (Table 4.3.1).

Table 4.3.1. Change in Albedo for the High-Resolution Study Regions. The values in the table below take into account only water volume of the thermokarst lakes greater than 0.5 ha.

Study Region	Total Study Area (ha)	1965 Area (ha)	2007 Area (ha)	1965 Total Albedo	2007 Total Albedo	Change in Albedo
Cherskii (All)	336,200.0			0.179	0.177	-0.002 (0.92%)
Land		289,085.1	285,392.7			
Water		47,114.9	50,807.3			
Duvanny Yar (All)	419,200.0			0.185	0.186	0.001 (0.43%)
Land		376,470.0	378,704.1			
Water		42,730.0	40,495.9			

In the Cherskii region, an increase in lake area of 3,622 ha resulted in a decrease in albedo of approximately 1%. In the Duvanny Yar region, a decrease in lake area of 2,238 ha resulted in an increase in albedo of almost 0.5%. These results are what is expected to occur based on the observed change in lake area.

4.4 Regional Study with Medium-Resolution Imagery

4.4.1 Lake Distribution in 2007

In the medium-resolution regional study area (Figure 3.5.2.1) there were 12,987 lakes greater than 5.0 ha in 2007 and 63.1% of these lakes were smaller than 25 ha (Table 4.4.1.1). This accounted for a total lake area of 703,319.4 ha. Although there are substantially more smaller lakes than larger lakes, the smaller lakes (less than 25 ha) account for less than 15% of the total lake area. Close to 50% of the lake area is from lakes larger than 200 ha (Figure 4.4.1.1).

Table 4.4.1.1. Lake Distribution for the Regional Study. Distribution of lakes larger than 0.5 ha for the 2007 lake layer.

	Lake Size (ha)	Total Lake Area (ha)	Total Lake Area (%)	Number of Lakes	Total Number of Lakes Accounted for by Each Size Category (%)
	< 10	29,054.6	4.1	4,045	31.1
	10 to 25	66,571.3	9.5	4,153	32.0
	25 to 50	77,942.6	11.1	2,199	16.9
	50 to 100	90,217.3	12.8	1,298	10.0
	100 to 200	101,816.9	14.5	734	5.7
	> 200	337,716.7	48.0	558	4.3
Totals	---------	703,319.4	100.0	12,987	100.0

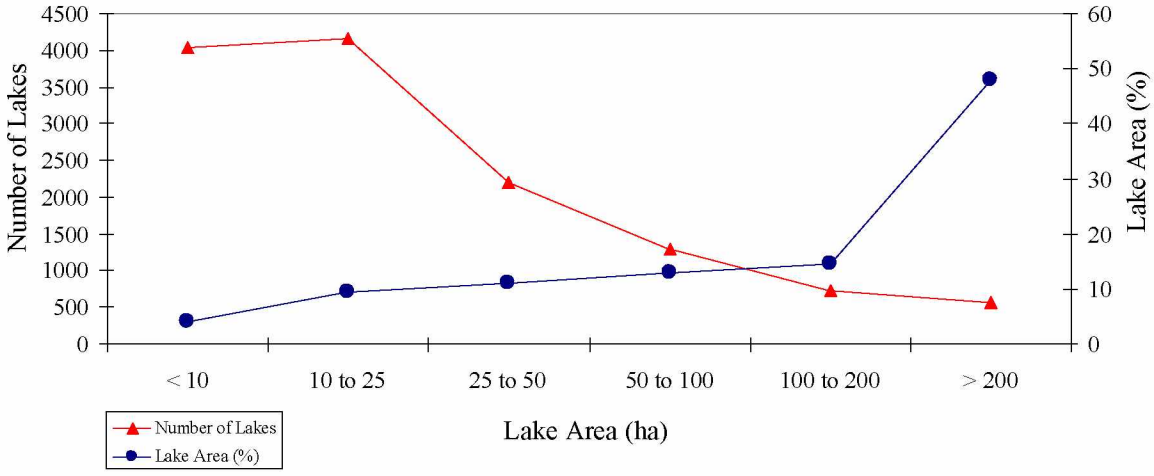

Figure 4.4.1.1. Lake Distribution for the Regional Study in 2007. Percent lake area distribution (right axis; blue line) is shown along with the number of lakes per size category (left axis; red line).

When the 2007 lakes were analyzed by geological unit, *am1V* deposits along with *lb1V* and $L111_{2\text{-}4}$ deposits accounted for the greatest amount of lake area (Figure 4.4.1.2).

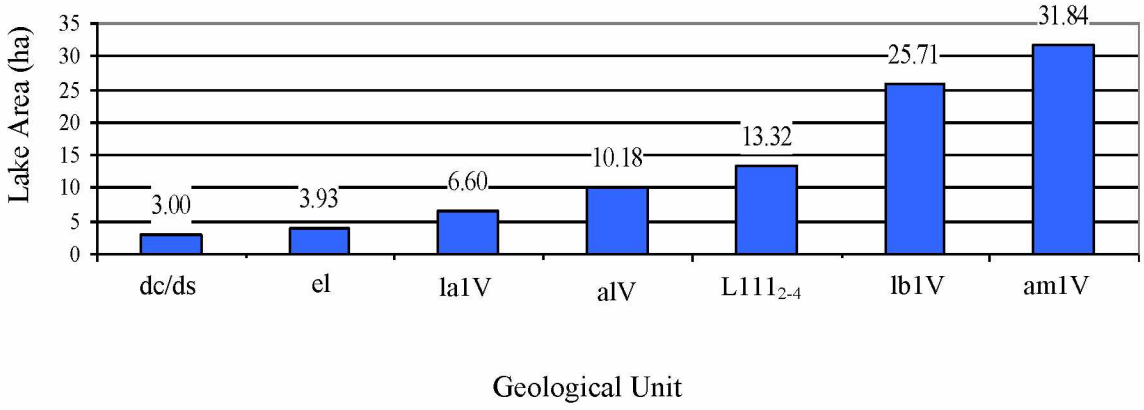

Figure 4.4.1.2. Limnicity by Geological Unit for the Regional Assessment.

4.4.2 Accuracy of TM 2006/2007 Lake File

To judge the accuracy of the medium-resolution regional study, which used Landsat images, lake areas from the 2006/2007 TM and the 2007 ALOS PRISM images from the Cherskii and Duvanny Yar regions were compared. The TM images date July 12, 2006 and July 10, 2007 and the ALOS PRISM images date July 29, 2007. For the Duvanny Yar region, lakes with an area greater than 5.0 ha on the ALOS PRISM images accounted for 37,274.4 ha. On the TM images, the lakes in the Duvanny Yar region greater than 5.0 ha accounted for 35,374.3 ha. Assuming the 2.5 m resolution ALOS PRISM images to be accurate, this is an underestimation of 1,900.1 ha (5.1%) of lake area or 19.0 km^2 on the TM data set. Upon visually scanning the two image sets for differences, the greatest discrepancies were found in two lake types: 1) lakes right around the 5.0 ha threshold were largely left out of the TM data set and 2) lakes in alluvial sediments nearest to the rivers. These lakes were usually narrow with a possible origin being an oxbow lake. These lakes often have slightly lighter spectral signatures on the TM image than lakes in the Yedoma deposits do. Areas for the lakes located within the Yedoma deposits are more accurately extracted from the TM images than are the lakes within alluvial deposits.

The Cherskii region had a much greater difference in lake area between the two image sets. On the ALOS PRISM images, lakes greater than 5.0 ha accounted for 47,375.1 ha of lake area while on the TM images, lakes greater than 5.0 within the same region accounted for 36,254.6 ha of lake area. This is an underestimation of 11,120.5 ha (23.5%) or 111.2 km^2 of lake area on the TM images. Like the Duvanny Yar region, many lakes around the 5.0 ha threshold and those nearest to the rivers were left out of the TM dataset. However, the majority of this underestimation is not from error in the digitizing of the lake boundaries on either image. The lake areas for the same lakes on the TM and ALOS PRISM image sets actually vary in size.

As described in section 4.2 of this thesis, lakes in the Cherskii region, especially the area designated as 'region A', which are connected to the river network experienced a high degree of possible lake area increase due to seasonal flooding caused by changes in

the river water level. In the TM image, these lakes were generally smaller than in the ALOS PRISM images (Figure 4.4.2.1). Likely, precipitation events between the two acquisition dates caused water level in the rivers and river tributaries to rise, thus strongly affecting those lakes connected to the river network in a short time period (less than 19 days). The Kolyma River, flowing thought the study region, also showed an increase in channel width between the two image sets. Increase in river width between July 10, 2007 and July 29, 2007, ranges from under 15 m to 73 m.

Lake areas were also inconsistent on what are presumably shallow lakes in alluvial deposits. The lighter spectral signatures of some lakes caused them to be reported as smaller than their actual size or not at all.

As a trend, the TM lake datasets underestimated lake area when Feature Analysts was used to extract the lakes. The mapping of lakes in uplands, away from rivers, streams, and tributaries was the most accurate. Long, narrow, sediment laden lakes, like those mostly found in alluvial sediments near rivers and their tributaries, were often left out or their area was underestimated in the automated extraction process. As the Cherskii region has more alluvial sediments and thermokarst lakes connected to the river network, the variation in lake area between the TM and ALOS PRISM images were expected to be greater.

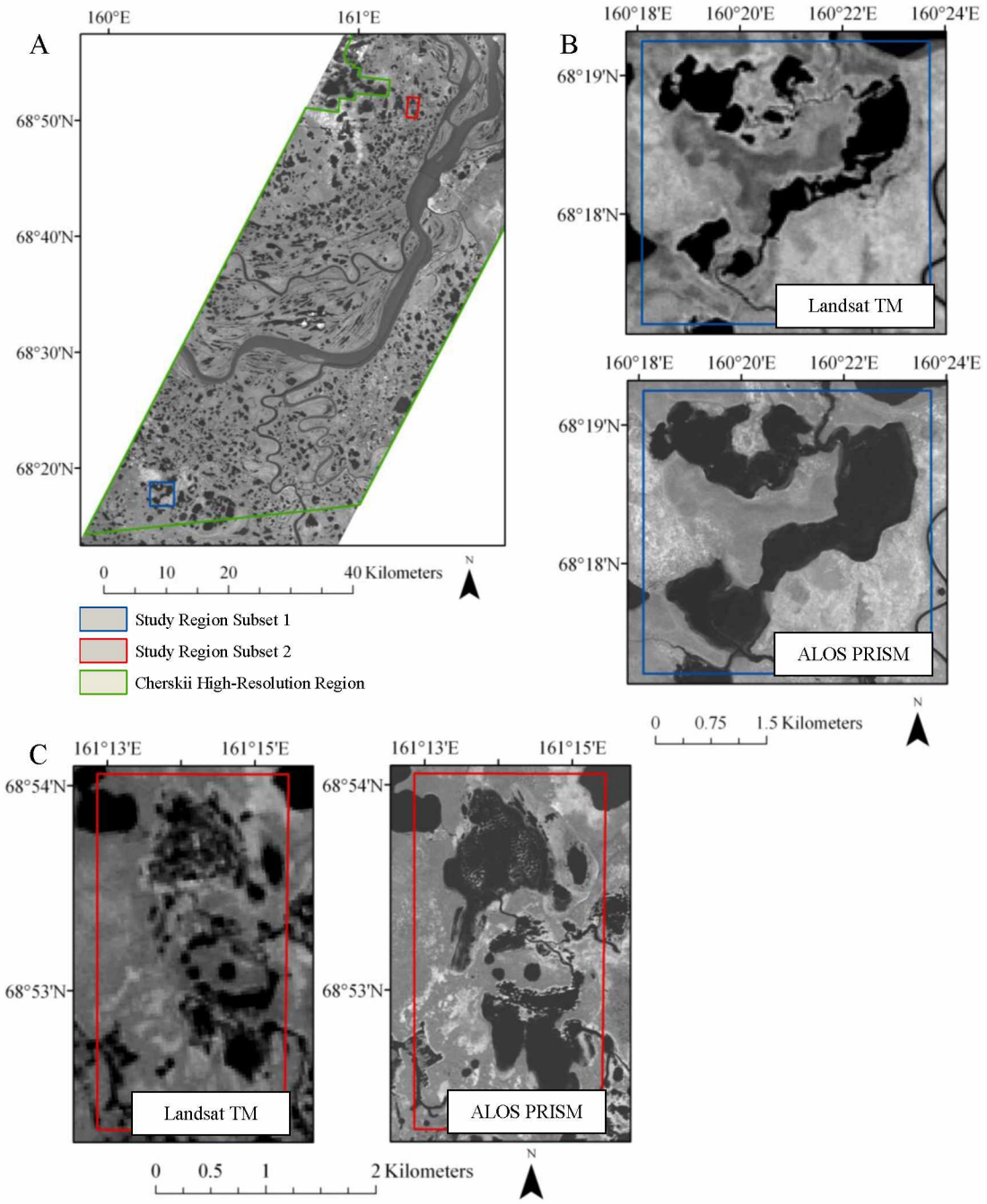

Figure 4.4.2.1. Discrepancies Between the 2007 ALOS PRISM and TM Images. A. Overview of the subsets in B and C within the Cherskii high-resolution study region. B. Difference in water levels of two lakes which are connected to the river network. C. Example of a varied spectral response in the TM images compared to a more uniform response for the same lake in the ALOS PRISM image.

4.4.3 Lakes Showing Substantial Area Loss

When analyzing the entire study region from 1965 to 2007, there were 409 lakes larger than 5.0 ha that experienced substantial lake area loss (greater than 20% of lake area, or larger lakes that loss a considerable area but less than 20%), and 65 lakes disappeared completely (> 90% area loss) (Table 4.4.3.1; Figure 4.4.3.1). In 1965 and 2007, the area of the lakes which showed substantial lake area loss was 39,928.2 ha and 25,678.8 ha respectively. This accounted for a lake area loss of 14,249.4 ha within this 42-year period (Figure 4.4.3.2).

Table 4.4.3.1. Distribution of Lake Area Loss in the Regional Study. Large lakes, greater than 200 ha, accounted for close to 50% of the lake area loss. Lakes smaller than 25 ha, although large in number, accounted for less than 10% of the total lake area loss.

	Number of Lakes	Lake Size (ha)	Lake Area 1965 (ha)	Lake Area 2007 (ha)	Lake Area Loss (ha)	Total Lake Area Loss Accounted for by Each Size Category (%)
	45	<10	344.9	47.4	297.5	2.1
	101	10 to 25	1,725.5	776.6	948.9	6.7
	90	25 to 50	3,267.2	1,985.3	1,281.9	9.0
	73	50 to 100	5,122.0	3,328.4	1,793.5	12.6
	57	100 to 200	7,848.4	4,528.8	3,319.5	23.3
	43	>200	21,620.2	15,012.2	6,608.0	46.4
Totals	409	-------	39,928.2	25,678.8	14,249.4	100.0

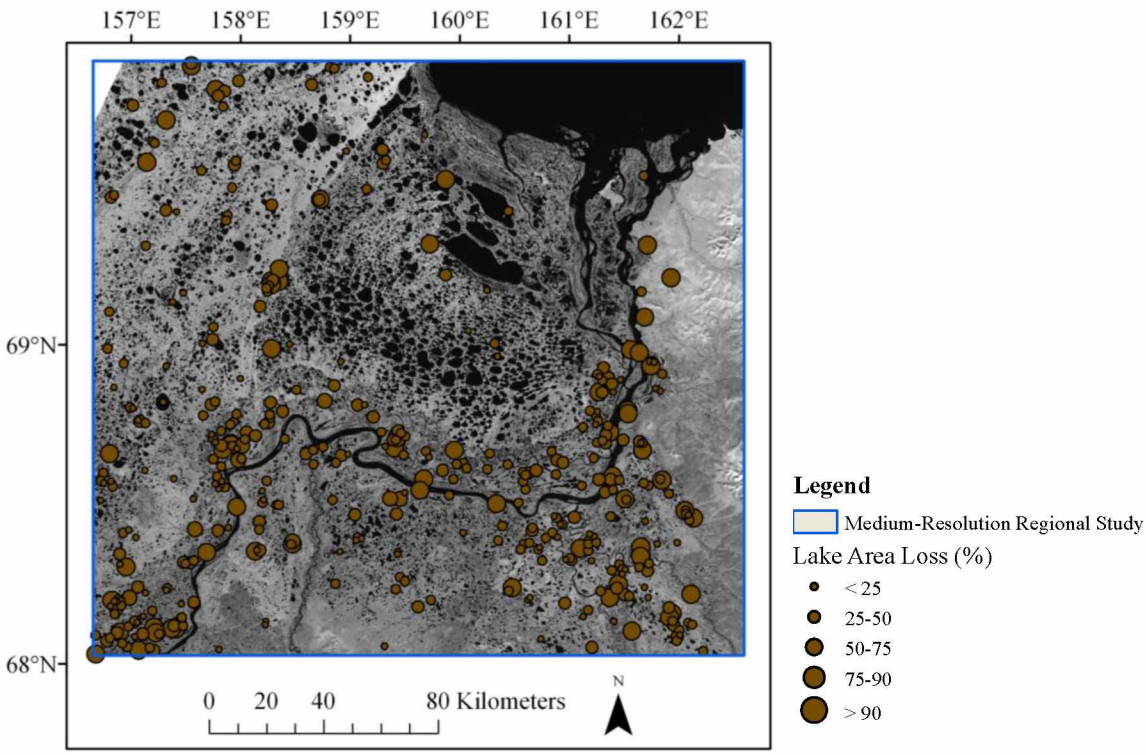

Figure 4.4.3.1. Lakes Exhibiting Substantial Area Loss by Percent Area Loss.

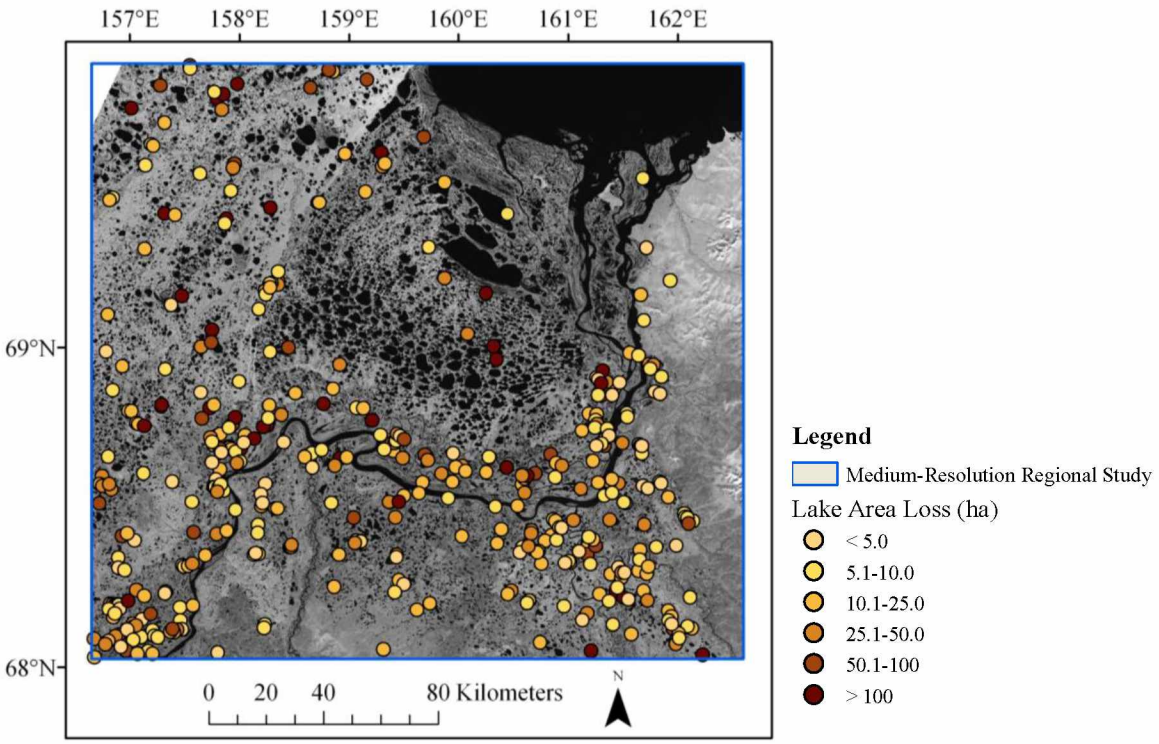

Figure 4.4.3.2. Lakes Exhibiting Substantial Area Loss by the Size of Area Loss.

Percent of lake area loss for the individual lakes was greatest in lakes smaller than 10 ha (Figure 4.4.3.3), 37 of the 45 lakes in this category completely disappeared. Of the 28 remaining lakes that completely disappeared, 25 were between 10 and 25 ha, and three were between 25 and 50 ha. Lakes greater than 25 ha in size experienced 50% less lake area loss than lakes with areas smaller than 10 ha.

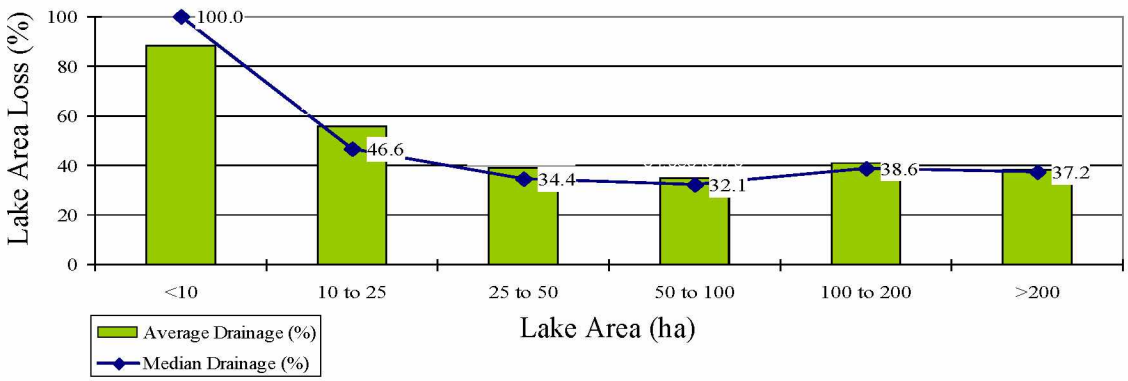

Figure 4.4.3.3. Percent Lake Area Loss Compared to Lake Size.

4.4.4 Geological Analysis of Lakes Showing Substantial Lake Area Loss

The regional assessment study region has seven different geological units present (Figure 4.4.4.1). Much of the assessment region (83.7%) is comprised of $L111_{2\text{-}4}$, *am1V*, and *alV* deposits. l*b1V* deposits make up 8.4% of the region. The majority of the *lb1V* deposits are scattered throughout the $L111_{2\text{-}4}$, *am1V*, and *alV* deposits.

lb1V deposits have the greatest normalized lake area (Figure 4.4.4.2). *alV* deposits have the second highest percent lake area and experienced the greatest lake area loss, -0.9%. This accounted for 36.0% of the total lake area loss in the assessment region. $L111_{2\text{-}4}$ deposits show a 0.2% decrease in lake area or 9.3% of the total lake area loss. Remaining statistical data analysis relating drained thermokarst lakes in the regional assessment to the underlying geology are presented in Table 4.4.4.1.

Like the Cherskii and Duvanny Yar study regions, the *alV* deposits accounted for the highest percentage of lake area loss (36.0%). Rates of lake area loss for 100 ha of *alV* deposits were 0.83, 0.70, and 0.86 ha in the Duvanny Yar, Cherskii and the regional assessment region respectively. *lb1V* deposits show substantial lake area loss as well, something not seen in the Cherskii and Duvanny Yar regions. For the *alV* unit, 292 lakes experienced substantial lake area loss, with an average lake size of 53 ha (median 26 ha). For the *lb1V* deposits, only 50 lakes showed substantial lake area loss. However, these lakes were much larger with average size of 168 ha (median 34 ha). Larger lakes experiencing drying would allow for a higher normalized rate of lake area loss.

dc/ds and *el* deposits, like for the Cherskii and Duvanny Yar regions, accounted for low percentages of the total lake area loss, both under eight percent. *am1V* deposits appear to be relatively stable. They showed a normalized decrease in lake area of 0.1 ha per 100 ha or 4.0% of the total lake area loss within this geological unit.

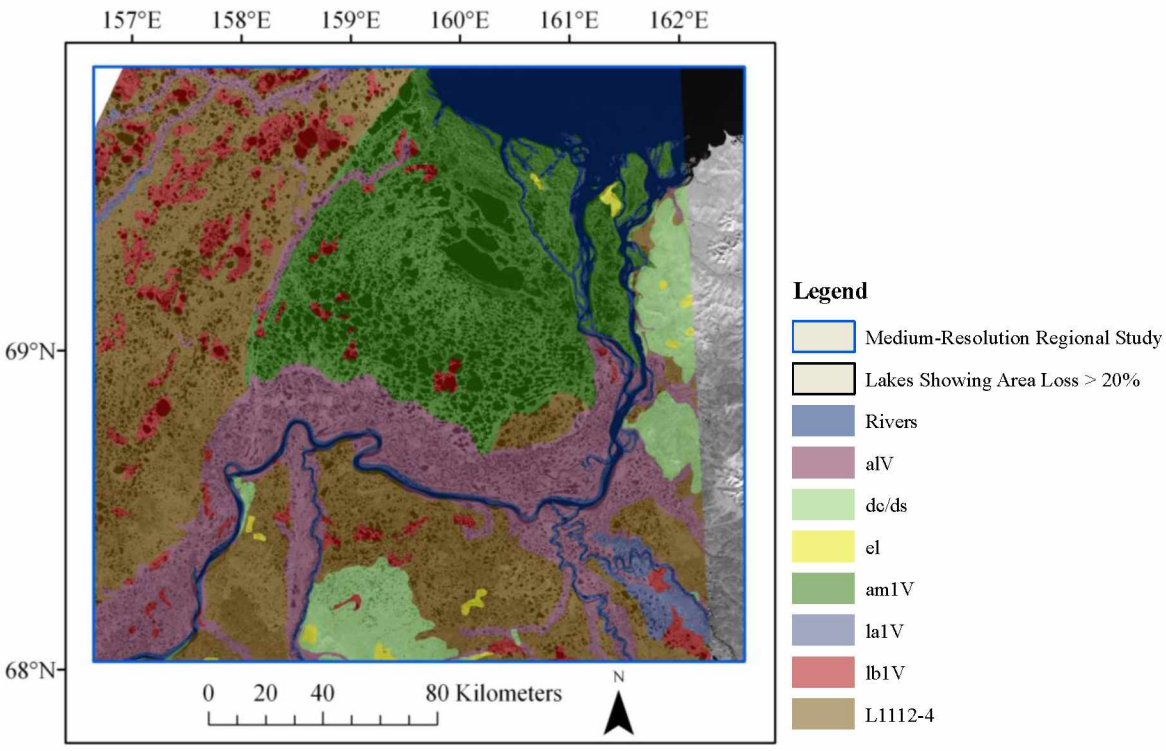

Figure 4.4.4.1. Locations of the 409 Drained Lakes by Regional Geological Unit. Geological map data is from Russian Geological Research Institute VSEGEI, 2000.

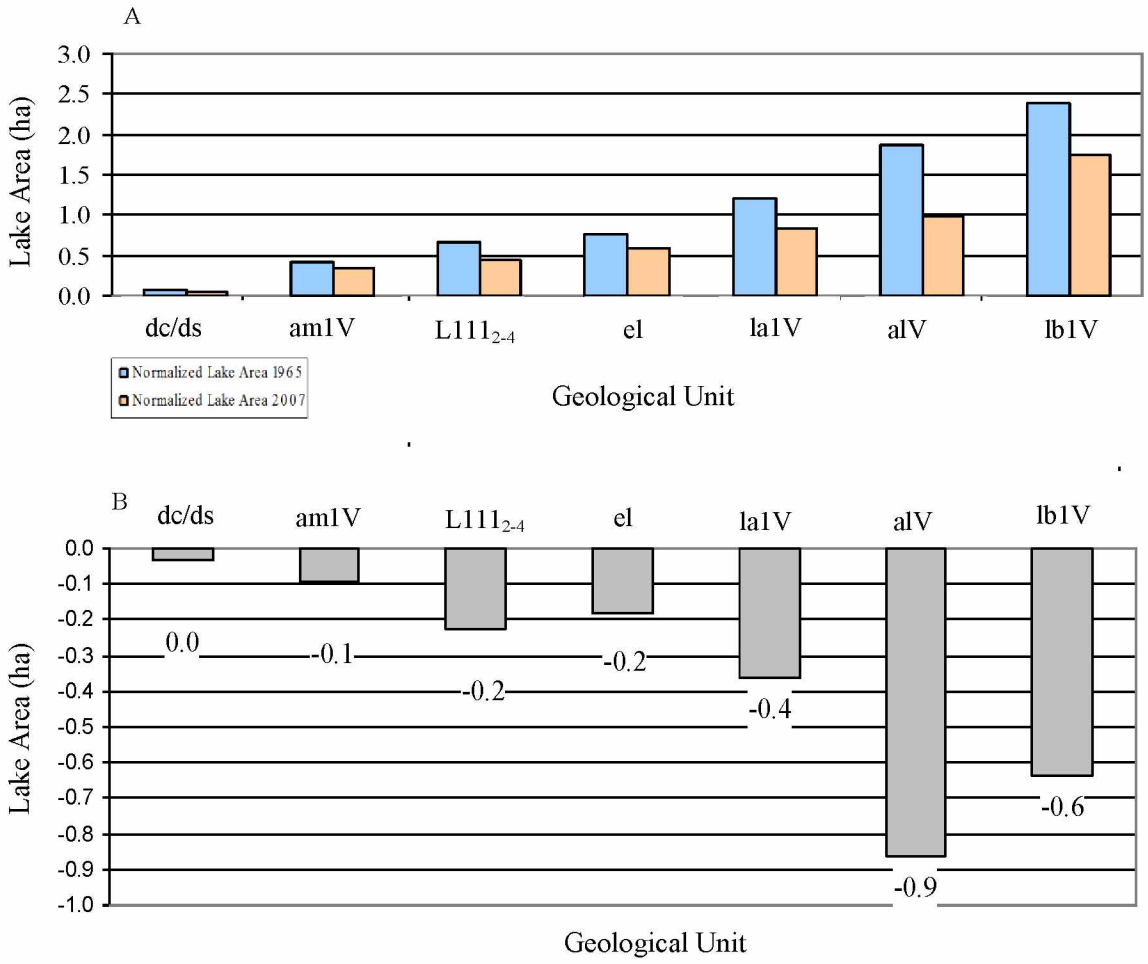

Figure 4.4.4.2. Normalized Lake Area for 100 ha of Geological Unit. A. Normalized lake area for each geological unit. B. Decrease in normalized lake area over the 42-year period for each geological unit. This analysis pertains to the 409 substantially drained lakes

Table 4.4.4.1. Geological Assessment and Lake Size Statistics of Lakes Showing Substantial Lake Area Loss.

Geological Unit	Area (ha)	1965 Lake Area (ha)	2007 Lake Area (ha)	1965 Lake Area per Unit (%)	2007 Lake Area per Unit (%)	Lake Area Loss (ha)	Percent of Total Lake Area Loss per Unit (%)	Difference in Lake Area Lost per Unit (%)	Normalized Percent of Total Lake Area loss Accounted for per Unit (%)
dc/ds	261,927.6	222.6	137.4	0.1	0.1	-85.2	-0.6	0.0	1.4
am1V	1,237,457.8	5,314.2	4,139.3	0.4	0.3	-1,175.0	-8.3	-0.1	4.0
L111 $_{2\text{-}4}$	1,449,480.3	9,585.2	6,353.1	0.7	0.4	-3,232.1	-22.8	-0.2	9.3
el	17,088.4	130.2	99.6	0.8	0.6	-30.6	-0.2	-0.2	7.5
la1V	55,298.1	663.1	461.5	1.2	0.8	-201.6	-1.4	-0.4	15.2
alV	837,339.9	15,565.2	8,335.0	1.9	1.0	-7,230.2	-50.9	-0.9	36.0
lb1V	352,696.9	8,403.2	6,151.7	2.4	1.7	-2,251.4	-15.8	-0.6	26.6
Totals		39,883.8	25,677.6	-----	-----	-14,206.1	-100.0	-2.40	100

4.4.5 Elevation Analysis of Lakes Showing Substantial Lake Area Loss

The 409 lakes that showed substantial lake area loss were analyzed by 20-meter elevation contours. Of these 409 lakes, 325 (79%), were located in lowlands with elevations less than 20 meters above sea level (Figure 4.4.5.1); 59 of the 65 lakes that completely disappeared were also located in such lowlands. Only eight lakes located at elevations of 60 m above sea level or higher exhibited substantial lake area loss. None of the substantially shrinking lakes were located above 100 m average sea level (a.s.l.) (Table 4.4.5.1.). This likely is also related to the overall small number of lakes in such higher elevations in our study region. Overall, there were only six lakes 100 m above sea level. The areas of these lakes are: 5.5 ha, 6.0 ha, 7.9 ha, 8.4 ha, 13.6 ha, and 16.5 ha. None of these lakes showed any substantial drainage.

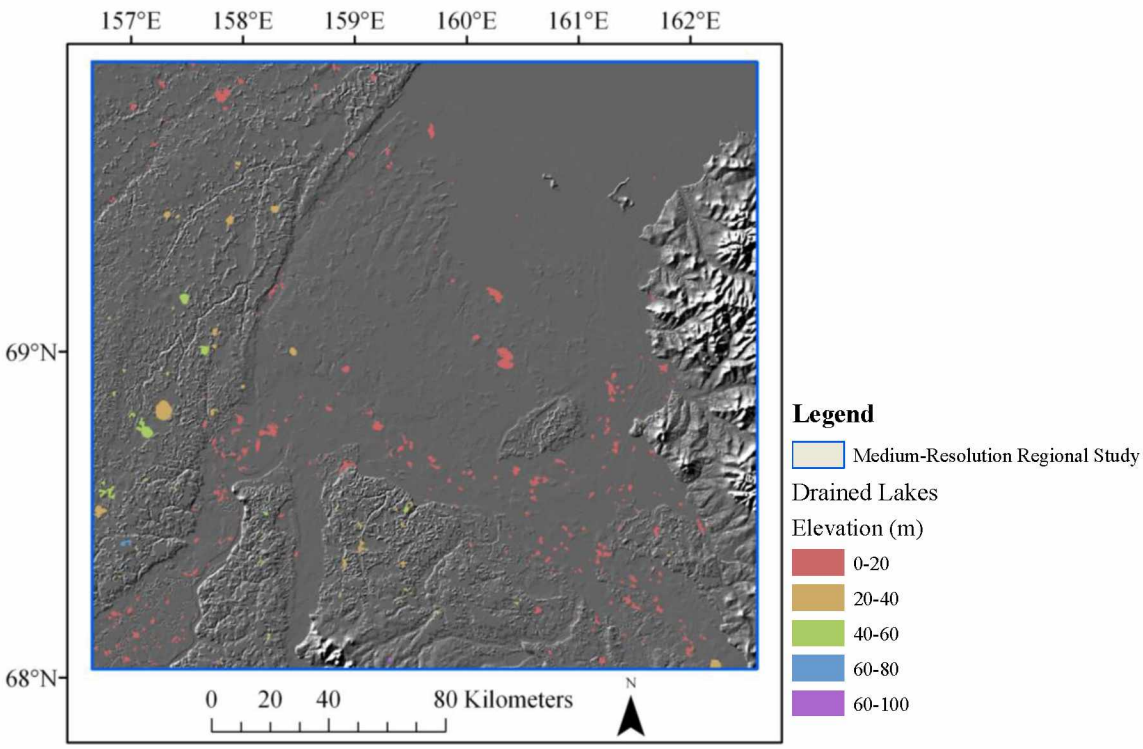

Figure 4.4.5.1. Elevation of Drained Lakes in the Regional Assessment Region. Lakes that showed substantial lake area loss are color-coded by elevation and overlaid on a hillshade.

Table 4.4.5.1. Elevation Analysis of Lakes Showing Substantial Lake Area Loss. No relationships were found relating percent drainage to elevation.

Elevation (m)	Number of Lakes	Number Completely Drained	Average Individual Lake Area (ha)	Median Individual Lake Area (ha)	Average Percent Drainage	Median Percent Drainage	Total Area 1965 (ha)	Total Area 2007 (ha)	Difference (ha)
0-20	325	59	81.7	36.2	49.6	44.1	26,543.0	15,514.7	11,028.3
20-40	36	0	227.0	76.9	34.1	30.1	8,171.2	6,308.8	1,862.4
40-60	40	4	119.1	44.2	36.2	29.8	4,762.4	3,546.8	1,215.6
60-80	7	2	49.8	15.4	52.8	48.4	348.3	227.1	121.2
80-100	1	0	103.3	103.3	21.2	21.2	103.3	81.4	21.8
Totals	409	65					39,928.2	25,678.8	14,249.4

4.4.6 Multi-Temporal Assessment of Lake Area Loss

Within the regional assessment, an area of 26,179 km^2 was cloud-free on all the image data sets. Within this zone, 211 lakes showed substantial lake area loss; 29 disappeared completely. These 211 lakes accounted for 22,380.9 ha and as a whole, showed a 34.3% decrease in lake surface area (Table 4.4.6.1). Figure 4.3.6.1 shows that lake area loss occurred at different rates throughout the observation period. A steeper slope represents a greater loss in lake area. The highest rate (271.5 ha/yr) occurred between 1980 and 1995, and the slowest rate (71.0 ha/yr) between 2002 and 2007 (Table 4.4.6.2).

Table 4.4.6.1. Rates of Lake Area Loss for the 211 Lakes within the Multi-Temporal Cloud-Free Zone of the Regional Assessment. Cumulative statistics using 1965 as the starting point.

Time Steps (years)	1965	1974	1980	1995	2002	2007
Total Lake Area (ha)	22,380.9	21,471.0	20,585.4	16,513.1	15,068.4	14,713.4
Percent Lake Area Lost Since 1965	0.0	4.1	8.0	26.2	32.7	34.3
Percent Lake Area Remaining (Starting Area:1965)	100.0	95.9	92.0	73.8	67.3	65.7

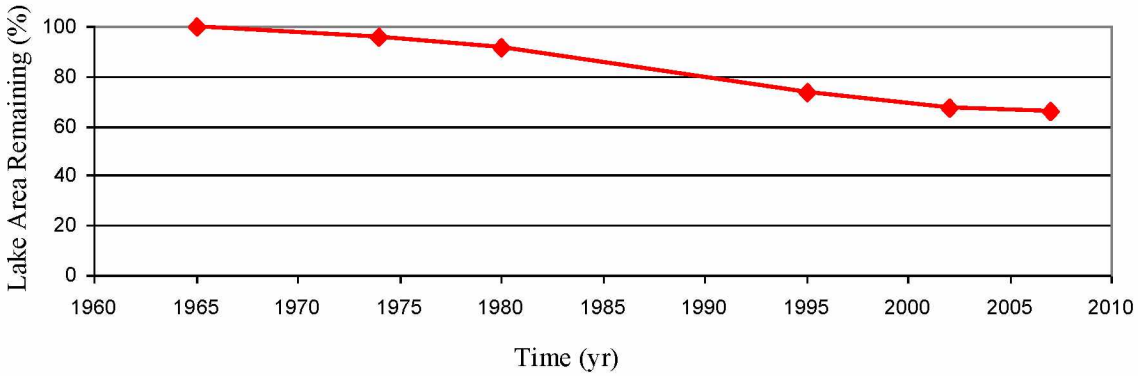

Figure 4.4.6.1. Lake Area Remaining with Time. Starting baseline: 1965.

Table 4.4.6.2. Lake Disappearance Rates for the Cloud-Free Image Region. Statistics were calculated between the individual time steps.

Time Steps (years)	1965	1974	1980	1995	2002	2007	Totals
Difference in Lake Area Between Consecutive Time Steps (ha)	0	909.9	885.5	4,072.4	1,444.6	355.0	7,667.5
Percent Lake Area Lost Between Consecutive Time Steps	0	4.1	4.1	19.8	8.7	2.4	
Number of Years Between Time Steps	0	9	6	15	7	5	42
Linear Rate of Lake Area Lost Per Year (ha)	0	101.1	147.6	271.5	206.4	71.0	

Of the 211 substantially drained lakes located within this cloud-free zone of the regional assessment area, 173 showed more than 20% lake area loss (L_{20} subset). The greatest linear rate of lake area loss (289.0 ha/year) occurred between 1980 and 1995. This was followed closely by the next time period, 1995 to 2002 (286.4 ha/year). The lowest linear lake area loss rate (91.2 ha/year) occurred between 2002 and 2007. These values vary slightly from the ones given in the table above as these only pertain to the

173 lakes from the L_{20} subset. The values previously listed are for all 211 lakes that showed substantial lake area loss. As an average trend for lake area loss, many lakes that decreased in area before 1995 began to stabilize and not continue to shrink after 1995. However, many other lakes had their initial episode of area loss between 1995 and 2002, giving that time period a high linear rate of lake area loss as well.

There are different trajectories of lake area loss occurring throughout the Kolyma Lowlands (Figure 4.4.6.2). Some lakes gradually decreased in area throughout the entire period from 1965 to 2007 (Figure 4.4.6.3), while others shrunk during a single time step, some early and some later. Some lakes disappeared completely or partially just to refill soon after. Still others disappeared completely and stayed empty.

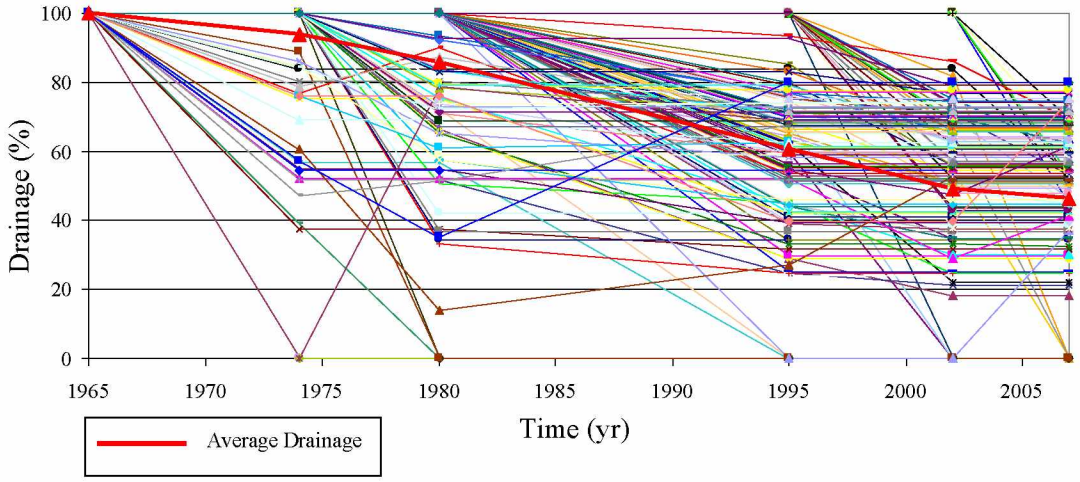

Figure 4.4.6.2. Lake Area Loss Patterns of the 173 Lakes which Showed L_{20}. With each line representing a single, individual lake, it is shown that between 1965 and 2007, numerous lake drainage patterns occurred.

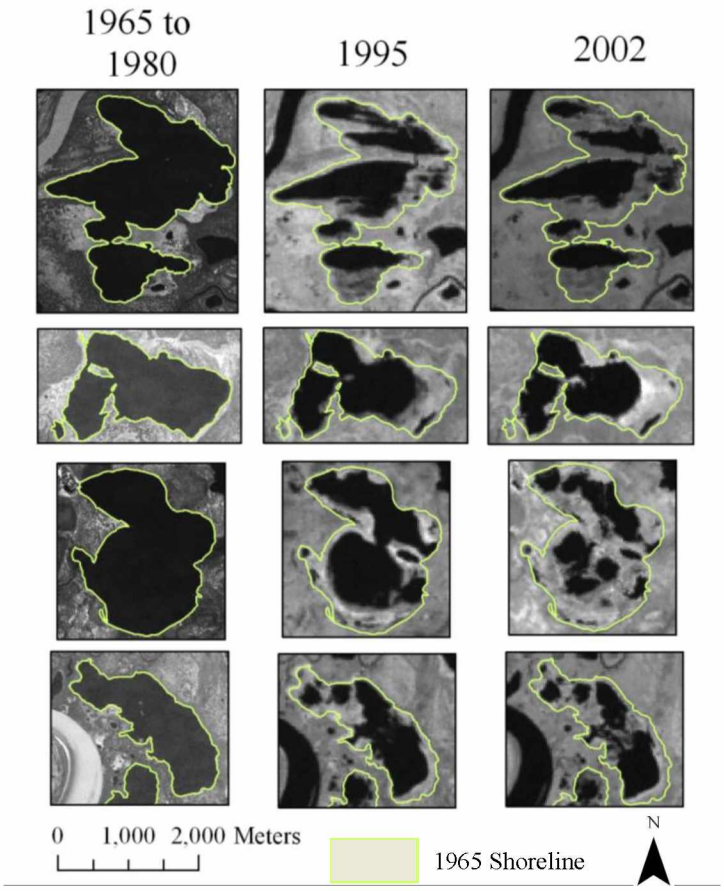

Figure 4.4.6.3. Four Lakes Showing Similar Lake Area Loss Patterns. These lakes experienced most of there area loss between 1980 and 1995. After 1995, a much smaller percentage of lake area was loss.

4.5 Climate Analysis

Temperature analysis from three weather stations around the Kolyma Lowlands, Cherskii, Bukhta Ambarcik, and Kolymskaya (Figure 3.3.3), all showed an increasing trend in the July mean monthly temperature and a decreasing trend in the January mean monthly temperature (Figure 4.5.1).

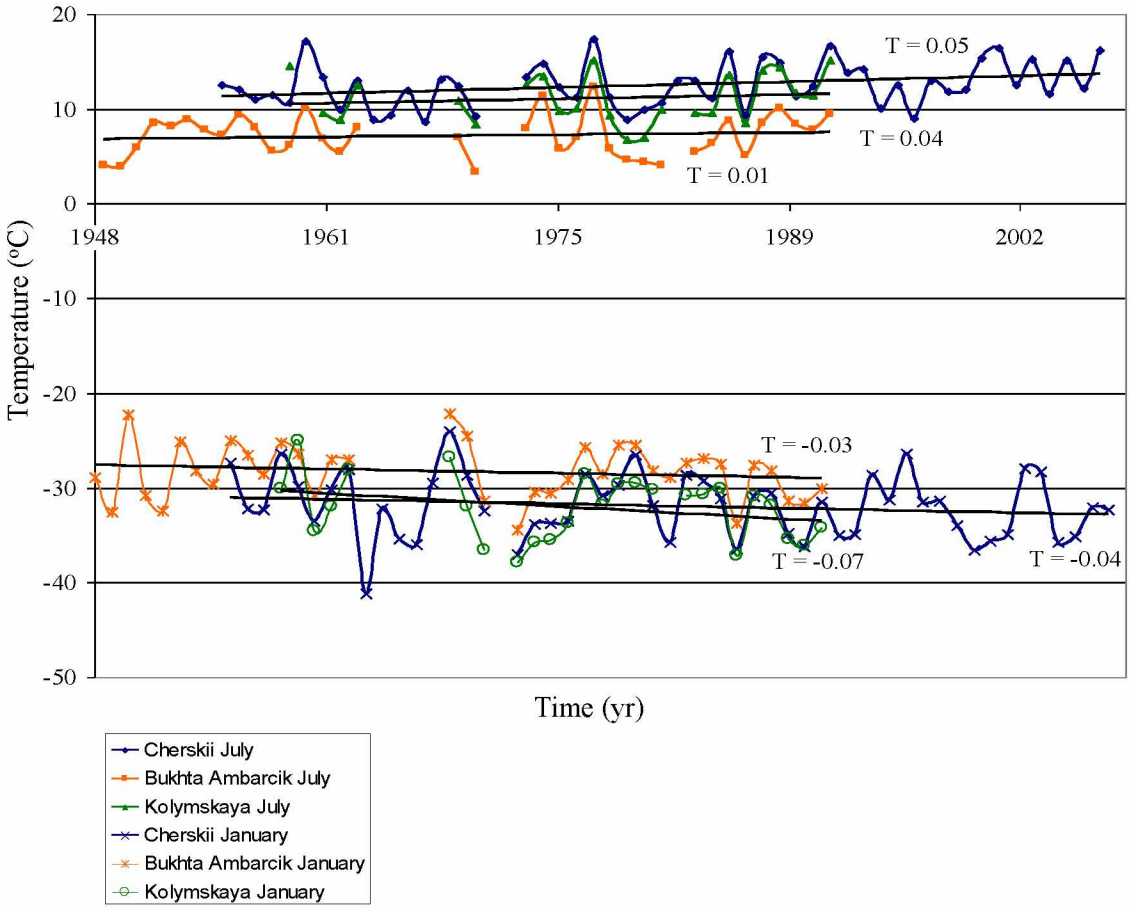

Figure 4.5.1. July and January Mean Monthly Temperatures.

Site	Latitude	Longitude	Elevation (m)
Cherskii	68° 75' 0"	161° 28' 3"	85.3
Kolymskaya	68° 73' 3"	158° 73' 3"	45.7
Bukhta Ambarcik	69° 37' 7"	162° 18' 0"	70.1

T = Linear temperature trend in °C/year.

Cherskii experienced an increasing trend in July mean monthly temperature over the period from 1955 to 2008; 0.05 °C year. Bukhta Ambarcik had an increasing trend of 0.01 °C/year from 1948 to 1994 and Kolymskaya had an increasing trend of 0.04 °C/year from 1959 to 2001. The average temperature for each weather station for the respective time period are as follows: Bukhta Ambarcik: 7 °C, Cherskii: 13 °C/year, and Kolymskaya: 11 °C.

Cherskii and Kolymskaya both had a mean January temperature of -32 °C. Bukhta Ambarcik was slightly warmer, averaging around -28 °C. All sites experienced a cooling trend in January mean monthly temperature; Bukhta Ambarcik experienced a cooling at the rate of -0.03 °C/year. Cherskii show a long-term trend around -0.04 °C/year while at the Kolymskaya station, the trend was around -0.07 °C/year.

The following analysis looks at the short-term temperature trends for individual time steps, which correspond to the image dates. The highest linear rate of thermokarst lake area loss occurred between 1980 and 1995. During this time period, from 1980 to 1991, the Kolymskaya and Bukhta Ambarcik sites showed a steep increase in July mean monthly temperature trends, 0.38 °C and 0.46 °C/year respectively. At the Cherskii site the entire time interval from 1980 to 1995 had a 0.13 °C/year increasing trend. However, if broken in two, from 1980 to 1991 the temperature was increasing with the rate of 0.29 °C/year. The highest periods of increasing temperature coincide with the highest linear rates of thermokarst lake drainage (Figure 4.5.2). The period from 1995 to 2002 also had a high rate of lake area loss. This stretch is following an increasing temperature trend and corresponds with the highest increasing temperature trend recorded at the Cherskii site (0.50 °C/year). The slight drop in the rate of lake area loss could be due to the sharp decreasing January mean monthly temperature trend (-0.94 °C/year). The January temperature trend for the previous time period was not nearly as strong (-0.33 °C/year) (Figure 4.5.3). A colder winter temperature would mean colder soil temperatures coming into summer. With colder soil temperatures, more solar radiation energy is needed to rise the surface temperature above freezing. Permafrost degradation will therefore be less severe than in years that have a warmer winter.

Between 1975 and 1980, there was a downward temperature trend at all three weather stations, the strongest being at Kolymskaya, -0.79 ^{o}C/year and the weakest being at Cherskii, -0.64 ^{o}C/year. The rate of lake area loss though was relatively high (147.59 ha/year). Two factors may have promoted drainage to occur. First, during this time period there was one year, 1977, which had an exceptionally warm July with temperatures 4 to 5 ^{o}C above average. Secondly, this time step was the only one to show an increasing trend in average January mean monthly temperature throughout the entire period (the later part of the Cherskii 1980 to 1995 time step did show an increasing temperature trend). A warmer winter air temperature would have allowed for warmer soil temperatures. With a warmer than normal January and July (1977) temperature 1) less heat energy would have been needed to warm the soil to above the freezing temperature and 2) there would have been a higher than normal amount of heat energy available. Combined, this could have allowed the permafrost to thaw slightly more than in the past creating a deeper active layer and thaw channels through which drainage could occur. In general, steeper warming temperature trends appear to coincide with higher rates of thermokarst lake area loss.

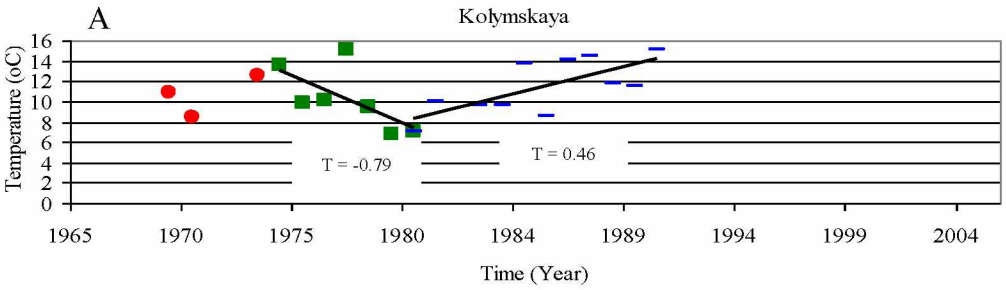

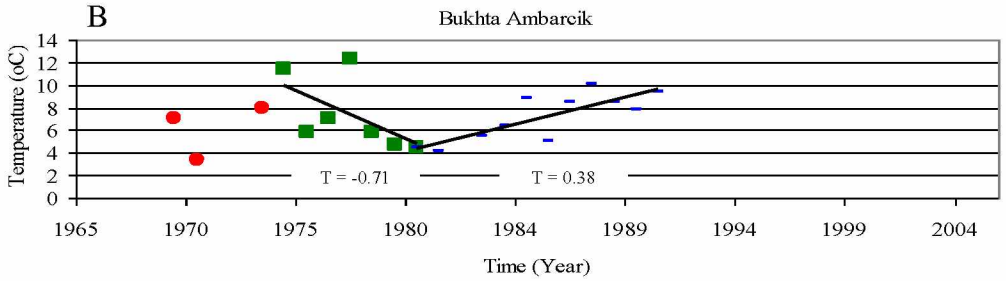

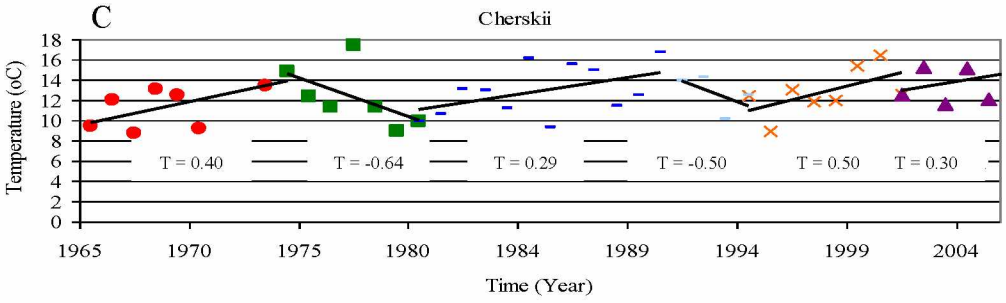

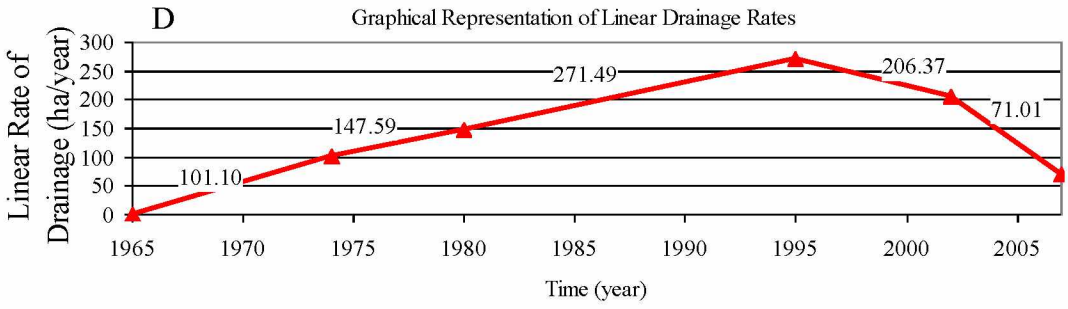

Figure 4.5.2. Average July Temperatures. Average July temperatures for weather stations in the Kolyma Lowlands (A-C). Rates of lake area loss are also shown (D) to allow comparison between linear drainage rates and temperature trends.
T = Linear temperature trend in ^{o}C/year

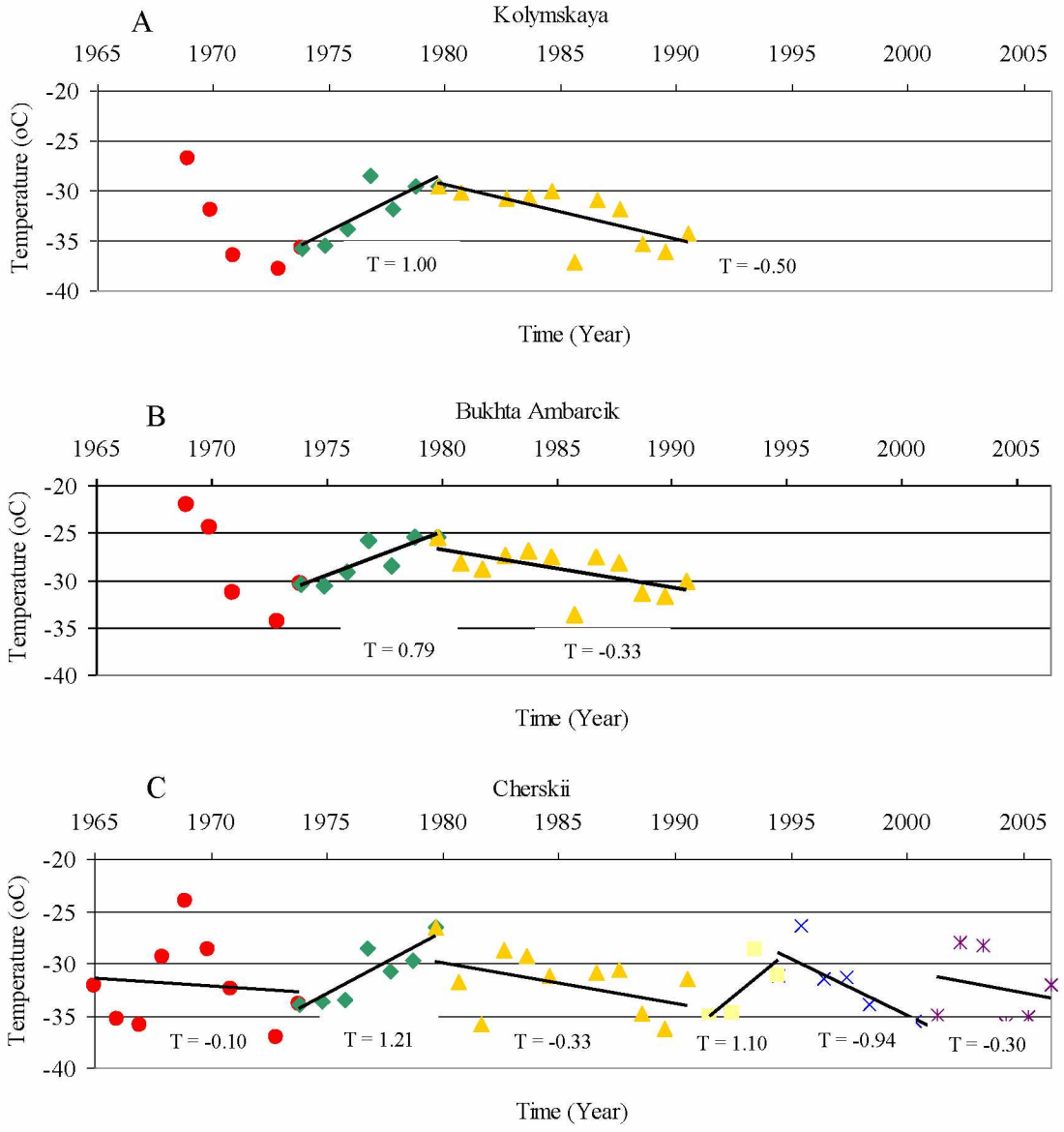

Figure 4.5.3. Average January Temperatures. Average January temperatures for three weather stations within the Kolyma Lowlands (A-C). Linear temperature trends are shown for each time step. The Cherskii weather station (C) between 1980 and 1995 is again split into two sections to allow for comparison with the other two stations.
T = Linear temperature trend in ^{o}C/year

Chapter 5: Discussion

5.1 Effects of Surface Geology and Geomorphology on Lake Distribution

When total lake area for the Kolyma Lowland region was analyzed by geological unit, the highest lake limnicity was found within the *lb1V* and $L111_{2\text{-}4}$ deposits. Both of these deposit types consist of silt (0.05 mm to 0.002 mm), clay (< 0.002 mm), and loam (a combination of sand (2.00 mm to 0.05 mm), silt, and clay particles) (soil particle and grain size information was obtained from the geological map (Russian Geological Research Institute VSEGEI, 2000)). Silt and clay have low permeability due to there small particle size which gives them low hydraulic conductivity and as a result produces poor drainage conditions. Loam, which is an unsorted material, also does not allow for good drainage as the pore space created by the largest particles is often filled by the smaller particles.

The *am1V* unit in the regional assessment region also showed high lake limnicity. These are highly permeable sand deposits but, nevertheless, many large stable lakes are found here. Perhaps the underlying geology is different than the surface geology and acts as an aquitard. This region is also not affected by a strong elevation gradient or a major river network thus keeping alluvial flooding and erosion to a minimum and pooling of water in lakes at a maximum.

The geological units with the lowest limnicity (*alV*, *el*, and *dc/ds* deposits) have larger grain sizes with sand, gravel (> 2.00 mm), and unrounded pebble (> 10.00 mm) sized particles. Larger particles have higher permeability and thus a higher hydraulic conductivity. Sand and gravel if not frozen would provide good drainage conditions, hinder lake development, and generally allow for low ice contents. *el* and *dc/ds* units are found at higher elevations with slope. Slope supports gravity-driven drainage limiting the occurrence of ponding. Higher elevations also have thinner overburden, a factor that would limit thermokarst lake expansion and growth. *alV* sediments had small lake sizes possibly due to the reworking of the sediments by river erosion and flooding. This likely prevents sediments from becoming stable long enough to develop large lakes.

Lake size is closely related to the distribution of lake area which is strongly affected by the surface geology. Those geological units with the highest limnicity often supported the largest lakes and had geological deposits which consisted of poorly drained silts, clays, and loam. The results described in Chapter 4 of this thesis support this conclusion.

5.2 Effects of Surface Geology and Geomorphology on Lake Dynamics

The greatest normalized amount of drainage occurred in the *alV* deposits and in the $L111_{2\text{-}4}$ unit. Lakes in the *alV* unit are highly affected by river flooding and meandering caused by erosion. These processes occur with changes in the rivers water velocity and volume. During times of high water and flooding, lake basins and other depressions in the river floodplain can easily flood with river water, and lakes connected to the river network may experience a back push of water and thus a lake level increase. When the river water level recedes, water can remain in the depressions creating a new, but possibly short-lived, arctic lake or pond. However, flooding and erosional processes can also cause lakes to drain. With higher water levels, lakes are more likely to overtop their banks creating drainage outlets. River erosion can also breach lake banks causing lake area loss.

The $L111_{2\text{-}4}$ unit also showed substantial lake area loss. A reason this unit shows substantial normalized lake area loss when compared to *alV* sediments may be because lake areas within *alV* deposits are expanding more quickly and new lakes are forming more rapidly due to the flooding and erosion patterns of the rivers. The refilling of depressions with water is not as prevalent in the Yedoma uplands. In addition, the scale of the geological map (1:1,000,000) (Russian Geological Research Institute VSEGEI, 2000) is much coarser than the scale of the lake data set (ground resolution 2.5 m). This means that the geological unit on the geological map, $L111_{2\text{-}4}$ for example, also contains other types of surface features, like alluvial plains and river valleys. More than only Yedoma surface deposit are located in the $L111_{2\text{-}4}$ map unit. An alluvial influence from rivers within the $L111_{2\text{-}4}$ unit may be the cause of the drainage of some substantially large lakes. The largest such lakes were 298.1 ha and 224.9 ha. There were also many other

lakes around 100 ha in size that experienced more than 20% loss of area. While many more lakes experienced lake area loss in the *alV* deposits, they were much smaller. The drainage of larger lakes would create a greater normalized lake area loss.

Another factor affecting lake dynamics is elevation. Higher elevations also have a thinner layer of soil to support lake development. These both hinder thermokarst lake formation. A region with lower elevation means there is very little slope present to encourage drainage and also, lower elevations allow river flooding and erosional processes to affect a larger area. The Duvanny Yar study region showed greater drainage possibly because of the steeper drainage gradient compared to the Cherskii region which has limited land surface elevation greater than 20 m above sea level.

Geomorphological features like mountains and rivers, uplands and lowlands, have been around for many millennia. However, in the last 50 years, lake dynamics have changed immensely. The presence of the permafrost table acts as an aquitard and prevents drainage (Ishikawa et al., 2005). Between 1954 and 2003, mean annual surface temperatures have increased between 2°C and 3°C in the arctic; winter temperatures for Siberia have increased 4°C (ACIA, 2005). This recent temperature increase has caused surface permafrost to start to degrade allowing increased groundwater infiltration and flow (ACIA, 2005). A lower permafrost table and a deeper active layer allow the geomorphological features to play a larger role in thermokarst lake dynamics. When the permafrost degrades, pore space, once filled with ice, thaws, opening up the soil allowing for increased permeability and possible drainage. Larger particles will have greater ice-free pore space to allow for greater lake drainage. The opposite is true for smaller particles.

5.3 Effects of Permafrost on Lake Distribution and Lake Dynamics

According to the Circum-Arctic Permafrost Map (Brown et al., 1997), the majority of the Kolyma Lowlands has continuous ice-rich (> 20% excess ice) permafrost. All lakes for this study were located within this region. The Kolyma Lowlands being labeled as all ice-rich is impractical. Factors like the surface geology, sediment and soil type, and the type of vegetation will cause differences to exist in ice content at a local

scale. With such low-resolution permafrost data available, spatial relationships between thermokarst lake changes and permafrost ice content and temperature cannot be studied in detail.

According to previous research (Jorgenson and Shur, 2007; Walter et al., 2007b), regions with low ice content will have limited thermokarst development upon permafrost thaw and degradation due to the limited surface subsidence that will occur. Ice-rich regions will experience substantial land subsidence and thus often have a higher limnicity.

5.4 Causes of Lake Area Loss

Many of the lakes, whether they disappeared completely or decreased in area partially during a single time step, appeared to do so catastrophically. One means of catastrophic disappearance is drainage by tapping of the lake bank by river erosion (Figure 5.4.1). Lakes also overtop their banks in times of high water (Are and Reimnitz, 2000; Brewer et al., 1993). This would cause drainage over the banks and start a process of downward erosion and the beginnings of a lake outlet (Mackay, 1988). Lake coalescence was also a common occurrence throughout the study region (Figure 5.4.2). A single lake may breach its bank and drain into a lower-lying, downstream lake (Harris, 2002). This rise in water level of the second lake would initially increase the lake area but it is often followed by the overtopping of its banks and the creation of a drainage outlet (Hinkel et al., 2007). Drainage outlets can be completely new, caused by downward erosion or further permafrost degradation, or be the enhancement of a previous outlet (Figure 5.4.3) (Mackay, 1988). Old drainage outlets can become blocked with sediment or no longer deep enough to continue draining the lake. Increased flow, water movement, and erosion can reopen or enhance an older outlet. In some circumstances, headward erosion of a river branch or stream will break through lake banks causing drainage into the river network (Hinkel et al., 2007). Other times, a river connecting multiple lakes could be the cause of drainage (Figure 5.4.4; Figure 5.4.5). If the lake outlet leading into the stream degrades enough to allow for excessive lake drainage, the water could flow into a second lake. This in return would increase the flow

of water out of the second lake (Hinkel et al., 2007). The higher volume of water could degrade the outlet enough to allow the second lake to drain through the river as well.

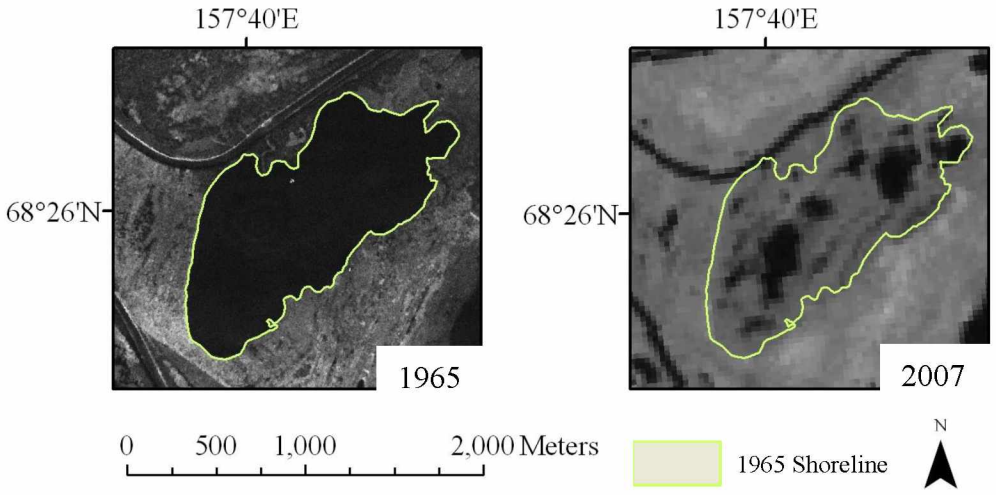

Figure 5.4.1. Lake Drainage by Riverbank Erosion. Lake area loss equals 94.6 ha.

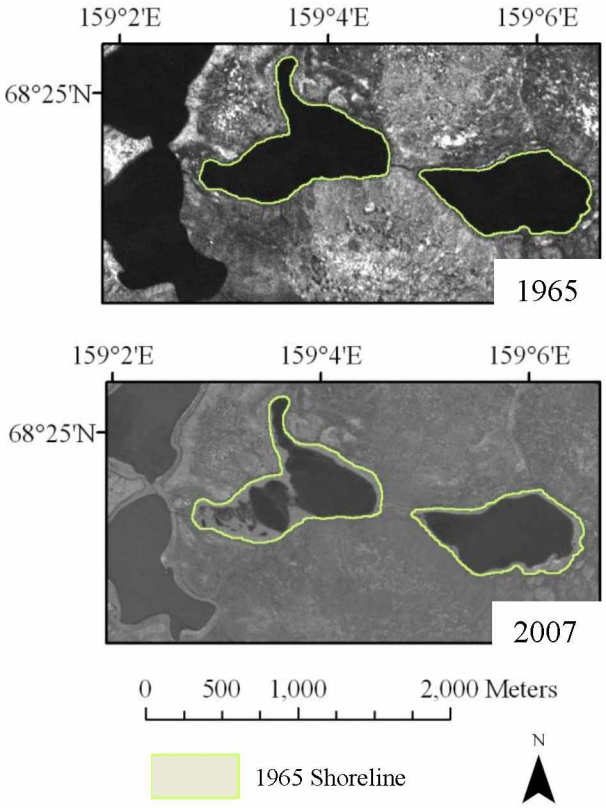

Figure 5.4.2. Lake Coalescence and Drainage. The lake on the far right drained through a small connecting channel into the middle lake, which drained into the larger lake on the left. Several more lakes downstream also drained, indicating that a cascade of lake drainages was initiated by the first drainage event.

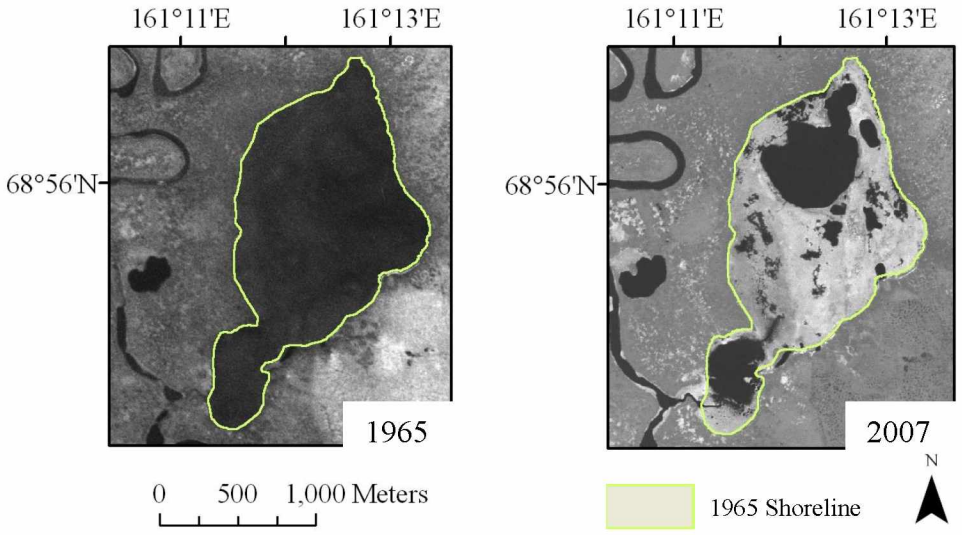

Figure 5.4.3. Lake Drainage by the Formation of a Drainage Outlet. Further degradation of an existing outlet decreased lake area by 127.8 ha.

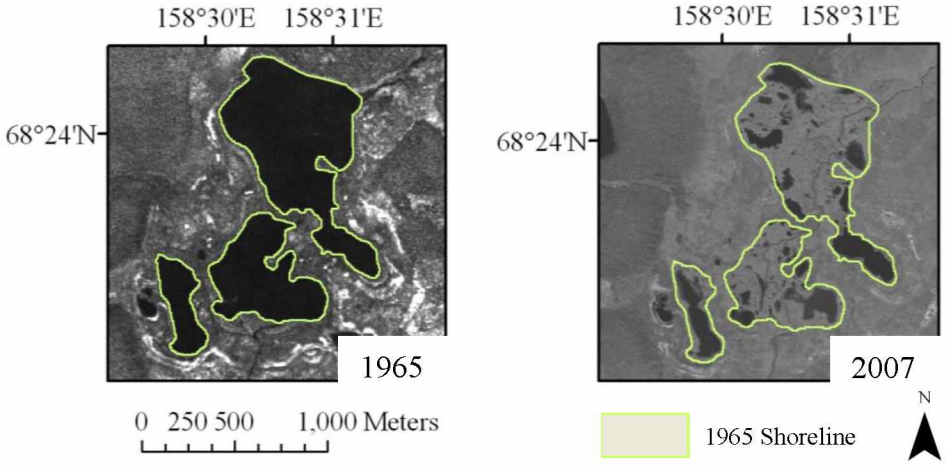

Figure 5.4.4. Lake Drainage Occurring by a River Connecting Multiple Lakes. Decrease in lake area of 60.0 ha.

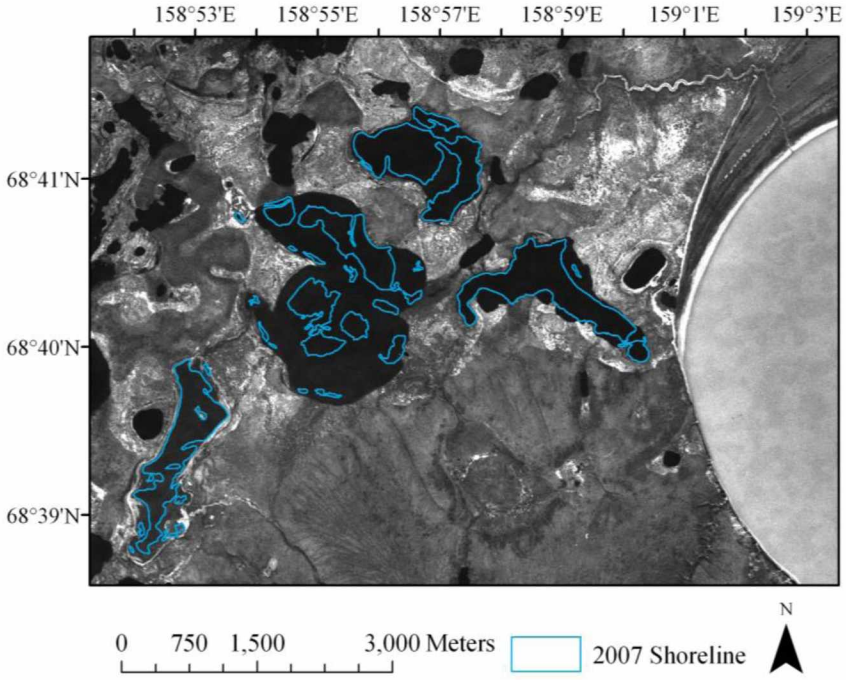

Figure 5.4.5. Drainage Occurring in Duvanny Yar *L111*$_{2\text{-}4}$ Unit. Base image is 1965. As seen in the image, all four lakes from L_{20} subset are connected by a stream (red line) which is draining into the Kolyma River on the right. Drainage could have occurred through this river. In the 2007 image (not shown) this river is not an obvious feature. The river may have dried up after the lakes drained, as the water source that fed the river was gone.

Some lakes drained by less obvious causes, one of which is subsurface drainage due to permafrost thaw (Marsh et al., 2009). This can be through interconnecting ice-wedge cracks (Mackay, 1988; Marsh et al., 2009) or complete thaw to the base of the permafrost layer. The latter is not likely to occur in the Kolyma Lowlands, where continuous permafrost is hundreds of meters thick. Water flow into thermal contraction cracks causes thermo-mechanical erosion of ice wedges at depth and allows drainage (Hinkel et al., 2007). Another possibility is drainage because of direct human impact. Two lakes in close proximity to the town of Cherskii completely drained, possibly due to human influence (Figure 5.4.6). Human influence could include vehicle traffic disturbing the surface and initiating permafrost degradation (Mackay et al., 1988) or intentional drainage of the lake by creating an outlet.

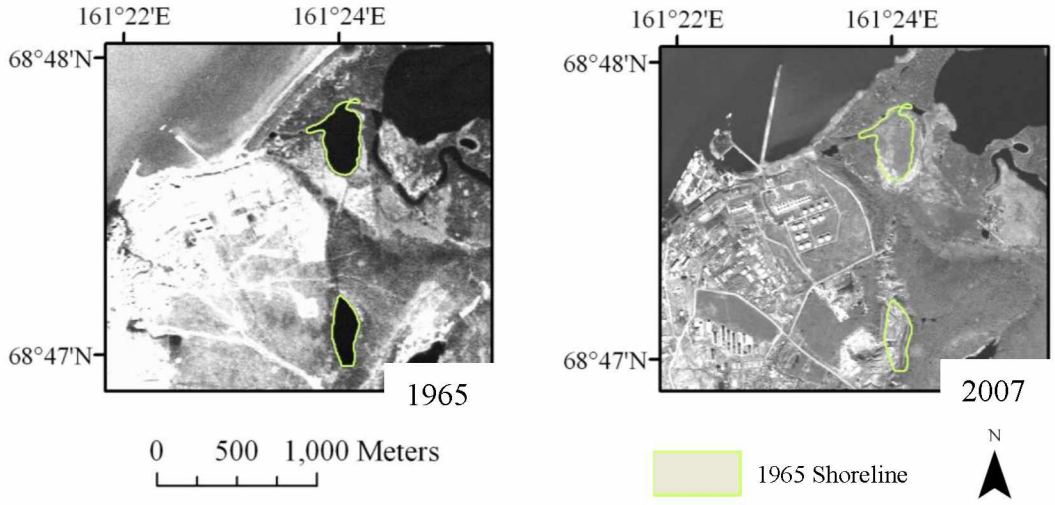

Figure 5.4.6. Drainage of Two Lakes near Cherskii. Possible drainage by human influence. The southern lake was artificially drained and is now being used as a landfill (personal communication, G. Grosse). The northern lake may have been artificially drained or there may have been a river influence. Combined lake area loss of 14.0 ha.

Besides lake drainage happening by the above-mentioned processes, lake drying can occur due to changes occurring to the arctic water balance. With increasing arctic temperatures, rates of precipitation and evaporation are likely to change (ACIA, 2005). Small and shallow lakes are the most susceptible to area changes due to changing climate conditions as they have low water volumes and high surface area to depth ratios (Smol and Douglas, 2007). Several lake change studies have been completed which showed lake drying being caused by changes to the water balance. Boike et al. (2008) recorded a disappearance of polygonal ponds in the Lena River Delta, Siberia during 1999. The cause was attributed to a negative water balance throughout the summer as a result of the limited precipitation. Riordan et al. (2006) saw an 11% decrease in closed basin ponds in Subarctic Alaska for the past 50 years. The cause was surmised to be increased evapotranspiration due to the increasing air temperatures. Smol and Douglas (2007) completed a study in the Canadian High Arctic on Ellesmere Island looking at lake changes that occur between the 1970's and 2006. Here, they noticed that ponds that had existed for many years were now drying; an increase in the evaporation/precipitation ratio was cited. In some cases however (Smith et al., 2005), lake drying is recorded despite parallel increases in precipitation.

Permafrost acts as an impermeable barrier to water infiltration. With continued permafrost degradation, water will be able to percolate deeper into the soil unrestricted (Yoshikawa and Hinzman, 2003). This may allow for less runoff and surface water to supply the wetlands and ponds with but it also could allow for groundwater recharge of the lakes (Yoshikawa and Hinzman, 2003; Zhang et al., 1999). A transformation from a permafrost to a non-permafrost arctic may cause a reduction of inland surface water by 40% (Smith et al., 2007). The rate of lake area loss in relation to the rate of permafrost degradation is uncertain, however, Smith et al. (2005) suggest that this could occur rapidly. Precipitation and evaporation data for this thesis research was not available for the Kolyma Lowlands. However, lakes that experienced drying were located near lakes that experienced little to no change in lake area. This suggests that the causes of lake

area loss were related to other factors than regional precipitation/evaporation balance (i.e. geology, permafrost degradation, river erosion, ect.).

5.5 Comparison with Previous Lake Change Studies

5.5.1 Comparison with Previous Studies on Siberian Lakes

Smith et al. (2005) studied an area of 515,000 km^2 in West Siberia and used a minimum lake size threshold of 40 ha. Between 1973 and 1998, the region experienced a net decrease in lake area of 6%, (92,000 ha). However, within the continuous permafrost zone, lake area showed an increase of 13,000 ha (12%). The number of lakes larger than 40 ha increased by 4%. The discontinuous permafrost zone showed a decline in lake area by 13%.

Walter et al. (2006) studied an area with continuous permafrost along the Kolyma River near Cherskii. The study area was 12,000 km^2 and located within the Yedoma geological unit. Between 1974 and 2000, there was an increase in lake area of 14.7%.

Veremeeva and Gubin (2009) studied an area of 6,500 km^2 that was located in the Kolyma Lowlands in Yedoma deposits. Lake changes were studied for the period between 1973 and 2009. All lakes larger than 0.1 ha were mapped. This study showed a decrease in lake area with the cause cited as a response to changes in the hydrological network. River valleys experienced the greatest reduction in lake area, 10.7%. Lake area in low-elevation Yedoma decreased by 6.6% while high-elevation Yedoma lake area decreased by 0.9%.

The results of this thesis research disagree with the conclusion that thermokarst lake area is increasing in continuous permafrost and decreasing in discontinuous permafrost as is stated in the Smith et al. (2005) study. The Duvanny Yar region, located all within continuous permafrost, showed a decrease in lake area of 5.23%. However, the 12% increase seen in continuous permafrost of west Siberia is on the same order of magnitude as the 7.84% increase in lake area seen in the Cherskii region. The fact that the Duvanny Yar region decreased in lake area could be due to difference in geology, permafrost, hydrological patterns, climate, and elevation.

The change in lake area of the Yedoma unit within the Cherskii region showed an increase of 12.4%, which very closely resembles the 14.7% increase in Yedoma lake area recorded by Walter et al. (2006). However, the Duvanny Yar region Yedoma unit experienced a net decrease in lake area. This could be a factor of elevation as the Duvanny Yar Yedoma uplands are not located at elevations less than 20 m above sea level like in the Cherskii region.

The Veremeeva and Gubin (2009) study agrees nicely with this thesis research. Alluvial sediments showed the greatest level of lake area loss throughout. The $L111_{2\text{-}4}$ unit drained less than the alV *unit*. The Cherskii lower-elevation Yedoma experienced greater lake area loss than the Duvanny Yar higher-elevation Yedoma. The overall trend in thermokarst lake changes agree. Alluvial sediments and lakes influenced by the river systems showed greater drainage than Yedoma sediments and those located at higher elevations.

5.5.2 Comparison with Previous Studies Completed within Alaska

5.5.2.1 Alaska Permafrost Conditions

Alaska's temperatures, soils, and permafrost properties allow for thermokarst development. In many ways, permafrost-related studies in Alaska can be compared to permafrost-related studies in Siberia. Alaskan surface permafrost deposits are of Pleistocene and Holocene age with the development of the current landscape, thermokarst lakes and basins, initiated primarily in the Holocene (Hamilton et al., 1983; Hinkel et al., 2003; Shur and Jorgenson, 2007; Jorgenson et al., 2008). The Arctic Coastal Plain and the Seward Peninsula are two regions heavily affected by permafrost and thermokarst processes. Between 15% and 40% of these regions are occupied by thermokarst lakes (Hinkel et al., 2005). Similar ice-rich, wind blown sediments, like the Siberian Yedoma, exists in parts of these regions (Zimov et al., 2006; Walter et al., 2007a). Mean annual air temperatures for Alaska vary from below -10.0 ^{o}C for the Arctic Coastal Plain to -6.0 ^{o}C on the Seward Peninsula to -3.5 ^{o}C for the central interior (Brown et al., 2000; Riordan et al., 2006; Plug and West, 2009; Wendler et al., 2010).

Permafrost of the Arctic Coastal Plain is continuous and measures between 300 and over 600 m in depth (Hopkins et al., 1955; Hinkel et al., 2005). The upper 20 meters have an ice content greater than 20% and active layer depths vary between 0.2 m and 0.8 m (Brown et al., 2000). The northern Seward Peninsula also lies in the continuous permafrost zone. The permafrost depth ranges from 5 m to over 85 m. The southern portion of the Seward Peninsula is in the discontinuous permafrost zone with permafrost thickness commonly between 30 m and 60 m. Active layer depths for the Seward Peninsula are between 0.53 and 0.73 m (Brown et al., 2000). The permafrost in central Alaska is discontinuous (Shur and Jorgenson, 2007) and has depths between 15 and 70 m. Active layer depths are greater than 0.40 m (Brown et al., 2000).

5.5.2.2 Comparison with Previous Studies on Alaskan Lakes

Riordan et al. (2006) looked at closed-basin lakes and ponds at several different locations throughout Alaska using various Landsat and aerial photos. Lake changes occurring between the 1950s and 2001/2002 were analyzed. All the study sites were located on alluvial or lacustrine plains with slopes no greater than five percent; lakes larger than 0.2 ha were analyzed. The results showed that lake area decreased in the discontinuous permafrost with values of decrease ranging from 4% to 31%. The Arctic Coastal Plain showed very little lake area change. All study regions showed between a 5% and 54% decrease in total number of closed basin ponds. Mechanisms possibly causing the decrease in lake area included increased evapotranspiration due to longer and warmer growing seasons, the expansion of the talik, allowing subsurface drainage, and wildfires, causing accelerated warming and thawing of the permafrost.

Yoshikawa and Hinzman (2003) researched shrinking thermokarst ponds near Council, Alaska, located on the southern half of the Seward Peninsula, between 1950 and 2000. 24 ponds were identified in the study region and 22 of them showed decrease in lake area. The two lakes that increased in size were controlled by terrain. Drainage was mostly by bank rupture and subsurface drainage through a well-developed ice-wedge polygon network and well-developed taliks beneath the lakes. The study showed active thermokarst and newly developed ponds forming, possibly indicating a response to the

slight warming trend occurring in the permafrost temperatures and the mean annual air temperatures. Minimal lake development occurred in regions with gentle slope.

In a third study, Hinkel et al. (2007) examined drainage occurring to thermokarst lakes on the western Arctic Coastal Plain (34,570 km^2) in northern Alaska. This study used MSS images from the mid-1970s and ETM+ imagery from 2002. Between the middle 1970s and 2002, lakes that were larger than 10 ha and showed significant drainage (> 25%) were identified. 50 lakes, out of 7,417, showed significant drainage. The majority of these lakes (> 75%) were smaller than 100 ha. Limnicity of the western Arctic Coastal Plain was 17.3% in 2001. Reasons for lake drainage included the establishment of a drainage channel between two lakes resulting with lake area loss in one lake and lake area rise in the other, bank overtopping, drainage through ice wedge networks, coastal erosion, and stream headward erosion.

A second part of the study compared 1955 and 1959 aerial photos and 2002 orthorectified radar imagery of the Barrow Peninsula. Lake area during this time decreased from 21.3% to 20.9%, a 0.4% change, and the number of lakes (> 10 ha) went from 301 to 271 (many of these 30 lakes experienced partial drainage putting them beneath the 10 ha threshold). The average lake size increased however, due largely to lake coalescence.

In this thesis research, many of the same conclusions were drawn as were cited in these Alaskan lake studies. A pattern of lake coalescence and flooding is seen, which is increasing the number of large lakes. This was observed in the Kolyma Lowlands as well as on the Barrow Peninsula. The smaller lakes, less than 100 ha, account for greater than 75% of the substantially drained lakes in the Kolyma Lowlands as well as on the Arctic Coastal Plain (Hinkel et al., 2007). Limnicity of the Arctic Coastal Plain is comparable to the limnicity of the Kolyma Lowlands, 17.3% and 16.2% respectively.

Several mechanisms of lake drainage were identified by Yoshikawa and Hinzman (2003) and Hinkel et al. (2007) including coastal erosion, initiation of a drainage outlet during times of high water, stream headward erosion, bank rupture, subsurface drainage, and stream meandering, along with direct human impacts. These causes of drainage, with

the exception of coastal erosion, are the dominant causes of lake area loss within the Kolyma Lowlands as well. On the Seward Peninsula, active thermokarst was observed creating new ponds. New thermokarst lakes are developing within the Kolyma Lowlands (Sections 4.1.1.3 and 4.1.2.3). These studies also concur that the presence of slope and increased elevation hinder lake development.

Lake change studies done in Alaska and Siberia can be compared. Both regions have thick continuous permafrost with cold annual temperatures. Lakes in both regions are experiencing drainage by many of the same mechanisms, yet lake expansion and new lake development are also occurring. Unfortunately, not many lake change studies have been completed within Alaska's continuous permafrost zone.

5.5.3 Comparisons to Other Lake Change Studies

Another lake change study was completed by Plug et al. (2008) on the Tuktoyaktuk Peninsula in the western Canadian Arctic. This region of Canada is located within continuous permafrost, generally between 200 and 600 meters thick with an elevation under 60 m above sea level, and has experienced warming of 1.7 ^{o}C over the last 100 years. The mean annual air temperature has been roughly -10 ^{o}C for the past 40 years. The southern Tuktoyaktuk Peninsula was glaciated during the last glacial advance and the northern region consists of sands and silts with low ice contents. Limnicity here is between 22% and 34%.

Plug et al. (2008) used Landsat MSS, TM, and ETM+ images from between 1978 and 2001 and used a minimum lake area of 1.3 ha. Between 1979 and 1991, lake area expanded by 14%. Conversely, between 1991 and 2001, lake area decreased by 11%. Overall, a 3% increase in lake area was observed. Larger lakes drained, increasing the number of smaller lakes in the region. There was a strong correlation relating thermokarst lake changes to changes in annual precipitation. These results agree most with results from the Alaska Arctic Coastal Plain (Riordan et al., 2006) that also exhibited limited lake area change.

The fact that this region was previously glaciated may play a role in lake change dynamics. Upon glacial retreat, depressions may have formed allowing lakes to form and

therefore they are not thermokarst lakes initiated by permafrost degradation. In addition, permafrost in this region is generally ice-poor (Plug et al., 2008). Because of that, many of the lakes here may have different origins and not be closed-system thermokarst lakes. Climatic warming would have less of an affect on non-thermokarst lakes in ice-poor regions than in an ice-rich region like the Yedoma sediments of Siberia. Upon warming, permafrost will thaw, however little thermokarst will form and limited land subsidence will take place. With limited thermokarst occurring, the amount of lake expansion and growth due to permafrost degradation caused by climate warming will be limited.

5.6 The Larger Scale Problem and How These Results Contribute

A larger problem that this study contributes information to is determining the effect thermokarst lake changes will have on the arctic environment. Changes in thermokarst lake dynamics and permafrost degradation results in changes to the arctic ecology, which encompasses the relationships between living organisms and the environment, the hydrological patterns, vegetation cover and thus ecosystem distribution (tundra/forest biomes and wetland/steep environment). Thermokarst lake changes will affect albedo values, freshwater discharge, and human infrastructure within the arctic (Hinzman et al., 2005; Lawrence and Slater, 2005; Romanovsky et al., 2007; Jorgenson et al., 2008). Permafrost degradation and lake formation and drying will affect aspects of the arctic in different ways. The results from this study will help predict future changes that will occur to the arctic environment.

The dominant process occurring to thermokarst lakes within the region of the Kolyma Lowlands is lake drainage. A large decrease in surface water would cause greater summer warming of the air (effects to albedo are discussed on the following page) (Bonan, 1995; Krinner and Boike, 2010). This would be because the large heat holding capacity of lakes has disappeared. Water has over twice the heat holding capacity of soils. The average heat capacity for water is 4.187 MJ/m^3K and for soils, the average heat capacity is 1.875 MJ/m^3K (Harris, 2002). A large percentage of the heat once absorbed by the lakes, is now absorbed into the soil or is being reflected. For the same reason, a large decrease in lake area would cause air-cooling in the fall. Lakes release

their heat more slowly when cooling than the soil surface will. The fall cooling effect would be stronger than the warming forced by the decreased lake area (Harris, 2002; Krinner and Boike, 2010). Lake area loss would be a negative feedback to global warming. Complete lake disappearance would mean a 10-20% reduction in the predicted warming trend, up to 30% regionally and seasonally (Krinner and Boike, 2010).

Dominant lake drainage and drying soils, the faster growing aspen, birch, and white spruce will move in from the south, as these species will already occupy the drier, permafrost-free soils in the southern boreal forests. These plants are more suited for a drying climate (Jorgenson et al., 2010). Dry, grassy steppe environments could also develop where there used to be wetlands. With drying, less water will be available to vascular plants. These environments create poor habitats for plants, birds, fish, and land-based mammals as the limited water supplies become high in acidity and low in productivity (Jorgenson et al., 2008, 2010). Vital feeding and nesting grounds for many migratory birds may also disappear (Smith et al., 2005).

Lakes also act as conduits to transfer heat deeper into the soil closer to the permafrost table. With lake drying, no convection currents, or wind-generated currents in the lakes will exist to transfer this heat deeper into the ground (Harris, 2002). Rivers whose water supply was thermokarst lakes may dry upon lake desiccation.

Transformation to a deciduous forest and a loss of lake area will help to increase the albedo of the arctic environment. This means less solar energy will be absorbed by the arctic; a larger percentage will be reflected back into the atmosphere (Harris, 2002; Jorgenson et al., 2010). This could help counteract the effect of a warming climate and lake development.

A second problem this thesis research will help to address is changes that are occurring to the global carbon budget. The fact that new lakes are forming in Yedoma, and most likely other sediments, and lakes are experiencing erosion along their banks, indicates that thermokarst lake area is increasing and permafrost is thawing. As the permafrost degrades, the ice melts and the soil thaws. Yedoma soils contain between two and five percent organic matter and have an ice content between 50% and 90% (Walter et

al., 2006; Zimov et al., 2006; Schirrmeister et al., 2008). Thawing permafrost soils in the Kolyma Lowlands are therefore a source of freshwater along with organic carbon. When the organic matter in the soil thaws, it will decompose and release either carbon dioxide or methane (Schuur et al., 2008).

This study will help determine the effect thermokarst lakes will have on methane and carbon dioxide fluxes. Upon soil thaw, organic matter within the soil will accumulate on the bottom of thermokarst lakes. Here, the organic matter can undergo anaerobic decomposition releasing methane into the atmosphere. Where permafrost is thawing and no lakes are forming, decomposition will occur in aerobic conditions, which will release carbon dioxide (Schuur et al., 2008). Walter et al. (2006) reported that the decomposition of organic matter beneath Siberian lakes in Yedoma deposits account for 3.7 Tg of CH_4/year.

Research done on ice cores from Greenland show an abrupt increase in temperature and precipitation followed by an increase in the concentration of atmospheric methane. The differences between the methane concentrations recorded in Greenland ice cores and Antarctic ice cores suggest the methane source is from an arctic region (Severinghaus et al., 1998). The period of increasing temperature, precipitation, and methane coincides with the end of the Younger Dryas cold period (13-11.5 k yr BP) and the beginning of the warmer Holocene period (11.5 to 9.5 k yr BP) (Severinghaus et al., 1998; Walter et al., 2007a). As mentioned before, the permafrost surface deposits, which include Yedoma, developed during the Pleistocene era and thermokarst started to develop at the Pleistocene/Holocene transition. The highest rates of thermokarst development occurred between 11k and 8k years ago (Walter et al., 2007a) which includes the Holocene Climatic Optimum (9 k to 8 k y BP) (Veremeeva and Gubin, 2009). During the Holocene Climatic Optimum, the annual average air temperature was 2 to 3 ^{o}C higher than present and the average July temperature was between 8 and 9 ^{o}C higher than present (Lozhkin et al., 1975 cited in Veremeeva and Gubin, 2009). It was during this time that over half of the Yedoma deposits experienced thermokarst development (Veremeeva and Gubin, 2009).

Walter et al. (2006) estimated that a 14.7% increase in lake area would results in a 58% increase in methane emissions or 1.4 Tg/year, if extrapolated throughout the Yedoma regions. Between 41% and 83% of the methane released from Siberian lakes is originating from Pleistocene organic carbon, deposited between 20,000 and 40,000 years ago. Today, there is an estimated 500 Pg of labile Pleistocene carbon located within Siberian Yedoma deposits (Zimov et al., 2006). Upon thaw, portions of this carbon will become available for decomposition and possible release into the atmosphere.

The highest amount of soil organic carbon in the entire permafrost regions is located within the first 100 cm of the soil (495.8 Pg). Between 100 and 300 cm, there is 528.2 Pg (Tarnocai et al., 2009). Permafrost thaw and degradation is going to affect the uppermost layer of permafrost first. When this occurs, large amounts of carbon will be released into the arctic atmosphere. A study by Raupach and Canadell (2008) estimated that if a 10% thaw of the permafrost were to occur, a 0.7 ^{o}C global temperature increase and an 80-ppm increase in atmospheric CO_2 would occur by 2100.

Our study shows that: 1) the dominant process in the Kolyma Lowlands occurring to thermokarst lakes is loss of lake area; 2) thermokarst lakes are expanding and new ones are forming; and 3) Yedoma deposits are eroding along the lake perimeters. These facts show that active thermokarst is ongoing in the Kolyma Lowlands. Landscapes characterized by newly formed thermokarst and lakes generate significantly higher emissions than stable lakes (Walter et al., 2007b). Furthermore, during the Holocene Climatic Optimum, a warming climate causes increased thermokarst formation and methane emissions in the Arctic.

Throughout the 21st century, permafrost degradation and thaw is likely to occur over 12-20% of the permafrost land area (ACIA, 2005). By the middle of the 21st century, permafrost in the northern hemisphere will likely decrease in area between 20% and 35% (IPCC, 2007). Active layer depth will likely increase 30-50% by 2080 over most of the permafrost areas (IPCC, 2007). The greatest increases are expected in northern Siberia and interior Alaska-Yukon regions (ACIA, 2005). This study will help scientist to be able to predict rates of future permafrost degradation and aggradation in

response to thermokarst lake formation, expansion, and drainage and thus the rate with which organic matter is thawing and becoming available for microbial decomposition. Knowing rates of decomposition, the amount of methane and/or carbon dioxide that will be released into the atmosphere can be calculated along with to what degree thermokarst lakes play a role in increasing the arctic carbon concentrations and forcing global climate change.

5.7 Future Trends

In the long-term, warming and permafrost thaw will lead to thermokarst lake drainage being the dominant process. However, initial permafrost warming likely will lead to the development of more thermokarst and thermokarst lakes. With further permafrost degradation, thermokarst lakes will drain (ACIA, 2005; Smith et al., 2005) as more lake area loss through subsurface drainage will occur (Smith et al., 2005). Eventually, the discontinuous/continuous permafrost boundary will move further north. By the end of the 21st century, the permafrost boundary is expected to move northward by several hundred kilometers (ACIA, 2005). The study by Smith et al., (2005) that was done across a portion of West Siberia reported that 85% of the drained lakes were within 200 km of the continuous permafrost boundary.

In addition, with continuing permafrost thaw, at least some part of the 1,672 Pg of organic carbon frozen within the permafrost of the northern hemisphere will thaw and decompose (Tarnocai et al., 2009). This amount of organic carbon, when released as methane or carbon dioxide, could prove to be a powerful element in future climate change. Both of these processes, permafrost degradation and the continued release of organic carbon are caused by climate warming. They will, in return, feed back into the system furthering yet more climate warming continuing the process of permafrost degradation and thawing.

Permafrost degradation and thaw will cause changes to occur to the dynamics of thermokarst lakes as well. Globally, as mentioned above, with long-term degradation, drying will be the dominate process (ACIA, 2005; Smith et al., 2005). In southern zones of discontinuous permafrost, lake drainage will most likely out pace lake expansion and

growth while in northern, continuous permafrost zones, lake formation will be dominant upon permafrost thaw (Hinzman et al., 2005; Smith et al., 2005; Riordan et al., 2006). However, on a local scale, the ratio of lake drying and formation cannot be determined solely based on a warming climate and the permafrost degradation that it is associated with. Variations in local factors including topography, surface water, ground water, soil properties, geology, vegetation, slope, snow cover, and ice content will allow both lake growth and drying to occur simultaneously and within close proximity to each other (Hinzman et al., 2005; Jorgenson et al., 2010). This study demonstrates how differences in geomorphology can allow lake expansion, growth, and drying to occur concurrently within the Kolyma Lowlands in continuous permafrost. Because of the positive and negative feedbacks associated with numerous environmental characteristics, at this time, one cannot accurately predict how thermokarst lake dynamics will change at a local scale.

5.8 Usability of Remote Sensing and GIS to Analyze Thermokarst Lakes

Remote sensing gives scientists the ability to map arctic lakes over large areas. There is high-resolution imagery available for most locations allowing the accuracy of remote sensing studies to increase and for the smallest lakes to be included into the research. With the higher accuracy, the need for extensive groundwork, while still essential, will be minimized.

As with all research methods, remote sensing has its limitations. One limitation in optical data as used in this study is cloud cover. Depending on application, spatial resolution can be another limitation. The image resolution of Landsat MSS (79 m resolution) and TM (30 m resolution) for example limited the minimum size of lakes mapped in this study to 5.0 ha for the medium-resolution regional study portion of this thesis.

The main GIS program used for lake extraction was Feature Analysts extension for ArcGIS. For the high-resolution ALOS PRISM and Corona images, the lake threshold was 0.5 ha. This was because Feature Analysts could not produce an accurate extraction which included the smallest of lakes due to the properties of panchromatic imagery. The smaller and shallow lakes had diverse spectral signatures that were, more

often than not, similar to land and not water. Shallow lakes and those that are sediment laden reflect more of the incoming radiation back to the sensor. Clear, deep water has a very low albedo and thus its spectral signature appears close to black. As the study region was too large to digitize all lakes less than 0.5 ha manually, they were left out of the research.

The same affect was seen on the Landsat images. Some lakes have shallow edges or more sediment-laden waters than others. These lakes therefore emit a lighter spectral signature and make it harder to distinguish the lake boundary from the surrounding land. This is especially true when a lake or pond is surrounded by a wetland or bog. When this is the case, as it was, for example, with the marine deposits in the regional assessment region, the lake bank could not accurately be determined manually or by Feature Analysts.

It was not possible to extract certain lake boundaries or lake types with Feature Analysts. Lakes that were narrow, or became narrow at there ends, would often be left out of the feature class produced by Feature Analysts. This is because of varied spectral signatures produced and the poor resolution of the Landsat images. When this occurred, manual correction had to be done. Overall, remote sensing is a time efficient and effective method for lake change studies.

Chapter 6: Conclusion

6.1 Overall Changes to Thermokarst Lakes in the Kolyma Lowlands

Between 1965 and 2007, thermokarst lakes located in the continuous permafrost of the Kolyma Lowlands have experienced drainage and expansion. New lake formation also occurred. These dynamics are occurring simultaneously in many regions and are caused by a variety of processes, including permafrost thaw and degradation (Harris, 2002; Hinzman et al., 2005), flooding, and erosion. In the Cherskii high-resolution region, there was an overall increase in lake area of 7.6% (87.91 ha/year from 1965 to 2007). In the high-resolution Duvanny Yar region, lake area has decreased by 5.2% (53.19 ha/year from 1965 to 2007). In the medium-resolution regional assessment a lake area loss of 14,250 ha was recorded for 409 substantially drained lakes over the period of 1965 to 2007. Overall change was not calculated, as it was not possible to derive a complete and qualitatively homogeneous lake dataset for this large region from the 1965 Corona imagery so far (Table 6.1.1).

Table 6.1.1 Summary of Lake Change Occurring in the Kolyma Lowlands.

Study Region	Area (km^2)	Number of Lakes from L_{20} subset or showing substantial drainage (regional study)	Lake Area Loss (ha) (accounted for by substantially drained lakes)	Number of Lakes which Completely Dried	Entire Lake Area 1965 (ha)	Entire Lake Area 2007 (ha)	Overall Lake Area Change
High-Resolution Cherskii	3,362	167 (>20%)	-1,762	14	47,187	50,809	7.6% Increase
High-Resolution Kolyma Lowlands	4,192	133 (>20%)	-2,281	13	42,740	40,502	5.2% Decrease
Medium-Resolution Region	43,543	409	-14,250	65	-----	703,319	-----

A number of factors played a role in determining the distribution of lake area and lake size, along with which regions experienced the most lake drainage. The largest lakes and the highest limnicity were found in lacustrine and bog deposits and Yedoma deposits. These sediments are located at elevations roughly less than 60 m, have high ice-contents, and small particle size. They exhibit poor drainage, and the high ice-content allows for a high degree of surface subsidence to occur upon permafrost thaw and degradation. Deluvial and eluvial deposits had the lowest limnicity. They consist of larger, coarse grained particles and a much lower ice content. They are also located at higher elevations with stronger slopes. Low ice-content means little surface subsidence and the slope and large particle size allows good, down-slope drainage. There is also limited alluvial flooding and erosion influence here. Deluvial and eluvial deposits have much smaller lake size as well.

Alluvial influences are a major control on the amount of normalized lake area. Changes in river water volume and velocity cause erosion and flooding to occur. This, in return, can cause both lake drainage and expansion. Alluvial deposits had a limnicity between that of the lacustrine deposits and the up-slope deposits in all three study regions. Rivers prevent the lakes from completely drying by erosional processes which cause drainage and flooding. Those processes refill the thermokarst depressions, preventing a long-term drainage trend from existing and breach lake banks preventing unlimited lake growth and expansion.

The amount of lake area that drains depends on the presence of rivers, the elevation, and lake size. Alluvial deposits accounted for the largest percentage of drained lake area. Many smaller lakes drained often due to river erosion. Lacustrine, bog and Yedoma deposits exhibited the next highest drainage levels. Here, fewer lakes drained but they were much larger. The sediments located at elevation with coarser particle size showed the least amount of drainage. There are much fewer lakes developing here and those that do are small.

Those regions which experienced the most significant changes in lake area, either expansion or lake area loss, are those with small sediment particle size, high ice content,

and an alluvial influence from rivers and streams. Locations experiencing increasing temperature trends also favor thermokarst lake expansion and drainage (ACIA, 2007).

Causes of lake drainage in the Kolyma Lowlands included rivers breaching lake banks, stream headward erosion, lake coalescence, the development or enhancement of an outlet, and human disturbances. Means of lake expansion included lake coalescence, further permafrost degradation, and river flooding.

Changes in thermokarst lake dynamics have severe ramifications on the Arctic environment. Changes in surface water area, which occurred throughout the study region, affected the local albedo values. The Cherskii region showed a decrease in albedo of just less than 1% while the Duvanny Yar region showed an increased in albedo of approximately 0.5%. The amount of organic carbon that undergoes microbial decomposition also changes with changing lake dynamics. With the dominant process being lake drainage, the ground is able to refreeze, slowing the rate of decomposition and thus the rate carbon is released into the atmosphere. However, new lakes are developing as well. The trends observed in this study cannot be extrapolated throughout the Arctic though.

Future development or drainage of thermokarst lakes depends on the degree of permafrost degradation that occurs. The stability of the permafrost thermal regime is dependent on many factors which include topography, water movement, soil properties, ice-content, snow cover, vegetation, geology, surface disturbances, and changes in air temperature (Schuur et al., 2008; Jorgenson et al., 2010). The impact thermokarst lakes will have on future climate change is based on the size of the organic carbon pool, the rate of release, and thus the rate of permafrost degradation (Sellmann et al., 1975; Smith et al., 2007; Schuur et al., 2008). Arctic air temperatures are expected to rise between 2.8 ^{o}C and 4.6 ^{o}C by 2100, more then anywhere else on earth (ACIA, 2005). This is going to greatly affect the stability of the surface permafrost, and cause degradation and thaw if negative feedbacks from outside factors do not help to sustain cold permafrost temperatures.

6.2 Outlook

Further studies are needed to allow precise calculations relating thermokarst lake formation and permafrost ice content. However, detailed permafrost data is unavailable for much of the Arctic, especially for Siberia. Having detailed permafrost analysis would allow for better estimates of the amount of surface subsidence and thermokarst development that could occur and the amount of freshwater that would be released upon permafrost thaw and degradation.

A second research gap is active layer monitoring. There was no available data for this study on active layer changes in the Kolyma Lowlands. This would help determine the amount of surface subsidence occurring along with the rate of permafrost degradation. Knowing changes in active layer depth would determine how much thaw is occurring, possibly allowing for subsurface drainage and changes in ground/surface water flow.

Continual permafrost research is pertinent to further understanding the ongoing changes, which are occurring to the Arctic environment, and to determine the degree to which thermokarst lakes act as a force for future climate change.

References

ALOS Data User Handbook (2007), Earth Observation Research Center, Japan Aerospace Exploration Agency, http://www.eroc.jaxa.jp/ALOS/doc/alos_userhb_en.pdf. Last accessed: 6/6/2010.

Arctic Climate Impact Assessment (ACIA) (2005), Impacts of a Warming Arctic: Arctic Impact Assessment, Cambridge, Mass.

Are, F., and E. Reimnitz (2000), An Overview of the Lena River Delta Setting: Geology, Tectonics, Geomorphology, and Hydrology, *Journal of Coastal Research,* 16(4), 1083-1093.

Avery, T.E., and G.L. Berlin (1992), Fundamental of Remote Sensing and Airphoto Interpretation, 5th edition, R. McConnin (ed.), Prentice-Hall, Inc.

Bakermans, C., H.L. Ayala-del-Rio, M.A. Ponder, T. Vishnivetskaya, D. Gilichinsky, M.F. Thomashow, and J.M. Tiedje (2006), Psychrobacter Cryohalolentis sp. Nov. and Psychrobacter Arcticus sp. Nov., Isolated from Siberian Permafrost, *International Journal of Systematic and Evolutionary Microbiology,* 56, 1285-1291.

Bayram, B., H. Bayraktar, C. Helvaci, and U. Acar (2004), Coast Line Change Detection Using Corona, Spot, and IRS 1D Images, *International Archives of Photogrammetry and Remote Sensing,* XXXV(B7), 437-441.

Boike, J., C. Wille, and A. Abnizova (2008), Climatology and Summer Energy and Water Balance of Polygonal Tundra in the Lena River Delta, Siberia, *Journal of Geophysical Research,* 113, GO3025.

Bonan, G.B. (1995), Sensitivity of a GCM Simulation to Inclusion of Inland Water Surfaces, *American Meteorological Society,* 8, 2,691-2,704.

Brewer, M.C., L.D. Carter, and R. Glenn (1993), Sudden Drainage of a Thaw Lake on the Alaskan Arctic Coastal Plain, in *Proceedings of the Sixth International conference on Permafrost,* 48-53, South China University of Technology Press, Wushan Guangzhou.

Brown, J., O.J. Ferrians Jr., J.A. Heginbottom, and E.S. Melnikov (1997), *Circum-Arctic Map of Permafrost and Ground-Ice Conditions,* Boulder, CO: National Snow and Ice Data Center/World Data Center for Glaciology, Digital Media.

Brown, J., K.M. Hinkel, and F.E. Nelson (2000), The Circumpolar Active Layer Monitoring (CALM) Program: Research Designs and Initial Results, *Polar Geography,* 24(3), 165-258.

Casana, J., and J. Cothren (2008), Stereo Analysis, DEM Extraction and Orthorectification of Corona Satellite Imagery: Archaeological Applications from the Near East, *Antiquity,*00, 1-18.

Castro, F.S.P., and J.A.S. Centeno (2010), Road Extraction from ALOS Images Using Mathematical Morphology, In: *ISPRS TC VII Symposium-100 Years ISPRS,* W. Wagner, and B. Szekely (eds), XXXVIII, 7B.

Chapin III, F.S., M. Strum, M.C. Serreze, J.P. McFadden, J.R. Key, A.H. Lloyd, A.D. McGuire, T.S. Rupp, A.H. Lynch, J.P. Schimel, J. Beringer, W.L. Chapman, H.E. Epstein, E.S. Euskirchen, L.D. Hinzman, G. Jia, C.L. Ping, K.D. Tape, C.D.C. Thompson, D.A. Walker, and J.M. Welker (2005), Role of Land-Surface Changes in Arctic Summer Warming, *Science,* 310, 657-660.

Dashora, A., B. Sreenivas, B. Lohani, J.N. Malik, and A.A. Shah (2006), GCP Collection for Corona Satellite Photographs: Issues and Methodology, *Journal of the Indian Society of Remote Sensing,* 34(2), 153-160.

Eugster, W., W.R. Rouse, R.A. Pielke Sr., J.P. McFadden, D.D. Baldocchi, T.G.F. Kittel, F.S. Chapin III, G.E. Liston, P.L. Vidale, E. Vaganov, and S. Chambers (2000), Land-Atmosphere Energy Exchange in Arctic Tundra and Boreal Forest; Available Data and Feedbacks to Climate, *Global Change Biology,* 6, 84-115.

Ferranti, J.D. (2009), Digital Elevation Model, Derived from Topographic Maps 1:200,000, Soviet Military Topographic Survey or Voenno-Topograficheskoe Upravlenie General'nogo Shtaba, VTU GSH.

Frazier, P.S., and K.J. Page (2000), Water Body Detection and Delineation with Landsat TM Data, *Photogrammetric Engineering and Remote Sensing,* 66(12), 1461-1467.

Friborg, T., H. Soegaard, T.R. Christensen, C.R. Lloyd, and N.S. Panikov (2003), Siberian Wetlands: Where a Sink is a Source, *Geophysical Research Letters,* 30(21), L017797.

Frohn, R.C., K.M. Hinkel, and W.R. Eisner (2005), Satellite Remote Sensing Classification of Thaw Lakes and Drained Thaw Lake Basins on the North Slope Alaska, *Remote Sensing of the Environment,* 97, 116-126.

Galiatsatos, N., D.N.M. Donoghue, and G. Philip (2008), High Resolution Elevation Data Derived from Stereoscopic Corona Imagery with Minimal Ground Control: An Approach Using Ikonos and SRTM Data, *Photogrammetric Engineering and Remote Sensing,* 74(9), 1093-1106.

Gonga-Saholiariliva, N., J. Xavier, M. Denoyelle, Y. Gunnell, and C. Mering (2008), Wetland and Aquatic Surface Inventory Using ALOS Satellite Images, Examples from Sologne (Central France) and Al'Tamin Province (Iraq), BALWOIS, May 2008.

Gradstein, F.M., J.G. Ogg, A.G. Smith, W. Bleeker, and L.J. Lourens (2004), A New Geological Time Scale, with Special Reference to Precambrian and Neogene, Excerpt from Geological Time Scale 2004, Cambridge University Press, 27(2), 83-100.

Grant, K.L., C.R. Stokes, and I.S. Evans (2009), Identification and Characteristics of Surge-Type Glaciers on Novaya Zemlya, Russian Arctic, *Journal of Glaciology,* 55(194), 960-972.

Grosse, G., L. Schirrmeister, V.V. Kunitsky, and H. Hubberten (2005), The Use of Corona Images in Remote Sensing of Periglacial Geomorphology: An Illustration from the NE Siberian Coast, *Permafrost, and Periglacial Processes,* 16, 163-172.

Grosse G., L. Schirrmeister. and T.J. Malthus (2006), Application of Landsat-7 Satellite Data and a DEM for the Quantification of Thermokarst-Affected Terrain Types in the Periglacial Lena-Anabar Coastal Lowland, *Polar Research,* 25, 51-67.

Grosse, G., V. Romanovsky, K. Walter, A. Morgenstern, H. Lantuit, and S. Zimov (2008), Distribution of Thermokarst Lakes and Ponds at Three Yedoma Sites in Siberia, In: *'Ninth International Conference on Permafrost'*, D.L. Kane, and K.M. Hinkel (eds.), Institute of Northern Engineering, University of Alaska Fairbanks, 551-556.

Hamilton, T.D., T.A. Ager, and S.W. Robinson (1983), Late Holocene Ice Wedges Near Fairbanks, Alaska, U.S.A.: Environmental Setting and History of Growth, *Arctic and Alpine Research,* 15(3), 157-168.

Harris, S.A. (2002), Causes and Consequences of Rapid Thermokarst Development in Permafrost of Glacial Terrain, *Permafrost and Periglacial Processes,* 13, 237-242.

Hese, S., G. Grosse, and S. Pocking (2010), Object Based Thermokarst Lake Change Mapping as Part of the ESA Data User Element (DUE) Permafrost, *The International Archives of the Photogrammetry, Remote Sensing and Spatial Information Sciences,* XXXVIII-4/C7.

Hinkel, K.M., W.R. Eisner, J.G. Bockheim, F.E. Nelson, K.M. Peterson, and X. Dai (2003), Spatial Extent, Age, and Carbon Stocks in Drained Thaw Lake Basins on the Barrow Peninsula, Alaska, *Arctic, Antarctic, and Alpine Research,* 35(3), 291-300.

Hinkel, K.M., R.C. Frohn, F.E. Nelson, W.R. Eisner, and R.A. Beck (2005), Morphometric and Spatial Analysis of Thaw Lakes and Drained Thaw Lake Basins in the Western Arctic Coastal Plain, Alaska, *Permafrost and Periglacial Processes,* 16, 327-341.

Hinkel, K.M., B.M. Jones, W.R. Eisner, C.J. Cuomo, R.A. Beck, and R. Frohn (2007), Methods to Assess Natural and Anthropogenic Thaw Lake Drainage on the Western Arctic Coastal Plain of Northern Alaska, *Journal of Geophysical Research,* 112, F02S16.

Hinzman, L.D., N.D. Bettez, W.R. Bolton, F.S. Chapin, M.B. Dyurgerov, C.L. Fastie, B. Griffith, R.D. Hollister, A. Hope, H.P. Huntington, A.M. Jensen, G.J. Jia, T. Jorgenson, D.L. Kane, D.R. Klein, G. Kofinas, A.H. Lynch, A.H. Lloyd, A.D. McGuire, F.E. Nelson, W.C. Oechel, T.E. Osterkamp, C.H. Racine, V. E. Romanovsky, R.S. Stone, C.A. Stow, M. Sturm, C.E. Tweedie, G.L. Vourlitis, M.D. Walker, D.A. Walker, P.J. Webber, J.M. Welker, K.S. Winker, and K. Yoshikawa (2005), Evidence and Implications of Recent Climate Change in Northern Alaska and Other Arctic Regions, *Climate Change,* 72, 251-298.

Hopkins, D.M. (1949), Thaw Lakes and Thaw Sinks in the Imuruk Lake Area, Seward Peninsula, Alaska, *Journal of Geology,* 57, 119-131.

Hopkins, D.M., T.N.V. Karlstrom, R.F. Black, J.R. Williams, T.L. Pewe, A.T. Fernald, and E.H. Muller (1955), Permafrost and Ground Water in Alaska, *Geological Survey Professional Paper,* 264-F, 113-144.

IPCC (2007), Summary for Policymakers, In: *Climate Change 2007: Impacts, Adaptation, and Vulnerability, Contribution of Working Group I &II to the forth Assessment Report of the Intergovernmental Panel on Climate Change,* M.L. Parry, O.F. Canziani, J.P. Palutikof, P.J. Van der Linden, and C.E. Hanson (eds.), Cambridge University Press.

Ishikawa, M., N. Sharkhuu, Y. Zhang, T. Kadota, and T. Ohata (2005), Ground Thermal and Moisture Conditions at the Southern Boundary of Discontinuous Permafrost, Mongolia, *Permafrost and Periglacial Processes,* 16(2), 209-216.

Jorgenson, M.T., and Y. Shur (2007), Evolution of Lakes and Basins in Northern Alaska and Discussion of the Thaw Lake Cycle, *Journal of Geophysical Research,* 112, F02S17.

Jorgenson, M.T., Y.L. Shur, and T.E. Osterkamp (2008), Thermokarst in Alaska, In: *'Ninth International Conference on Permafrost'*, D.L. Kane, and K.M. Hinkel (eds.), Institute of Northern Engineering, University of Alaska Fairbanks, 869-876.

Jorgenson, M.T., V. Romanovsky, J. Harden, Y. Shur, J. O'Donnell, E.A.G. Schuur, M. Kanevskiy, and S. Marchenko (2010), Resilience and Vulnerability of Permafrost to Climate Change, *Canadian Journal of Forest Research,* 40, 1219-1236.

Kaplina, T.N., and A.V. Lozhkin (1982), Vegetational History of Coastal Lowlands of Yakutia during the Holocene, In: *Environmental Evolution of USSR during Late Pleistocene and Holocene,* A.A. Velichko, I.I. Spasskaya, and N.A. Kohtinskiy (eds.), Nauka, Moscow, 207-220.

Katamura F., M. Fukuda, N.P. Bosikov, R.V. Desyatkin, T. Nakamura, and J. Moriizumi (2006), Thermokarst Formation and Vegetation Dynamics Inferred From a Palynological Study in Central Yakutia, Eastern Siberia, Russia, *Arctic, Antarctic, and Alpine Research,* 38, 561-570.

Kosterin O.E., and L.V. Sivtseva (2009), Odonata of Yakutia (Russia), with Description of Calopteryx Splendens Njuja ssp. Nov. (Zygoptera: Calopterygidae), *Odonatologica,* 38(2), 113-132.

Kotlyakov, V. and N. Koronkevitch (2002), Maps of Permafrost, Ground Ice, and Climate Data, In: V. Stolbovoi, and I. McCallum (2002), CD-ROM Land Resources of Russia, Laxenburg, Austria: International Institute for Applied Systems Analysis and the Russian Academy of Science, www.iiasa.ac.at/research/FOR/Russia-cd.

Krinner, G., and J. Boike (2010), A Study of the Large-Scale Climatic Effects of a Possible Disappearance of High-Latitude Inland Water Surfaces during the 21st Century, *Boreal Environment Research,* 15, 203-217.

Lawrence, D.M., and A.G. Slater (2005), A Projection of Severe Near-Surface Permafrost Degradation during the 21st Century, *Geophysical Research Letters,* 35, L24401.

Lillesand, T.M., R.W. Kiefer, and J.W. Chipman (2004), Remote Sensing and Image Interpretation, 5th edition, R. Flahive, and D. Powell (eds.), John Wiley & Sons, Inc.

Lloyd, A.H., T.S. Rupp, C.L. Fastie, and A.M. Starfield (2003), Patterns and Dynamics of Treeline Advance on the Seward Peninsula, Alaska, *Journal of Geophysical Research,* 108, JD000852.

Lozhkin, A.V., T.P. Prokhorova, and V.P. Parij (1975), Radiocarbon Dating and Palynological Characteristics of the Kolyma Lowlands Alas Deposits, *Reports of the USSR Academy of Science,* 224(6), 1395-1398.

Mackay, J.R. (1988), Catastrophic Lake Drainage, Tuktoyaktuk Peninsula Area, District of Mackenzie, In: *Current Research, Part D, Geological Survey of Canada,* 88-1D, 83-90.

Marsh, P., and M. Hey (1989), The Flooding Hydrology of Mackenzie Delta Lakes Near Inuvik, N.W.T., Canada, *Arctic,* 42(1), 41-49.

Marsh, P., M. Russell, S. Pohl, H. Haywood, and C. Onclin (2009), Changes in Thaw Lake Drainage in the Western Canadian Arctic from 1950 to 2000, *Hydrological Processes,* 23, 145-158.

Martin, P.D., J.L. Jenkins, F.J. Adams, M.T. Jorgenson, A.C. Matz, D.C. Payer, P.E. Reynolds, A.C. Tidwell, and J.R. Zelenak (2009), Wildlife Response to Environmental Arctic Change: Predicting Future Habitats of Arctic Alaska, *Report of the Wildlife Response to Environmental Arctic Change (WildREACH): Predicting Future Habitats of Arctic Alaska Workshop,* November 2008, Fairbanks, Alaska, 1-138.

McDonald, R.A. (1995), Corona: Success for Space Reconnaissance, A Look into the Cold War, and a Revolution for Intelligence, *Photogrammetric Engineering and Remote Sensing,* 41(6).

Nakano, T., S. Kuniyoshi, and M. Fukuda (2000), Temporal Variation in Methane Emission from Tundra Wetlands in a Permafrost Area, Northeastern Siberia, *Atmospheric Environment,* 34, 1205-1213.

O'Donnell, J.A., V.E. Romanovsky, J.W. Harden, and A.D. McGuire (2009), The Effect of Moisture Content on the Thermal Conductivity of Moss and Organic Horizons from Black Spruce Ecosystems in Interior Alaska, *Soil Science,* 174(12), 646-651.

Peterson, B.J., R.M. Holmes, J.W. McClelland, C.J. Vorosmarty, R.B. Lammers, A.I. Shiklomanov, I.A. Shiklomanov, and S. Rahmstorf (2002), Increasing River Discharge to the Arctic Ocean, *Science,* 298(5601), 2171-2178.

Ping, C.L., G.J. Michaelson, M.T. Jorgenson, J.M. Kimble, H. Epstein, V.E. Romanovsky, and D.A. Walker (2008), High stocks of Soil Organic Carbon in the North American Arctic Region, *Nature Geoscience*, doi10.1038/ngeo, 284.

Plug, L.J., C. Walls, and B.M. Scott (2008), Tundra Lake Changes from 1978 to 2001 on the Tuktoyaktuk Peninsula, Western Canadian Arctic, *Geophysical Research Letters,* 35, L03502.

Plug, L.J., and J.J. West (2009), Thaw Lake Expansion in a Two-Dimensional Coupled Model of Heat Transfer, Thaw Subsidence, and Mass Movement, *Journal of Geophysical Research,* 114, 1-4.

Raupach, M.R., and J.G. Canadell (2008), Observing a Vulnerable Carbon Cycle, In: *The Continental-Scale Greenhouse Gas Balance of Europe,* H. Dolman, R. Valentini, and A. Freibauer (eds.), Springer, Berlin.

Riordan, B., D. Verbyla, and A.D. McGuire (2006), Shrinking Ponds in Subarctic Alaska Based on 1950-2002 Remotely Sensed Images, *Journal of Geophysical Research,* 111, G04002.

Rohde, W.G. (1978), Digital Image Analysis Techniques Required for Natural Resource Inventories, *Collection of the Computer History Museum: National Computer Conference,* 93-105.

Romanovskii, N.N. (1993), Osnovy Kriogeneza Litosfery, Izdatelstvo Moscow State University, Moscow, (in Russian).

Romanovsky, V.E., S. Gruber, H. Jin, S.S. Marchenko, S.L. Smith, D.Trombotto, and K.M. Walter (2007), Frozen Ground: Chapter 7, In: *Global Outlook for Ice and Snow,* Earthprint, United Nations Environmental Program, Nairobia, 181-200.

Russian Geological Research Institute VSEGEI (2000), Quaternary Geological Map R-55-(57) Nizhnekolymsk, scale 1:1,000,000.

Schirrmeister, L., H. Meyer, S. Wetterich, C. Siegert, V.V. Kunitsky, G. Grosse, T.V. Kuznetsova, and A.Y. Derevyagin (2008), The Yedoma Suite of the Northeastern Siberian Shelf Region: Characteristics and Concept of Formation, In: *'Ninth International Conference on Permafrost',* D.L. Kane, and K.M. Hinkel (eds.), Institute of Northern Engineering, University of Alaska Fairbanks, 1595-1600.

Schneider, J., G. Grosse, and D. Wagner (2009), Land Cover Classification of Tundra Environments in the Arctic Lean Delta Based on Landsat 7 ETM+ Data and its Application for Upscaling of Methane Emissions, *Remote Sensing of the Environment,* 113, 380-391.

Schuur, E.A.G., J. Bockheim, J.G. Canadell, E. Euskirchen, C.B. Field, S.V. Goryachkin, S. Hagemann, P. Kuhry, P.M. Lafleur, H. Lee, G. Mazhitova, F.E. Nelson, A. Rinke, V.E. Romanovsky, N. Shiklomanov, C. Tarnocai, S. Venevsky, J.G. Vogel, and S.A. Zimov (2008), Vulnerability of Permafrost Carbon to Climate Change: Implications for the Global Carbon Cycle, *BioScience,* 58(8), 701-714.

Sellmann, P.V., J. Brown, R.I. Lewellen, H. McKim, and C. Merry (1975), The Classification and Geomorphic Implications of Thaw Lakes on the Arctic coastal Plain, Alaska, *United States Army, CRREL Research Report,* 344, A622120.

Severinghaus, J.P., T. Sowers, E.J. Brook, R.B. Alley, and M.L. Bender (1998), Timing of Abrupt Climate Change at the End of the Younger Dryas Interval From Thermally Fractionated Gases in Polar Ice, *Nature,* 391, 141-146.

Shur, Y.L., and M.T. Jorgenson (2007), Patterns of Permafrost Formation and Degradation in Relation to Climate and Ecosystems, *Permafrost and Periglacial Processes,* 18, 7-19.

Smith, C.A.S., D.K. Swanson, J.P. Moore, R.J. Ahrens, J.G. Bockheim, J.M Kimble, G.G. Mazhitova, C.L. Ping, and C. Tarnocai (1995), A Description and Classification of Soils and Landscapes of the Lower Kolyma River, Northeastern Russia, *Polar Geography and Geology,* 19(2), 107-126.

Smith, L.C., Y. Sheng, G.M. MacDonald, and L.D. Hinzman (2005), Disappearing Arctic Lakes, *Science,* 308, 1429.

Smith, L.C., Y. Sheng, and G.M. MacDonald (2007), A First Pan-Artic Assessment of the Influence of Glaciation, Permafrost, Topography and Peatlands on Northern Hemisphere Lake Distribution, *Permafrost and Periglacial Processes,* 18, 201-208.

Smol, J.P., and M.V. Douglas (2007), Crossing the Final Ecological Threshold in High Arctic Ponds, *Proceedings of the National Academy of Science of the United States of America,* 104(30), 12,395-12,397.

Surazakov, A., V. Aizen, and E. Aizen (2008), Towards a New High Resolution Orthophoto Mosaic Circa 1976 for the Northern Eurasia: Assessing the Potential of Declassified Hexagon KH-9 Images (Tien Shan Region, Central Asia Case Study), *American Geophysical Union: Fall 2008,* GC41A-0701.

Tappan, G.G., A. Hadj, E.C. Wood, and R.W. Lietzow (2000), Use of Argon, Corona, and Landsat Imagery to Assess 30 Years of Land Resource Changes in West-Central Senegal, *Photogrammetric Engineering and Remote Sensing,* 66(6), 727-735.

Tarnocai, C., J.G. Canadell, E.A.G. Schuur, P. Kuhry, G. Mazhitova, and S. Zimov (2009), Soil Organic Carbon Pools in the Northern Circumpolar Permafrost Region, *Global Biogeochemical Cycles,* 23, GB2023.

Tucker, C.J., D.M. Grant, and J.D. Dykstra (2004), NASA's Global Orthorectified Landsat Data Set, *Photogrammetric Engineering and Remote Sensing,* 70(3), 313-322.

Veremeeva, A., and S. Gubin (2009), Modern Tundra Landscape of the Kolyma Lowland and their Evolution in the Holocene, *Permafrost and Periglacial Processes,* 20, 399-406.

Walker, D.A., H.E. Epstein, V.E. Romanovsky, C.L. Ping, G.J. Michaelson, R.P. Daanen, Y. Shur, R.A. Peterson, W.B. Krantz, M.K. Raynolds, W.A. Gould, G. Gonzalez, D.J. Nicolsky, C.M. Vonlanthen1, A.N. Kade, P. Kuss, A.M. Kelley, C.A. Munger, C.T. Tarnocai, N.V. Matveyeva, and F.J.A. Daniëls (2008), Patterned-Ground Ecosystems: A Synthesis of Field Studies and Models Along a North American Arctic Transect, *Journal of Geophysical Research,* 113, G03S01.

Walter, K.M., S.A. Zimov, J.P. Chanton, D. Verbyla, and F.S. Chapin III (2006), Methane Bubbling from Siberian Thaw Lakes as a Positive Feedback to Climate Warming, *Nature,* 443, 71-75.

Walter, K.M., M.E. Edwards, G. Grosse, S.A. Zimov, and F.S. Chapin III (2007a), Thermokarst Lakes as a Source of Atmospheric CH_4 during the Last Deglaciation, *Science,* 318, 633-636.

Walter, K.M., L.C. Smith, and F.S. Chapin III (2007b), Methane Bubbling from Northern Lakes: Present and Future Contributions to the Global Methane Budget, *Philosophical Transactions of the Royal Society,* 365, 1657-1676.

Wendler, G., M. Shulski, and B. Moore (2010), Changes in the Climate of the Alaskan North Slope and the Ice Concentration of the Adjacent Beaufort Sea, *Theoretical and Applied Climatology,* 99, 67-74.

Williams, D. (2009), Landsat-7 Science Data Users Handbook, National Aeronautics and Space Administration (NASA), http://landsathandbook.gsfc.nasa.gov. Last accessed: 3/10/2011.

Yoshikawa, K., and L.D. Hinzman (2003), Shrinking Thermokarst Ponds and Groundwater Dynamics in Discontinuous Permafrost near Council, Alaska, *Permafrost and Periglacial Processes,* 14, 151-160.

Yoshikawa, K., W.R. Bolton, V.E. Romanovsky, M. Fukuda, and L.D. Hinzman (2003), Impacts of Wildfire on the Permafrost in the Boreal Forests of Interior Alaska, *Journal of Geophysical Research,* 108, JD000438.

Zhang, T., R.G. Barry, K. Knowles, J.A. Heginbottom, and J. Brown (1999), Statistics and Characteristics of Permafrost and Ground-Ice Distribution in the Northern Hemisphere, *Polar Geography,* 31, 47-68.

Zimov, S.A., Y.V. Voropaev, I.P. Semiletov, S.P. Davidov, S.F. Prosiannikov, F.S. Chapin III, M.C. Chapin, S. Trumbore, and S. Tyler (1997), North Siberian Lakes: A Methane Source Fueled by Pleistocene Carbon, *Science,* 277, 800-802.

Zimov, S.A., E.A.G. Schuur, and F.S. Chapin III (2006), Permafrost and the Global Carbon Budget, *Science,* 312(5780), 1612-1613.